Intra- and interlaminar excitatory synaptic connections of layer 4 spiny neurons and layer 6A pyramidal cells in rat barrel cortex

Von der Fakultät für Mathematik, Informatik und Naturwissenschaften der

RWTH Aachen University zur Erlangung des akademischen Grades eines

Doktors der Naturwissenschaften

genehmigte Dissertation

vorgelegt von

Master of Science

Guanxiao Qi

aus Shandong, China

Berichter: Universitätprofessor Dr. rer. nat. Dirk Feldmeyer

Universitätprofessor Dr. rer. nat. Marc Spehr

Tag der mündlichen Prüfung: 6. Juli 2011

Diese Dissertation ist auf den Internetseiten der Hochschulbibliothek online verfügbar.

To my family

Table of Contents

- **1 Introduction** 1
  - 1.1 The neocortex of the mammalian brain 1
  - 1.2 The somatosensory cortex of rodents 2
  - 1.3 Excitatory neurons and their microcircuits 4
  - 1.4 Previous related studies 6
  - 1.5 Aims of this study 7
- **2 Materials and Methods** 9
  - 2.1 Slice preparation 9
  - 2.2 Solutions 9
  - 2.3 Patch clamp technique 10
    - 2.3.1 Cell identification 10
    - 2.3.2 Electrophysiological recordings 11
    - 2.3.3 Synaptic pharmacology 12
  - 2.4 Electrophysiological analysis 12
    - 2.4.1 Passive properties of postsynaptic neurons 12
    - 2.4.2 Synaptic physiology 12
  - 2.5 Morphological reconstructions and analysis 14
    - 2.5.1 Histological procedures 14
    - 2.5.2 Morphological reconstructions 14
    - 2.5.3 Number and locations of synaptic contacts 16
  - 2.6 Innervation domain calculations 16
    - 2.6.1 Axonal and dendritic density maps 16
    - 2.6.2 Innervation domains 16
  - 2.7 Neuronal modeling 17
  - 2.8 Statistical analysis 18
- **3 Results** 19
  - 3.1 Diverse types of excitatory neurons in L4 and L6A 19
    - 3.1.1 L4 spiny neurons 19
    - 3.1.2 L6A short pyramidal cells 21
    - 3.1.3 Other L6A excitatory neurons 23
  - 3.2 Monosynaptic L4-L4 and L6A-L6A excitatory connections 25
    - 3.2.1 L4-L4 pairs 25
    - 3.2.2 L6A-L6A pairs 33

- 3.2.3 Summary of data 41
- 3.3 Monosynaptic L4-L6A excitatory connections 46
  - 3.3.1 Three connection phenotypes 46
  - 3.3.2 L4 spiny stellate-L6A pyramidal cell pairs 48
  - 3.3.3 L4 star pyramid-L6A pyramidal cell pairs with fast synapses 55
  - 3.3.4 L4 star pyramid-L6A pyramidal cell pairs with slow synapses 62
  - 3.3.5 Summary of data 68
- 3.4 Several interesting findings 77
  - 3.4.1 Tight correlation between geometric and functional properties 77
  - 3.4.2 Incomplete prediction of the synaptic location based solely on axo-dendritic overlap 80
  - 3.4.3 Modeling the origins of ‘slow’ and ‘fast’ synapses 82
  - 3.4.4 Pre but not postsynaptic cell-type specific selection of the postsynaptic target region 84

4 Discussion 87

- 4.1 The functional role of L4-L6A connections 87
- 4.2 Different roles of L4 spiny neurons 87
- 4.3 Development of L4-L6A connections 88
- 4.4 Comparison with previous findings 90
- 4.5 Advantage and shortcoming of present methods 92
- 4.6 Future directions 94

5 Abbreviations 96

6 Summary 97

7 Acknowledgements 99

8 References 101

9 Curriculum Vitae 114

1 Introduction

1.1 The neocortex of the mammalian brain

The mammalian and in particular the human brain is a structured but very complex system. To understand its structure and function and their relationship, diverse methods including morphological, electrophysiological, molecular, genetic and other related approaches have been developed since the pioneering work of Santiago Ramón y Cajal more than a century ago.

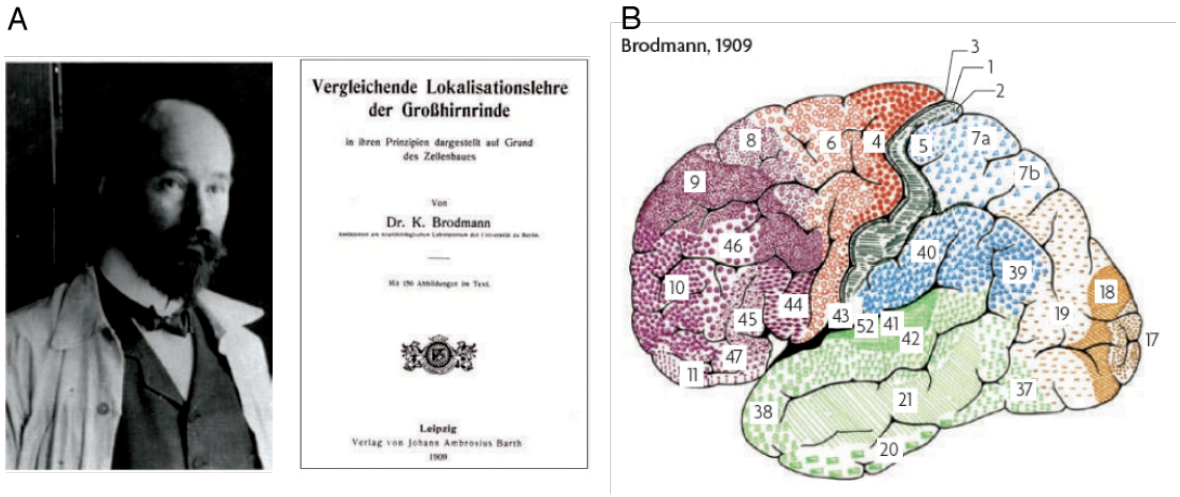


Fig. 1.1 Brodmann's map of the human cortex. A, Korbinian Brodmann and the cover page of Brodmann's seminal monograph from 1909. B, Lateral view of the cortical map of Brodmann. Areas 3, 1 and 2 are the primary somatosensory cortex. Images are adapted and modified from (Zilles and Amunts 2010).

Brodmann's map is one of the most influential works illustrating the cortical cytoarchitectonic organisation of neurons in the human brain (see Fig. 1.1). In Brodmann's map, the cerebral cortex is segregated into 43 cortical areas belonging to 11 regions. Each of these areas is characterised by a particular cytoarchitecture (Zilles and Amunts 2010). Many of the areas Brodmann defined solely on their neuronal organisation have since been correlated closely to diverse cortical functions. For example, Brodmann areas 3, 1 and 2 are the primary somatosensory cortex (S1); area 4 is the primary motor cortex; area 17 is the primary visual cortex; and areas 41 and 42 correspond closely to primary auditory cortex. Due to many limitations in studying the human brain itself and the

similarity between the human brain and other mammalian brains, some model systems (*e.g.*, brains from rats, mice, cats and monkeys) have been used extensively in many laboratories.

The neocortex is a multi-layered structure, that usually consists of six horizontally oriented layers between the pial surface and the white matter. In addition, sensory cortices have been demonstrated to be organised in functional, vertically oriented units, the so-called cortical columns (Mountcastle 1957; Hubel and Wiesel 1959; Hubel and Wiesel 1962; Mountcastle 1997). Therefore, cortical layers and columns are two most important concepts for understanding the structure and function of the neocortex of mammalian brain.

1.2 The somatosensory cortex of rodents

In rodents (*e.g.*, rats and mice) the mystacial whiskers are organised in rows and arcs on the snout. Mechanoreceptors at the base on the whisker hairs transduce sensory information, which is first relayed via afferent axons in the trigeminal nerve to different trigeminal relay nuclei in the brainstem, mainly the principal and the spinal nucleus. From there, sensory signals are relayed to the thalamus, and here predominantly to the ventroposterior medial nucleus (VPM) and the posterior medial nucleus (POm). Finally, thalamic afferents arising either from neurons in the VPM or POm project to different cortical laminae in the somatosensory barrel field of the neocortex (Lubke and Feldmeyer 2007) (see Fig. 1.2). Besides the two aforementioned afferent pathways (*i.e.,* the *lemniscal* via VPM and *paralemniscal* via POm pathways) (Ahissar, Sosnik et al. 2000), there is a third pathway called the *extralemniscal* pathway which was only discovered recently (Pierret, Lavallee et al. 2000; Yu, Derdikman et al. 2006). Neurons in the caudal part of the interpolar trigeminal nuclei are clustered into whisker-related barrelettes. They project to the ventrolateral domain of the VPM (VPMvl), where neurons are clustered into the ‘tails’ of barreloids in the dorsomedial section of VPM (VPMdm). The axons of VPMvl neurons project to the septa between

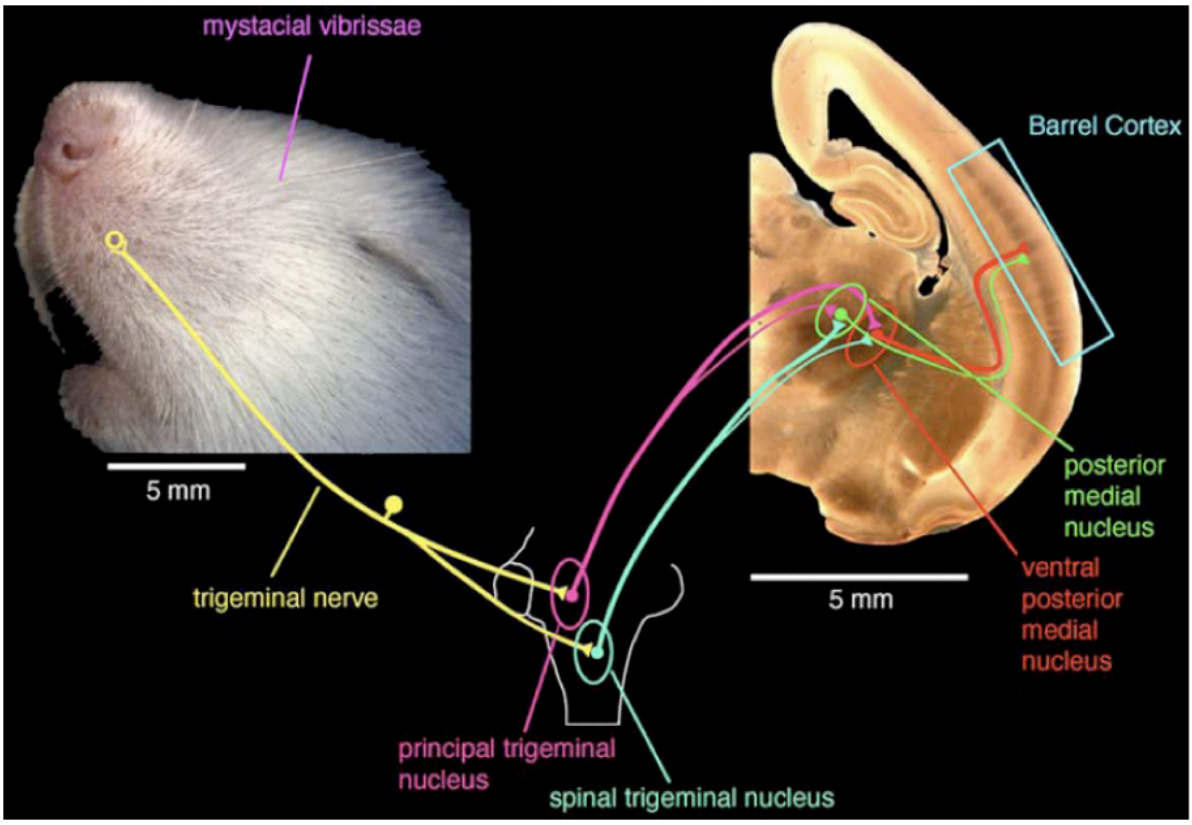


Fig. 1.2 The whisker to barrel cortex pathway. In rodents the mystacial whiskers are organised in rows and arcs on the snout. Mechanoreceptors at the base of the whisker hairs transduce sensory information, which is first relayed via afferent axons in the trigeminal nerve to different trigeminal relay nuclei in the brainstem, mainly the principal and the spinal nucleus. From there, sensory signals are relayed to the thalamus, and here predominantly to the ventroposterior medial nucleus (VPM) and the posterior medial nucleus (POm). Finally, thalamic afferents arising either from neurons in the VPM (red pathway) or POm (green pathway) project to different cortical laminae in the somatosensory barrel field (framed area) of the neocortex. Images are adapted and modified from (Lubke and Feldmeyer 2007).

the barrels of S1 and the secondary somatosensory cortex. The function of each of these three different pathways has not yet been directly tested and hypotheses vary across research groups. One hypothesis is that the paralemniscal neurons in the POm convey information about whisking kinematics, extralemniscal neurons in the VPMvl convey contact timing, and lemniscal neurons in the VPMdm convey detailed whisking and touch information (Diamond, von Heimendahl et al. 2008). Very recently, a fourth pathway, ascending from the principal trigeminal nuclei through the

'heads' of the barreloids in the VPMdm, has been reported (Urbain and Deschenes 2007). However, the cortical target neurons of this pathway have not yet been determined.

The barrel field in the somatosensory cortex (barrel cortex) of rodents is remarkable with respect to the clearly visible somatotopic cortical representation of the sensory periphery (Woolsey and Van der Loos 1970; Welker and Woolsey 1974). Here, each whisker hair and its arrangement on the rodent's snout is represented topographically in the form of a barrel in layer 4 (L4) of the somatosensory cortex. These barrels and their extension into other cortical layers, termed barrel columns, are thought to be the structural correlates of cortical columns. In other sensory cortices (*e.g.*, the primary visual cortex), such a clear structural correlate of a cortical column is not found.

1.3 Excitatory neurons and their microcircuits

The barrel cortex comprises diverse types of excitatory neurons in different layers and columns. Most excitatory neurons are pyramidal cells with triangle-shape somata and a typical apical dendrites pointing towards the pial surface except in granular layer 4 where spiny stellate and star pyramidal neurons dominate. These excitatory neurons are also called principal neurons and they represent the majority of neocortical neurons. Other neurons are inhibitory interneurons, which is a highly heterogeneous population, representing the remaining ~10-20% (Helmstaedter, de Kock et al. 2007; Lubke and Feldmeyer 2007; Ascoli, Alonso-Nanclares et al. 2008).

The microcircuits formed by excitatory neurons through chemical synapses are the backbone of the neocortical network, while inhibitory interneurons participate in sculpturing the information processed by the excitatory microcircuits. There are mainly three parallel neuronal networks in the barrel cortex: the 'canonical' microcircuit receiving lemniscal thalamic input from the VPM predominantly in layer 4 and to a lesser degree in layers 5B and 6A; the intracortical microcircuit

involved in the processing of signals arriving from the paralemniscal pathway (input from POm to L5A pyramidal neurons); and synaptic connections involved in the thalamo-cortical-cortico-thalamic feedback circuit between L4 spiny neurons, L6 pyramidal cells and the VPM (Lubke and Feldmeyer 2007) (see Fig. 1.3).

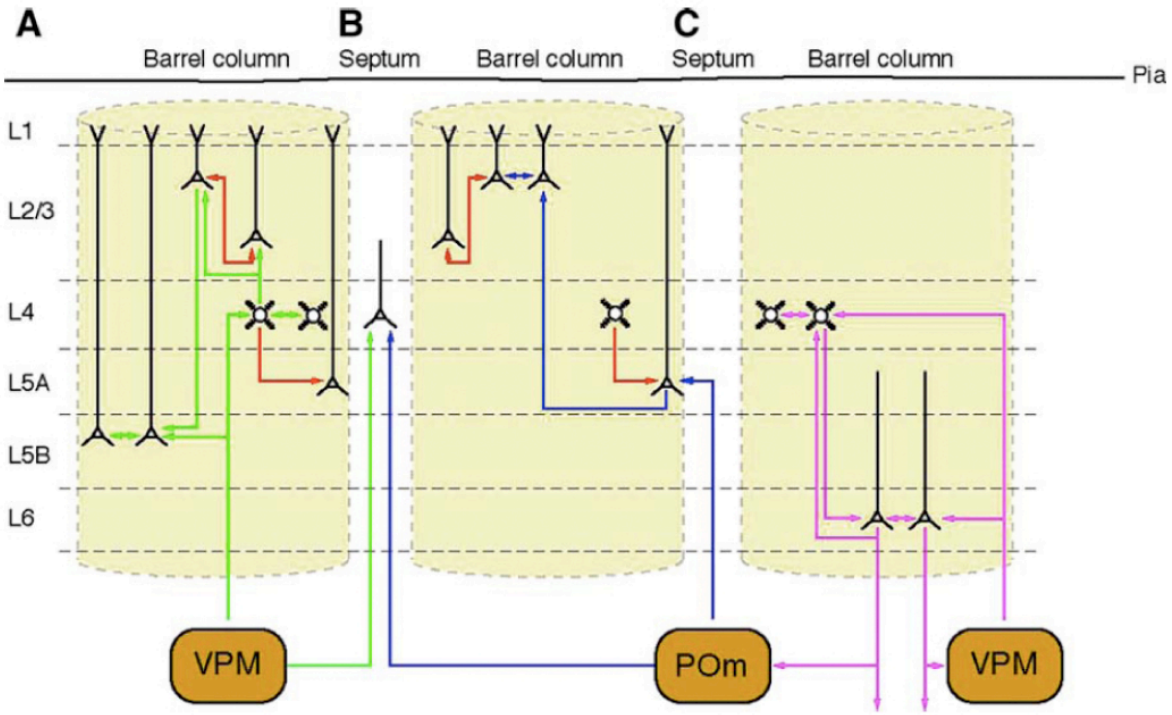


Fig. 1.3 Simplified scheme of parallel cortical microcircuits in the barrel cortex. A, The 'canonical' microcircuit receiving lemniscal thalamic input from the ventroposterior medial nucleus (VPM) predominantly in layer 4 (L4) (and to a less degree in layer 5B). B, Intracortical microcircuit involved in the processing of signals arriving from the paralemniscal pathway (input from the posterior medial thalamic nucleus, POm, to L5A pyramidal neurons). C, Synaptic connections involved in the thalamo-cortical-cortico-thalamic feedback circuit between L4 spiny neurons, L6 pyramidal cells and the VPM. Note that L4 barrel neurons are intrinsic elements of all three microcircuits and that L4 septal neurons receive both VPM and POm input. Colour code: Green, 'canonical' microcircuit, blue, 'paralemniscal' pathway, red, intracortical microcircuits interdigitating 'lemniscal' and 'paralemniscal' microcircuits, violet, thalamo-cortical-cortico-thalamic loop. Images are adapted from (Lubke and Feldmeyer 2007).

Information flow in the 'canonical' microcircuit has been extensively studied: A single whisker deflection will signal primarily through activity in the homologous thalamic barreloid projecting largely to a single barrel in layer 4. The L4 barrel neurons are therefore the first cortical neurons to

be activated. The excitatory L4 neurons send their axons primarily to other neurons in layer 4 and to neurons in layer 2/3 within the same barrel column. The L2/3 neurons lying above a barrel receive their major input from L4 barrel neurons. In addition, they receive substantial intralaminar synaptic input from within layer 2/3. Because the axons of L2/3 pyramidal cells can span large horizontal distances in layer 2/3, these synaptic connections are not necessarily within the same barrel column (Adesnik and Scanziani 2010; Feldmeyer 2010). L2/3 pyramidal cells synapse onto L5 neurons, providing a major route for excitation of the infragranular layers. Then L5 pyramidal cells themselves form recurrent synaptic connections and send axons to other cortical and subcortical regions. Finally, L6 neurons receive synaptic input from layer 5 and within layer 6 itself and send interlaminar synaptic output to L4 neurons (Gilbert and Wiesel 1979; Douglas and Martin 2004). The two microcircuits, *i.e.,* paralemniscal and thalamo-cortical-cortico-thalamic microcircuits, are less well characterised and need to be further studied.

1.4 Previous related studies

It has been shown previously that, L4 spiny neurons in the rat barrel cortex establish synaptic connections mainly with other spiny neurons in layer 4 (Feldmeyer, Egger et al. 1999) or pyramidal cells in layer 2/3 (Feldmeyer, Lubke et al. 2002) and layer 5A (Feldmeyer, Roth et al. 2005), whereas L6A pyramidal cells receive synaptic input mainly from other L6A and L5B pyramidal cells (Beierlein and Connors 2002) (see Fig. 1.4). Monosynaptic L4-to-L6 connections were rarely found: only one pair in cat visual cortex (Stratford, Tarczy-Hornoch et al. 1996; Tarczy-Hornoch, Martin et al. 1999) and only three pairs in mouse barrel cortex (Lefort, Tomm et al. 2009) have been observed and their electrophysiological and especially morphological properties have not been well documented. In addition to paired intracellular recording results, indirect evidence for the existence of L4-to-L6 connections were supplied by other experimental approaches: Data from multi-electrode array measurements in the rat barrel cortex demonstrated the existence of an excitatory

L6-L4-L6 loop (Wirth and Luscher 2004). *In vivo* recordings from neurons in layer 6 of rat auditory cortex suggested that L6 neurons might receive excitatory input from L4 neurons (Zhou, Liu et al. 2010). Furthermore, in monkey and rat visual cortex, photostimulation results showed different sources of excitatory synaptic input to L6 neurons including a sparse input from layer 4 (Briggs and Callaway 2001; Zarrinpar and Callaway 2006). Very recently, a similar input pattern from layer 4 to layer 6 in rat barrel cortex was also discovered by means of laser scanning photostimulation (Hooks, Hires et al. 2011).

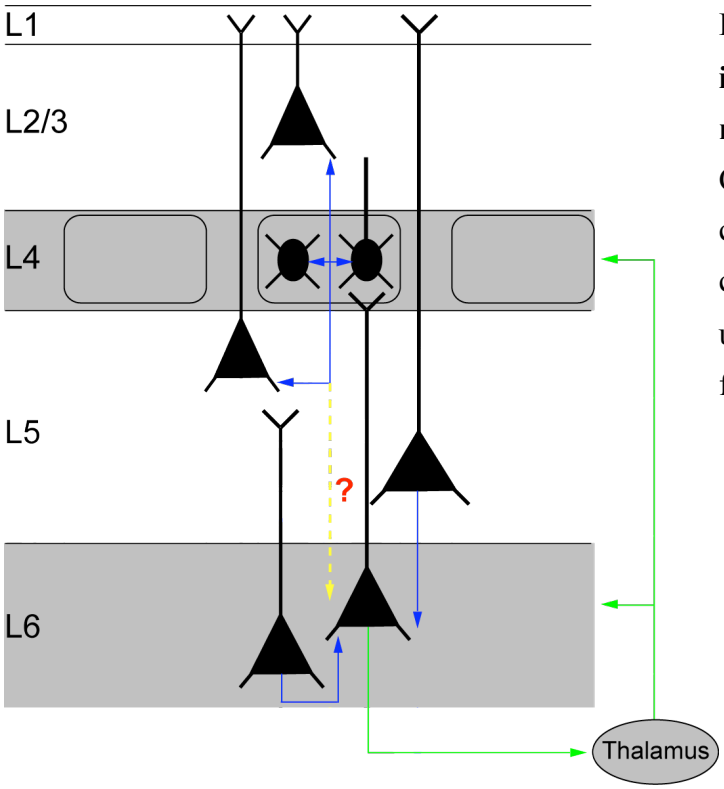


Fig. 1.4 Brief summary of synaptic input and output patterns of two main thalamorecipient layers 4 and 6. Colour code: Blue, intracortical connections, green, thalamocortical or corticothalamic connections, yellow, unidentified intracortical connections from layer 4 to layer 6.

1.5 Aims of this study

In the primary sensory cortices of mammals, layer 4 and upper layer 6 are the main recipient layers of VPM projections from the thalamus. In addition, layer 6 provides direct projections back to both VPM and POm of the thalamus. Thus it forms a thalamo-cortical-cortico-thalamic feedback circuit as described above. To better understand the role of the corticocortical unit in this feedback circuit, we studied the anatomical and functional properties of interlaminar excitatory synaptic connections

from layer 4 to layer 6A in the rat barrel cortex by making dual whole-cell recordings with simultaneous dye injection from L4 spiny neurons and L6A pyramidal cells in acute brain slices. As a comparison, we studied the characteristics of intralaminar excitatory synaptic connections within layer 4 and layer 6A using paired intracellular recordings.

2 Materials and Methods

2.1 Slice preparation

Wistar rats (18-22 days old) were anaesthetised with isoflurane and decapitated, and oblique coronal slices of somatosensory cortex were cut at 45° to the midline (Chmielowska, Carvell et al. 1989; Finnerty, Roberts et al. 1999) in cold extracellular solution using a vibrating microslicer (MICROM HM 650V, Walldorf, Germany) (see Fig. 2.1). Slices were cut at 350 µm thickness and incubated at room temperature (22-24°C) in an extracellular solution containing 5 mM $MgCl_2$/1 mM $CaCl_2$ to reduce synaptic activity.

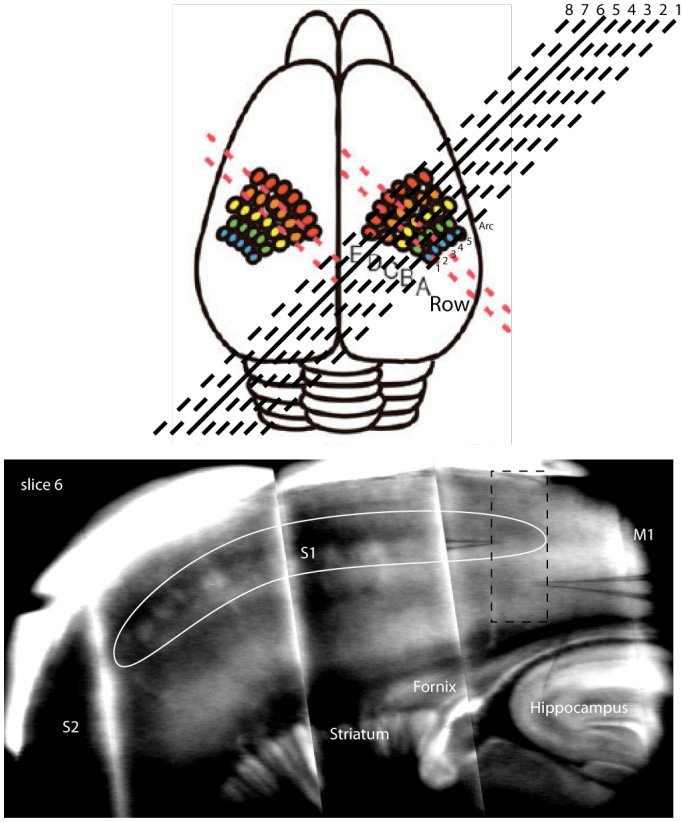


Fig. 2.1 Oblique coronal slice preparations of rat barrel cortex. Top, A schematic of the rat brain with the barrel structure shown from above. Each barrel row is marked by a different colour. A-E and 1-5 indicate barrel rows and arcs, respectively. Black lines with numbers denote the serial sections. Images are adapted and modified from (Ajima and Tanaka 2006). Bottom, Photomicrograph of the 6th slice. S1, primary somatosensory cortex, S2, secondary somatosensory cortex, M1, primary motor cortex. The barrel region of S1 is enclosed by a white contour. The area framed by a dotted black line is shown at higher magnification in Fig. 2.2.

2.2 Solutions

Slices were continuously superfused (perfusion speed ~5 ml/min) with an extracellular solution containing the following (in mM): 125 NaCl, 2.5 KCl, 25 glucose, 25 $NaHCO_3$, 1.25 NaH_2PO_4, 2 $CaCl_2$, and 1 $MgCl_2$ (bubbled with 95% O_2 and 5% CO_2). The composition of the pipette (intracellular) solution was as follows (in mM): 135 K-gluconate, 4 KCl, 10 HEPES, 10 phosphocreatine-Na, and 4 ATP-Mg (adjusted to pH 7.3 with KOH); the osmolarity of the solution

was around 300 mOsm. Biocytin (Sigma, Munich, Germany) at a concentration of 5 mg/ml was routinely added to the internal solution, and cells were filled during recording. For cell-attached stimulation (see below), we used a solution containing the following (in mM): 105 Na-gluconate, 30 NaCl, 10 HEPES, 10 phosphocreatine, 4 ATP-Mg, and 0.3 GTP (adjusted to pH 7.3 with NaOH).

2.3 Patch clamp technique

2.3.1 Cell identification

Slices were placed in the recording chamber under an upright microscope (fitted with 4×, 0.13 numerical aperture and 40×, water immersion, 0.80 numerical aperture objectives; Olympus, Tokyo,

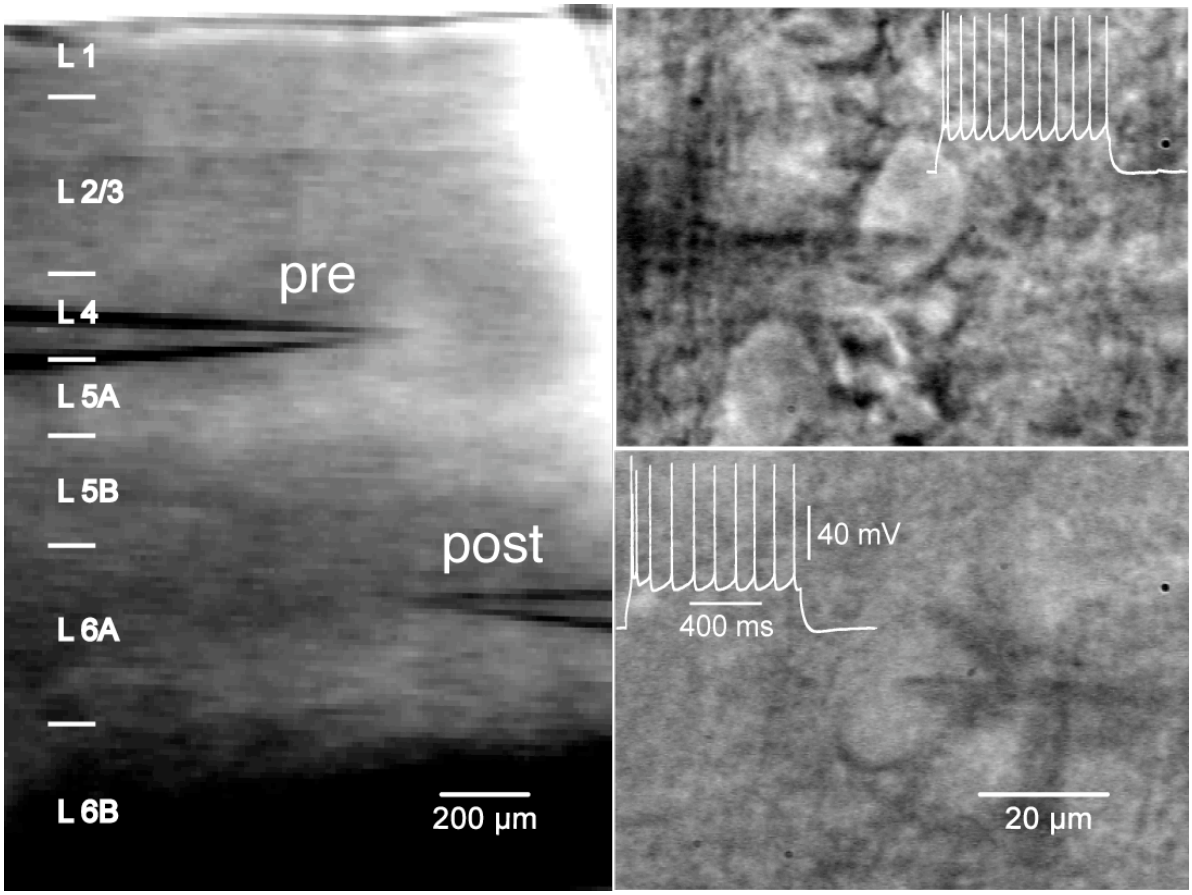


Fig. 2.2 IR-DIC image of a L4-to-L6A connection. Left, Infrared differential interference contrast (IR-DIC) image of the framed area in Fig. 2.1. The pipettes mark the positions of the presynaptic L4 spiny neuron and the postsynaptic L6A pyramidal cell. Right, High-magnification images of the presynaptic L4 spiny neuron (top) and the postsynaptic L6A pyramidal cell (bottom). Insets, the corresponding firing patterns of pre- and postsynaptic neurons.

Japan). The barrel field was visualised at low magnification under bright-field illumination and can be identified in layer 4 as narrow dark stripes with evenly spaced, light "hollows". Barrel structures were present in 6-8 slices. However, the orientation of axonal and dendritic structures of L4 and L6A neurons was optimal only in the last 2-3 slices; these were therefore used for the paired recording experiments. Individual L4 and L6A neurons were identified in the barrel-related column just above the hippocampus at 80× magnification using infrared differential interference contrast (IR-DIC) microscopy (Dodt and Zieglgansberger 1990; Stuart, Dodt et al. 1993). Furthermore, the regular firing pattern with some adaptation is also a good criterion for identifying the excitatory neurons by its electrophysiological characteristics (Connors and Gutnick 1990) (see Fig. 2.2).

2.3.2 Electrophysiological recordings

Whole-cell voltage recordings from postsynaptic neurons were made using patch pipettes of ~4-8 MΩ resistance pulled of thick borosilicate glass capillaries (outer diameter, 2.0 mm; inner diameter 1.0 mm). After patching the postsynaptic L6A pyramidal cell, connections were searched using extracellular "loose-seal" stimulation in the cortical barrel (layer 4) directly above the pyramidal cell, as described previously (Feldmeyer, Egger et al. 1999; Feldmeyer, Lubke et al. 2002; Feldmeyer, Roth et al. 2005; Feldmeyer, Lubke et al. 2006). When an action potential (AP) was evoked by loose-seal stimulation, this was visible as a small deflection on the voltage trace. When the AP resulted in an excitatory postsynaptic potential (EPSP) in the postsynaptic L6A pyramidal cell at short latency (*i.e.,* within 10 ms), the "searching" pipette was withdrawn. The presynaptic cell was then repatched with a new recording pipette (5-9 MΩ) filled with biocytin-containing intracellular solution, and APs were elicited in the whole-cell (current-clamp) mode. Somatic whole-cell recordings were performed at 32-33°C. Signals were amplified using an EPC10-triple patch clamp amplifier (HEKA Elektronik, Lambrecht, Germany), filtered at 2.9 kHz, and sampled at 10 kHz.

2.3.3 Synaptic pharmacology

In some experiments aimed at determining the size of the α-amino-3-hydroxy-5-methyl-4-isoxazolepropionic acid (AMPA) or N-Methyl-D-Aspartate (NMDA) component of the EPSP, 10 μM 6-cyano-7-nitroquinoxaline-2,3-dione (CNQX) or 50 μM (2R)-amino-5-phosphonovaleric acid (AP5) was added in the extracellular solution, respectively. For control conditions, 10-20 sweeps were recorded. Then, after adding the drugs (CNQX or AP5) to the extracellular solution, consecutive sweeps were recorded until the EPSP amplitude became stable. Last, at the start of washing in the standard external solution, as many as possible EPSPs were recorded until a (partial) wash-out of the drug was achieved.

2.4 Electrophysiological analysis

2.4.1 Passive properties of postsynaptic neurons

The resting membrane potential was measured immediately after establishing the whole-cell recording configuration. The time constant of the membrane was calculated as the average value of individual time constant obtained by fitting a single exponential function to the membrane potential deflection in response to current injection from -50 to 50 pA with 10 pA step (0 pA was not included). The input resistance was calculated as the slope of the linear fit to the current-voltage relationship for the same currents as for time constant calculation; transient membrane potential values before some channels (*e.g.*, HCN channels) open were used.

2.4.2 Synaptic physiology

Acquired data were stored on the hard disk of a Macintosh computer for off-line analysis using Igor (WaveMetrics, Lake Oswego, OR). EPSP amplitude, latency and kinetics were determined as described previously (Feldmeyer, Egger et al. 1999; Feldmeyer, Lubke et al. 2002; Feldmeyer, Roth et al. 2005; Feldmeyer, Lubke et al. 2006). All sweeps were aligned to their corresponding

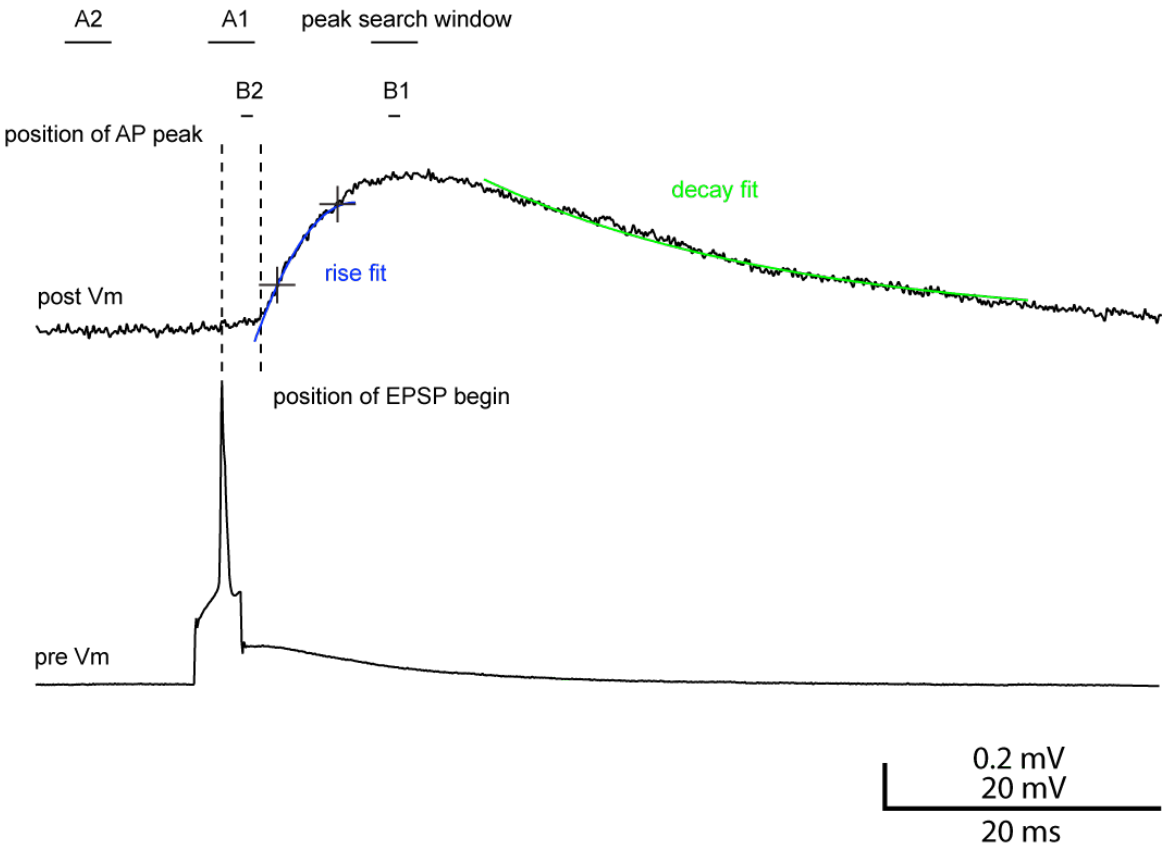


Fig. 2.3 Analysis of synaptic characteristics (amplitude, 20-80% rise time, latency and decay time constant). A single presynaptic action potential (AP) (bottom) in a L4 spiny neuron and the excitatory postsynaptic potential (EPSP) (top) in a L6A pyramidal cell are recorded in a L4-to-L6A connection (V_m, membrane potential). The two pluses mark 20% and 80% of the peak EPSP amplitude between which the rise time is calculated. The latency is defined as the interval between the peak of the presynaptic AP and the onset of the EPSP (dashed vertical lines). The onset of the EPSP is obtained from a quadratic fit (blue line, here, for slow synapses) or a linear fit (for fast synapses) of the EPSP rising phase to the baseline. The EPSP decay is fitted with a single exponential function to the falling phase of the EPSP (green line). The windows selected for the measurement of the noise-contaminated EPSP amplitude and the baseline noise are denoted A1, B1 and A2, B2, respectively.

presynaptic AP peaks and averaged to generate the mean EPSP. Then the EPSP peak amplitude for each individual sweep was determined within a "peak search window" of 5 ms after the presynaptic AP and averaged over 1 ms; subsequently, a baseline potential measured within a window of similar duration just preceding the EPSP was subtracted (for details, see Fig. 2.3 and (Feldmeyer, Egger et al. 1999)). All records were inspected visually. Paired-pulse ratio (PPR) was defined as the 2nd EPSP amplitude divided by the 1st EPSP amplitude of the mean EPSP elicited by paired APs.

Failures were defined as events with amplitudes <1.5× the standard deviation (SD) of the noise within the baseline window. So as not to misclassify small responses as failures, care was taken to verify that the failure average was near zero. The coefficient of variation (CV) was calculated as the SD divided by the mean of EPSP amplitude. For all data, means ± SD were given.

2.5 Morphological reconstructions and analysis

2.5.1 Histological procedures

After recording, slices were fixed at 4°C for at least 24 h in 100 mM PBS, pH 7.4, containing either 4% paraformaldehyde or 1% paraformaldehyde and 2.5% glutaraldehyde. Slices containing biocytin-filled neurons were processed using a modified protocol described previously (Lubke, Egger et al. 2000). Slices were incubated in 0.1% Triton X-100 solution containing avidin-biotinylated horseradish peroxidase (ABC-Elite; Camon, Wiesbaden, Germany); subsequently, they were reacted using 3,3-diaminobenzidine as a chromogen under visual control until the dendritic and axonal arborization was clearly visible (usually after 2-4 min). Slices were then mounted on slides, embedded in Mowiol (Clariant, Sulzbach, Germany), and enclosed with a coverslip. Or slices were further dehydrated and then processed as above but the embedding material was replaced to Eukitt (Marienfeld Lab. Glassware, Lauda-Königshop, Germany).

2.5.2 Morphological reconstructions

Biocytin-labelled pairs of neurons were examined under the light microscope at high magnification to identify putative synaptic contacts. Representative pairs were photographed at low magnification to document the dendritic and axonal arborization. Subsequently, neurons were reconstructed with the aid of Neurolucida software (MicroBrightField, Colchester, VT) using an Olympus Optical (Hamburg, Germany) BX61 microscope at a magnification of 1000× (see Fig. 2.4). The reconstructions provided the basis for the quantitative morphological analysis. To estimate

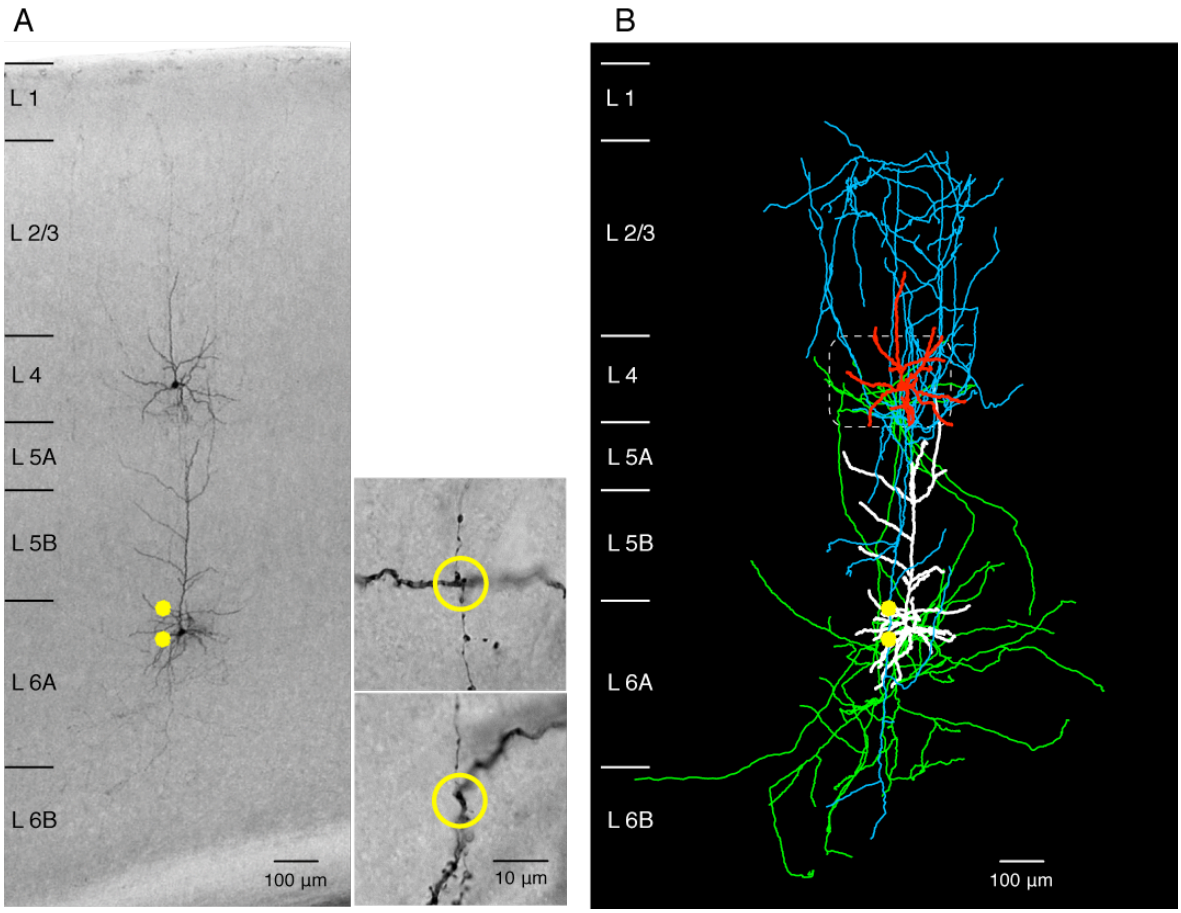


Fig. 2.4 Photomicrographs of a stained L4-to-L6 cell pair, its putative synaptic contacts and Neurolucida reconstructions. A, Left, Half-tone photomicrograph of a biocytin-filled pair between a spiny neuron (here, a star pyramid) in layer 4 and a pyramidal cell in layer 6A. Light-microscopically identified putative synaptic contacts are marked by filled yellow circles. Right, Higher magnification half-tone photomicrographs of two putative synaptic contacts marked by open yellow circles. One putative synaptic contact is located on the proximal apical oblique dendrite and the other on the basal dendrite of the L6A pyramidal cell. B, 2D projection of 3D Neurolucida reconstructions. The axonal arbor (blue) and the somatodendritic arbor (red) of the L4 spiny neuron and the axonal arbor (green) and the somatodendritic arbor (white) of the L6A pyramidal cell are shown. The barrel is indicated by a dashed contour. Light-microscopically identified putative synaptic contacts are marked by filled yellow circles.

shrinkage in the xy-plane, we compared the distance between the two somata of paired recordings in acute state (using the xy coordinate of pre- and postsynaptic neuron somata recorded during the experiment) and after fixation (using the computer reconstruction). Shrinkage factor in the xy-plane was 1.1 ± 2.2% (range 1.4-4.4%, n = 12) when Mowiol was used as embedding medium and 12.9 ± 7.7% (range 5.8-22.6%, n = 6) when Eukitt was used. Corrections for shrinkage in the xy-plane

were performed from pair to pair based on the calculated shrinkage factor for each individual pair. Shrinkage in the z-direction was not corrected due to the inhomogeneity of the shrinkage in the case of Mowiol (Egger, Nevian et al. 2008).

2.5.3 Number and locations of synaptic contacts

Potential synaptic contacts were identified as close apposition of a presynaptic axonal bouton and the postsynaptic dendrite in the same focal plane at a final magnification of 1000× (100× objective and 10× eyepiece). The synapse-to-soma distance was calculated as the path length along the dendrite from the location of synaptic contact to the soma in three-dimensional (3D) space.

2.6 Innervation domain calculations

2.6.1 Axonal and dendritic density maps

2D maps of axonal and dendritic "length density" were constructed using the computerised 3D reconstructions (for details, see (Lubke, Roth et al. 2003)). The length of all axonal and dendritic branches was projected in the 2D plane and measured in a 50 × 50 μm Cartesian grid, yielding a raw density map. To align these maps with respect to the barrel centre, barrel borders were identified in the low power (4× objective) bright-field photomicrographs made from the acute brain slice (Lubke, Egger et al. 2000; Lubke, Roth et al. 2003; Feldmeyer, Roth et al. 2005). Spatial low-pass filtering of these maps was performed by 2D convolution with a Gaussian kernel (σ = 50 μm), and continuous 2D density functions were constructed using bicubic interpolation in Mathematica 4.1 (Wolfram Research, Champaign, IL) (see Fig. 2.5).

2.6.2 Innervation domains

The presynaptic axonal and postsynaptic dendritic length density maps thus obtained were then multiplied to calculate the predicted 'innervation domain' between L4 spiny neurons and L6A

pyramidal cells (Lubke, Roth et al. 2003). Similar spatial low-pass filtering of 'innervation domain' maps were done as above (see Fig. 2.5).

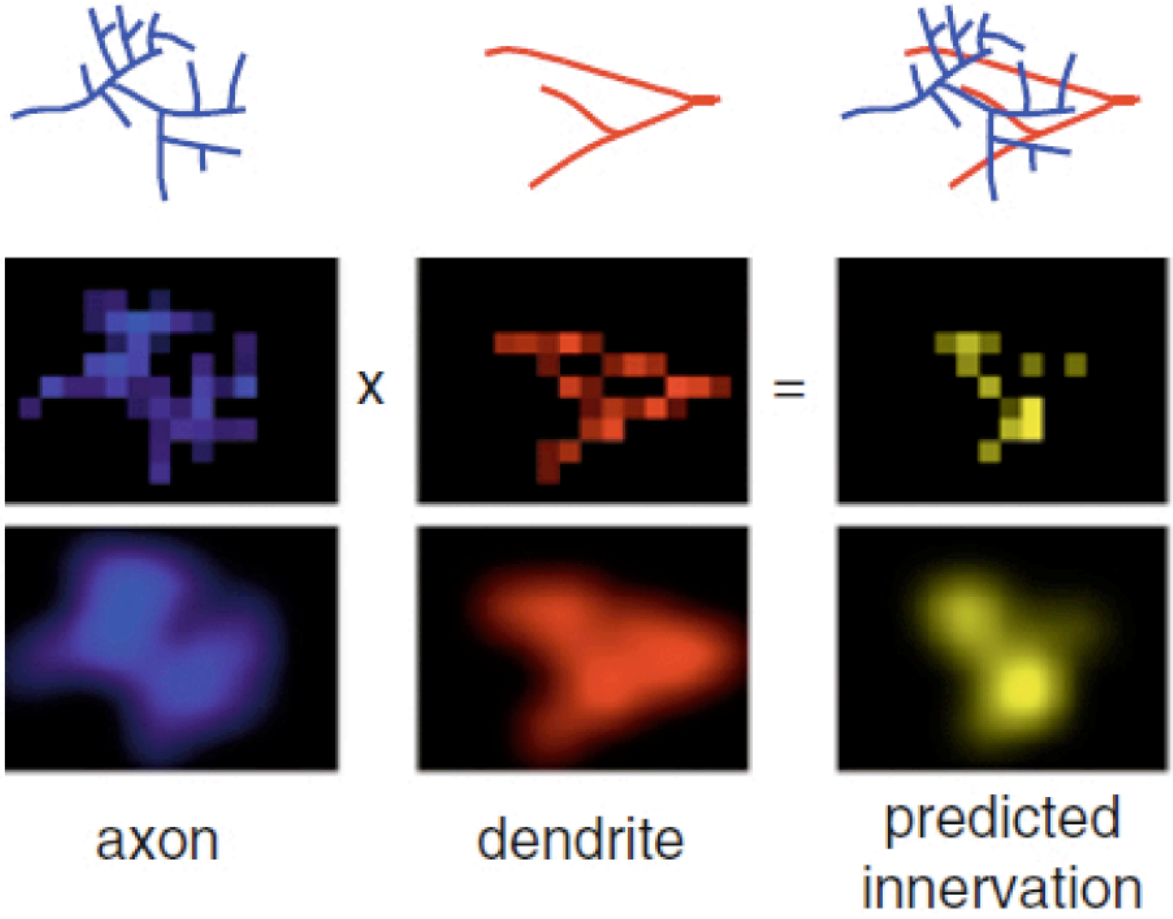


Fig. 2.5 Schematic of how axonal projections can be used to infer synaptic connectivity. Quantification of axo-dendritic overlap interpreted as the probability of synaptic innervation: neurite trees (top row) are converted to neurite path length density maps (middle row), which can be low-pass filtered and interpolated (bottom row). The product of axonal and dendritic length density can be interpreted as the probability of establishing a synaptic contact (predicted innervation probability). Images are adapted and modified from (Helmstaedter and Feldmeyer 2010).

2.7 Neuronal modeling

Modeling was carried out using the NEURON simulation environment (Hines and Carnevale 1997). A 3D reconstruction of a representative L6A pyramidal cell was obtained by the Neurolucida system and its somatodendritic structure was converted to the NEURON format, where a correction for the area of missing dendritic spines was included by adding 0.83 μm^2 surface area per linear micrometer of length to dendritic compartments (Mainen and Sejnowski 1996). A stereotypic axon

was attached to the soma (Mainen, Joerges et al. 1995). Typical conductance types (Na^+, K^+, Ca^{2+}) and their distributions were used (Mainen and Sejnowski 1996). The excitatory synaptic conductance is composed of both AMPA and NMDA components, which were modeled using double exponential functions (Sarid, Bruno et al. 2007).

2.8 Statistical analysis

One-way ANOVA followed by *post hoc* Tukey's test was used in Igor for statistical comparisons of multiple groups. Correlation analysis was performed by calculating Pearson correlation coefficients.

3 Results

3.1 Diverse types of excitatory neurons in L4 and L6A

3.1.1 L4 spiny neurons

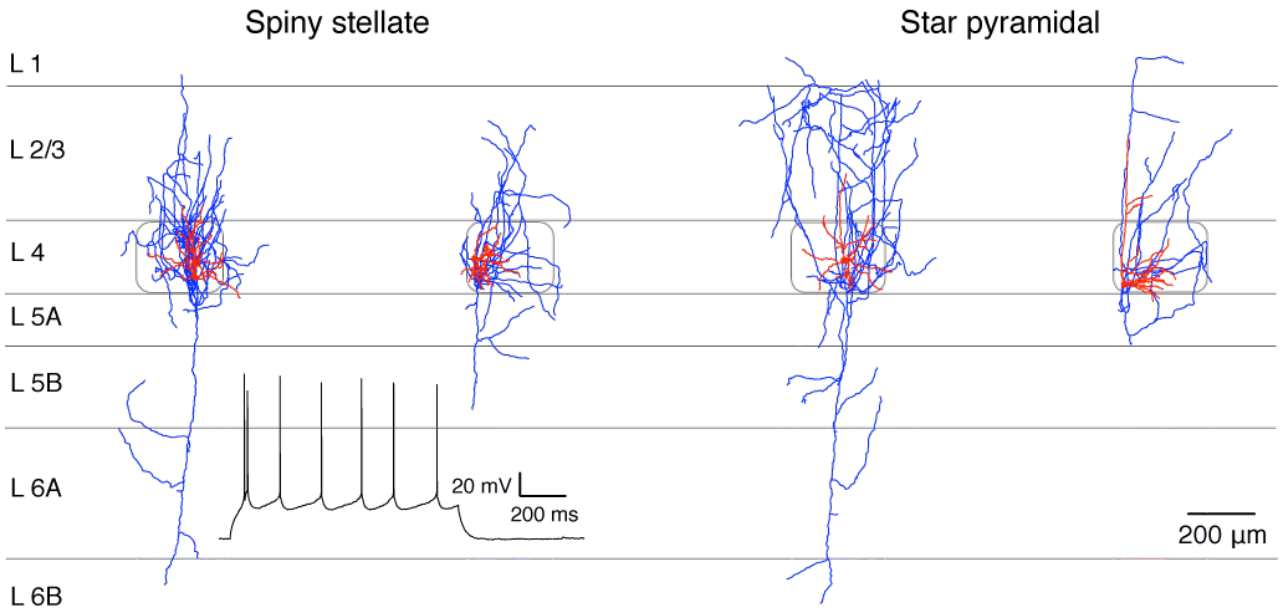


Fig. 3.1 Spiny stellate and star pyramidal neurons in layer 4. Two examples of spiny stellate neurons are shown on the left while two examples of star pyramidal neurons are shown on the right. Somatodendritic and axonal structures are shown in red and blue, respectively. Layer (grey lines) and barrel (grey contours) borders are also shown. Inset, representative firing pattern of L4 spiny neurons.

In L4 barrels, most neurons are excitatory spiny neurons, apart from a fraction of ~10-20% of inhibitory interneurons (Lubke and Feldmeyer 2007). These spiny neurons can be morphologically divided into two categories: spiny stellate (SS) and star pyramidal (SP) neurons ((Feldmeyer, Egger et al. 1999; Lubke, Egger et al. 2000; Egger, Nevian et al. 2008), but see (Staiger, Flagmeyer et al. 2004)). The SS neuron, which has several basal dendrites restricted to the barrel border and no apical dendrite, is the major neuron type. SP cells, in contrast, possess an apical dendrites in addition to their basal dendrites, which project out of the barrel into supragranular layers without forming an elaborate tuft. Furthermore, if the neuron soma is located near the barrel border, the basal dendrites of this neuron are largely confined to a single barrel in layer 4 and often display an asymmetric orientation towards the barrel centre (see Figs. 3.1 and 3.2). The axonal domain of SS

and SP neurons shows a similar asymmetric orientation towards the centre of barrel column and is largely confined to the column in which it resides. The highest density of axonal collaterals is in

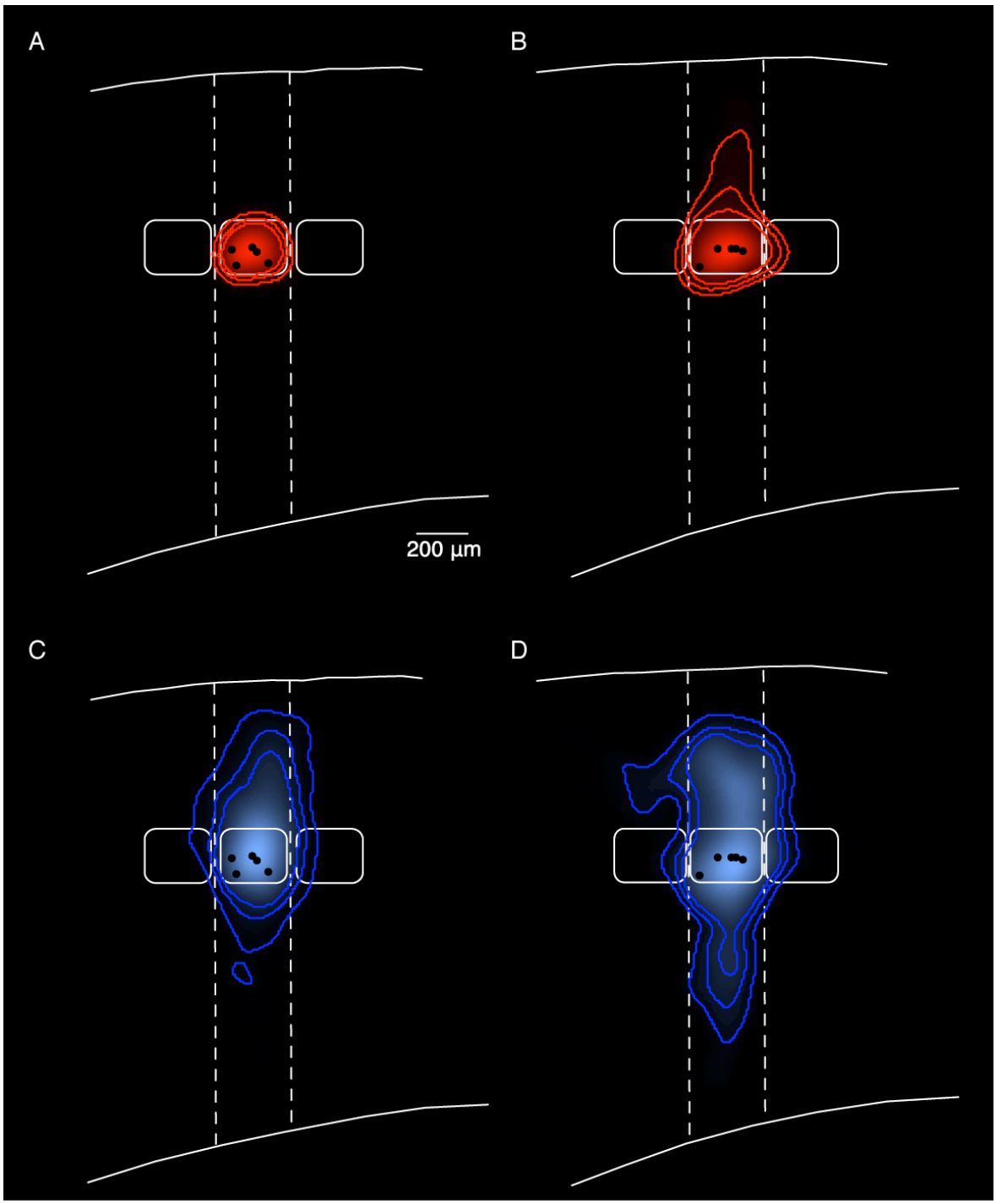


Fig. 3.2 Density maps of L4 spiny neuron dendritic and axonal arbors. Black dots mark neuron somata within the barrel, while dendritic and axonal densities are shown in red and blue, respectively. Red and blue contours show 70-, 80- and 90-percentile of the dendritic and axonal densities, respectively. A, C from five spiny stellate neurons while B, D from five star pyramidal neurons. Two vertical dashed lines mark the boundary of a barrel-related column. Scale bar in A also applies to B, C and D.

layers 4 and 2/3, where the predominant target structures of these neurons are located. The primary axon goes also deep into infragranular layers 5 and 6 but with many fewer collaterals (see Figs. 3.1 and 3.2). No obvious difference in the passive membrane properties and the action potential firing pattern of these two cell types was observed (Feldmeyer, Egger et al. 1999; Cowan and Stricker 2004).

3.1.2 L6A short pyramidal cells

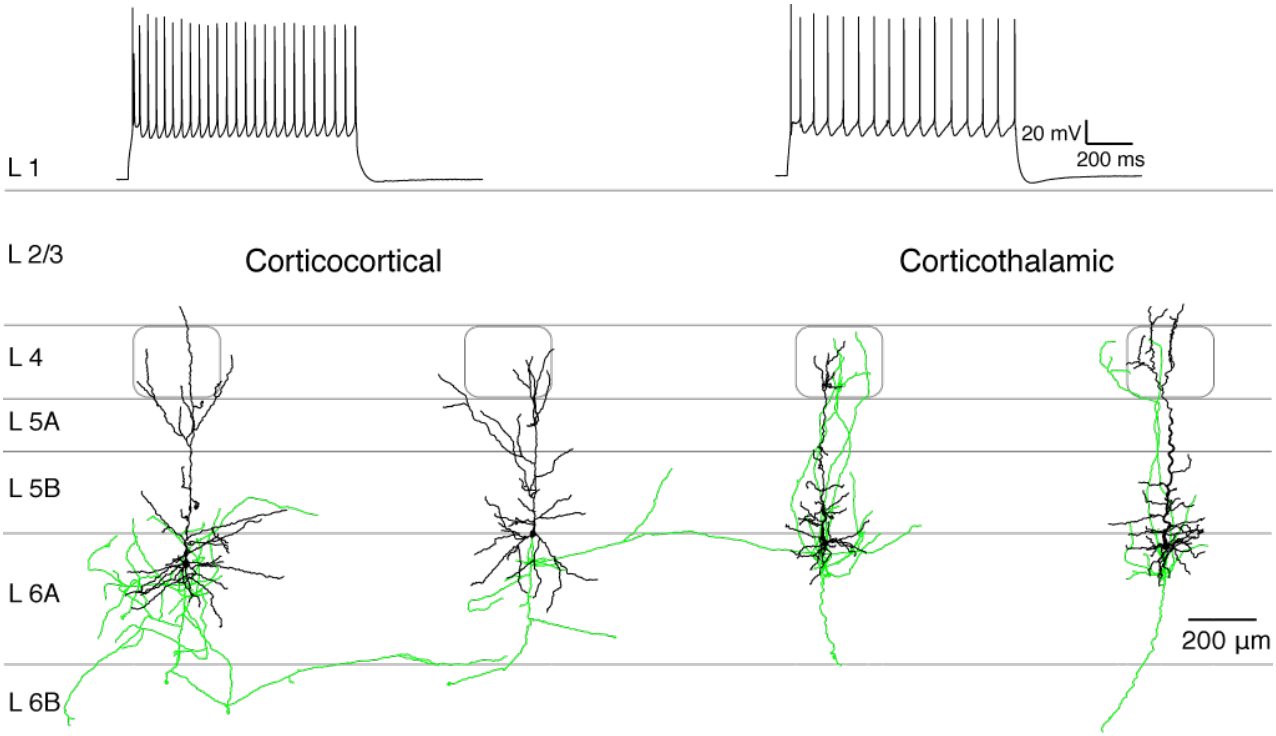


Fig. 3.3 Corticocortical and corticothalamic short pyramidal cells in layer 6A. Two examples of corticocortical short pyramidal cells are shown on the left while two examples of corticothalamic short pyramidal cells on the right. Somatodendritic and axonal structures are shown in black and green, respectively. Layer (grey lines) and barrel (grey contours) borders are also shown. Insets, the representative firing patterns of L6 corticocortical (left) and corticothalamic short pyramidal cells, respectively.

Layer 6A is composed of diverse types of pyramidal and non-pyramidal cells (Zhang and Deschenes 1997; Kumar and Ohana 2008). The majority of L6A excitatory neurons are short pyramidal cells which send a vertically oriented apical dendrite that terminates in layer 3 or layer 4 either forming a slender tuft or several small branches but no clear tuft (see Fig. 3.3), a feature also

reflected in the density maps (see Fig. 3.4). Two distinct populations of short pyramidal cells have been identified on the basis of their axonal projection patterns: the so-called corticocortical (CC)

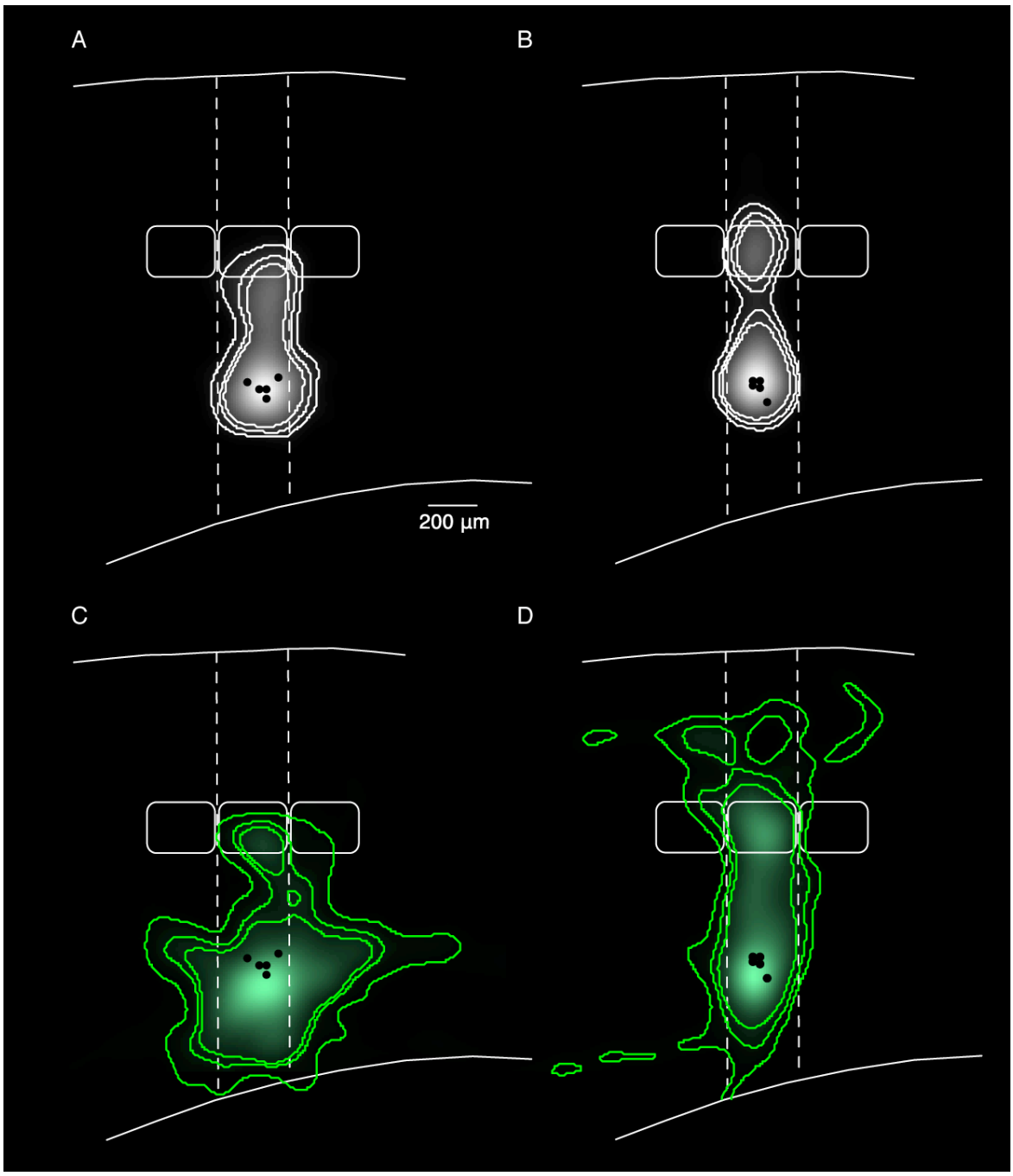


Fig. 3.4 Density maps of L6A short pyramidal cell dendritic and axonal arbors. Black dots mark cell somata in layer 6A, dendritic and axonal densities are shown in white and green, respectively, white and green contours show 70-, 80- and 90-percentile of the dendritic and axonal densities, respectively, for five corticocortical short pyramidal cells (A, C) and for five corticothalamic short pyramidal cells (B, D). Two vertical dashed lines mark the boundary of a barrel-related column. Scale bar in A also applies to B, C and D.

and corticothalamic (CT) neurons (Zhang and Deschenes 1997; Kumar and Ohana 2008). The axon of L6A CC short pyramidal cells forms a dense plexus in layers 5 and 6A and sends a few collaterals into sublamina 6B. A characteristic feature is the existence of a long-range horizontal projection to the secondary somatosensory cortex and/or to the motor cortex that are located exclusively in layer 6 (Zhang and Deschenes 1997). In addition, the axon sends a single fiber to the S1 cortex of the contralateral hemisphere via the corpus callosum (Zhang and Deschenes 1997). In contrast, L6A CT short pyramidal cells display a largely columnar organization of their axon with vertically oriented axonal collaterals that terminate at the layer 4/layer 2/3 border, occasionally giving rise to numerous short collaterals in layer 4 (see Figs. 3.3 and 3.4). These CT neurons can be further subdivided according to their intracortical projection patterns and termination zones: neurons projecting exclusively to the VPM; those projecting both to the VPM and POm; and those projecting either the ventromedial nucleus of the thalamus or to the POm (Zhang and Deschenes 1997). It should be noted that, although our data including the morphological reconstructions and the density maps confirm previous studies (Zhang and Deschenes 1997; Kumar and Ohana 2008), the exact projection types or the cortical and subcortical target regions of L6A pyramidal cells has only been inferred indirectly from the axonal projection pattern. Electrophysiologically, the two types of L6A short pyramidal cells demonstrate distinct firing patterns: CC neurons generally fire a train of spikes with a doublet or triplet at the beginning following the injection of a sustained depolarising current; while CT neurons exhibit a regular spike train with less spike frequency adaption using the same current injection (Kumar and Ohana 2008).

3.1.3 Other L6A excitatory neurons

Except for the typical short pyramidal cells described above, there is a minor population of excitatory neurons in layer 6A with different dendritic structures. For example, tall pyramidal cells show a tall apical dendrite which terminates in layer 1 with a small tuft. This neuron type might be

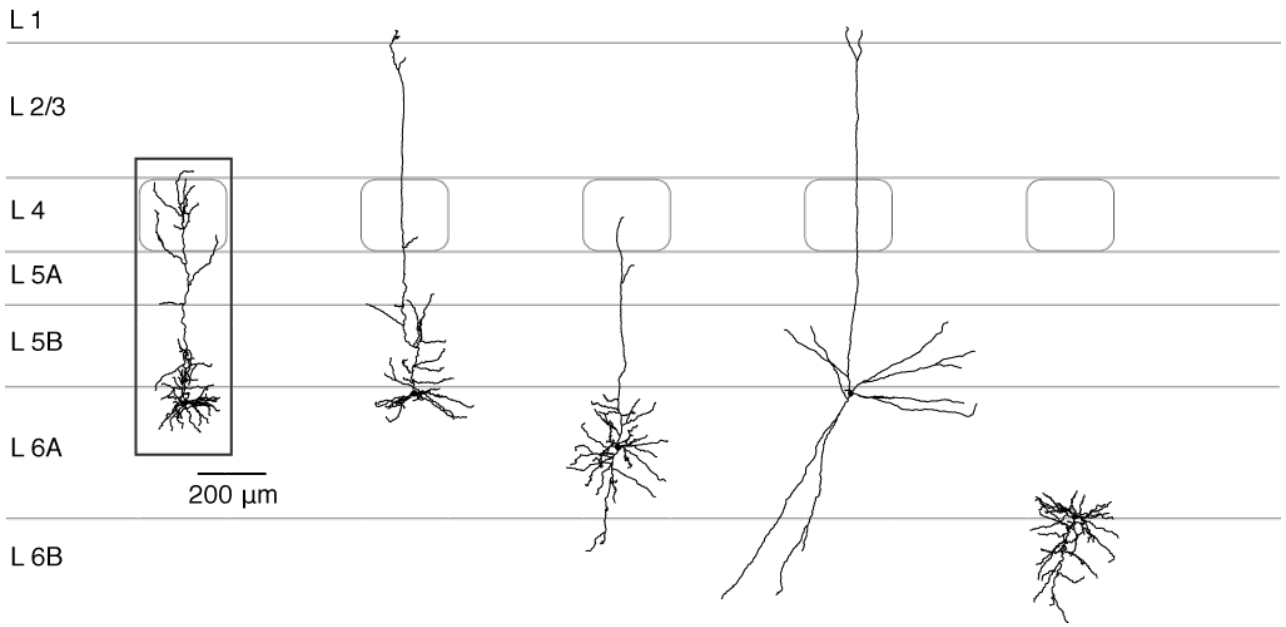


Fig. 3.5 Diverse types of excitatory neurons in layer 6A. Leftmost, a typical short pyramidal cell is shown within the frame. Then from the left to the right, a tall pyramidal, a short spiny bipolar, a claustrum-projecting-like and an inverted pyramidal cell are shown sequentially. Somatodendritic structures are shown in black; axonal structures are not shown. Layer (grey lines) and barrel (grey contours) borders are also shown.

a transitional neuronal type from L5B thick-tufted pyramidal cells to L6A short pyramidal cells. Short spiny bipolar neurons give rise to two primary dendrites one of which is oriented to the pial surface and the other to the white matter. Claustrum-projecting neurons have a very long, slender apical dendrite that reaches layer 1, with little if any branching in layer 4 and at best a meagre apical tuft (Katz 1987). Inverted pyramidal neurons possess a primary dendrite projecting to the white matter instead of to the pial surface as is the case for typical apical dendrites (Mendizabal-Zubiaga, Reblet et al. 2007). Inverted pyramidal neurons are mostly located in the deep layer 6A near the layer 6A/6B border and layer 6B (see Fig. 3.5). All of these atypical L6A excitatory neurons (except for claustrum-projecting neurons) are corticocortical neurons because they send axonal collaterals only to other cortical areas (*e.g.*, the ipsi- and contralateral S1, the secondary somatosensory cortex and the motor cortex) (Zhang and Deschenes 1997). Up to now, layer 6 has not been well studied and its functional role in neocortical information processing needs to be further investigated.

3.2 Monosynaptic L4-L4 and L6A-L6A excitatory connections

3.2.1 L4-L4 pairs

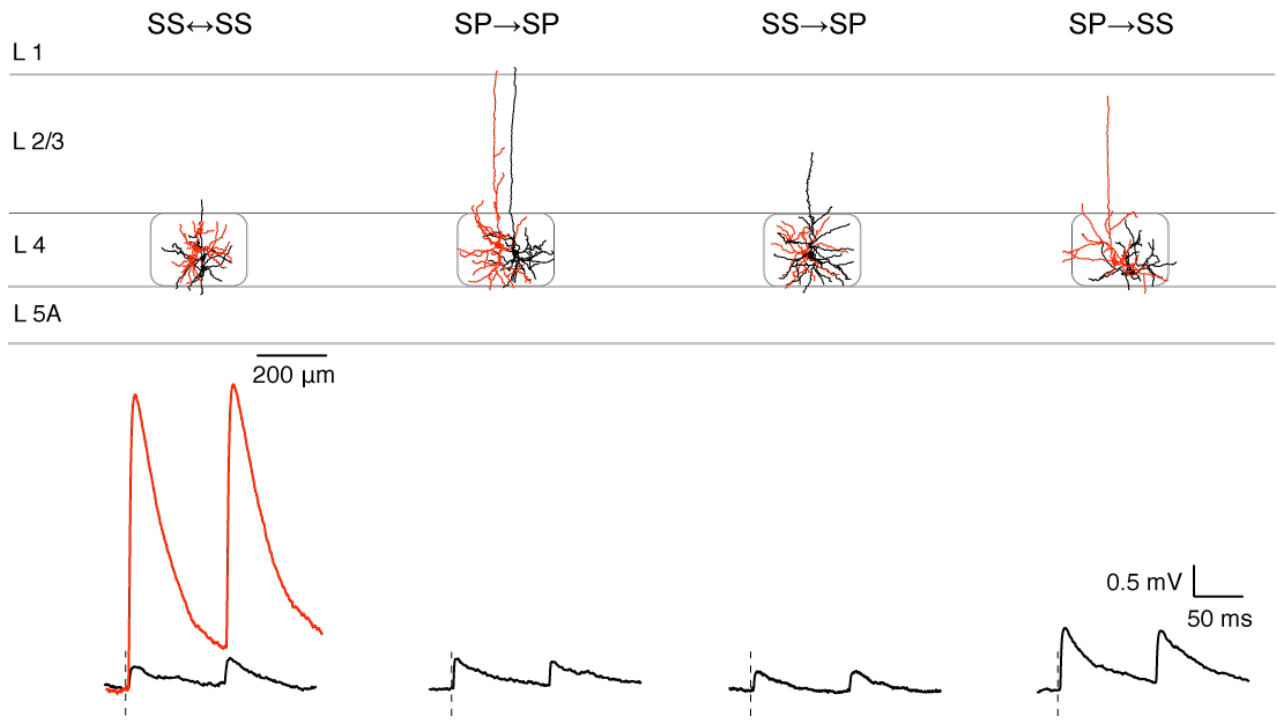


Fig. 3.6 Summary of L4-L4 excitatory connection phenotypes. Top, four L4-L4 excitatory connection phenotypes: spiny stellate-spiny stellate (SS-SS), star pyramid-star pyramid (SP-SP), spiny stellate-star pyramid (SS-SP) and star pyramid-spiny stellate (SP-SS). Pre- and post-somatodendritic structures are shown in red and black, respectively. Layer (grey lines) and barrel (grey contours) borders are also shown. Bottom, the corresponding mean EPSP waveforms. Note that the leftmost pair of neurons is reciprocally coupled.

Excitatory connections between L4 spiny neurons have been extensively studied by paired intracellular recordings in acute brain slices of juvenile and adult animals (Egger, Feldmeyer et al. 1999; Feldmeyer, Egger et al. 1999; Petersen and Sakmann 2000; Petersen 2002; Cowan and Stricker 2004; Bannister and Thomson 2007; Lefort, Tomm et al. 2009). It was shown that the probability of finding a connected pair between two randomly selected L4 spiny neurons is around 30%. We found a similarly high connectivity in our experiments: Out of 40 potential connections tested, ten L4-L4 excitatory connections were found, including two reciprocal ones. Therefore, the connection probability is about 25%. Considering the neuron type in L4 barrels, there are four possible excitatory connection types: spiny stellate-spiny stellate (SS-SS), star pyramid-star

pyramid (SP-SP), spiny stellate-star pyramid (SS-SP), and star pyramid-spiny stellate (SP-SS). All of these connection types were found among the ten recorded L4-L4 connections (see Fig. 3.6). Due

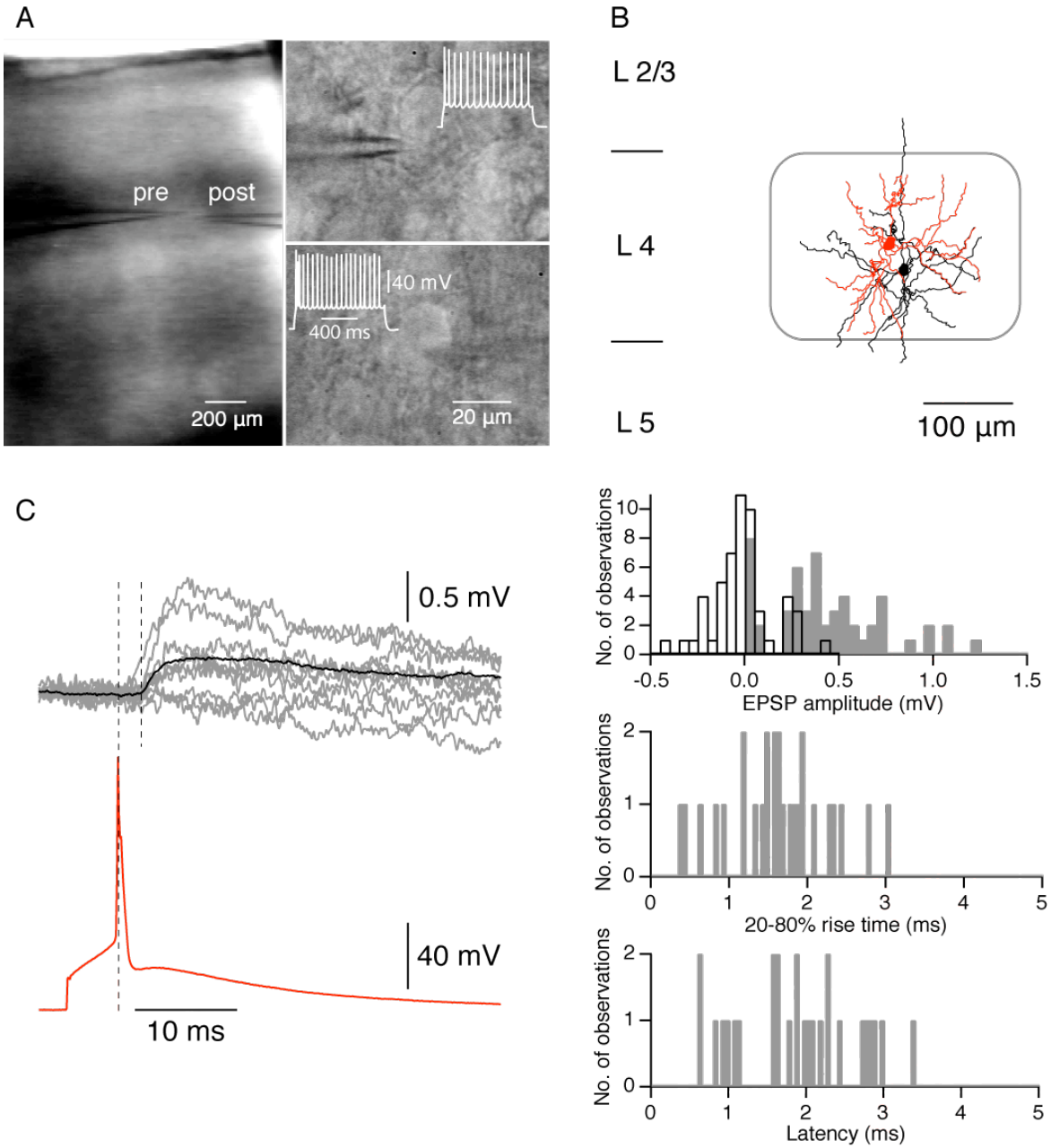


Fig. 3.7 Representative example of a L4-L4 excitatory connection (BC 190309 CD). A, Left, IR-DIC image of the slice. The pipettes mark the positions of the pre- and postsynaptic L4 spiny neurons. Right, High-magnification images of the pre- (top) and postsynaptic (bottom) neurons. Insets, the corresponding firing patterns of pre- and postsynaptic neurons. B, Neurolucida reconstruction of the pair shown in A. Pre- and post-somatodendritic structures are shown in red and black, respectively. C, Left, A presynaptic AP (red trace) and 10 consecutive EPSPs (grey traces) superimposed with the mean EPSP waveform (black trace) are shown. Right, EPSP amplitude (top, black open bars are for noise), 20-80% rise time (middle) and latency (bottom) histograms for this connection.

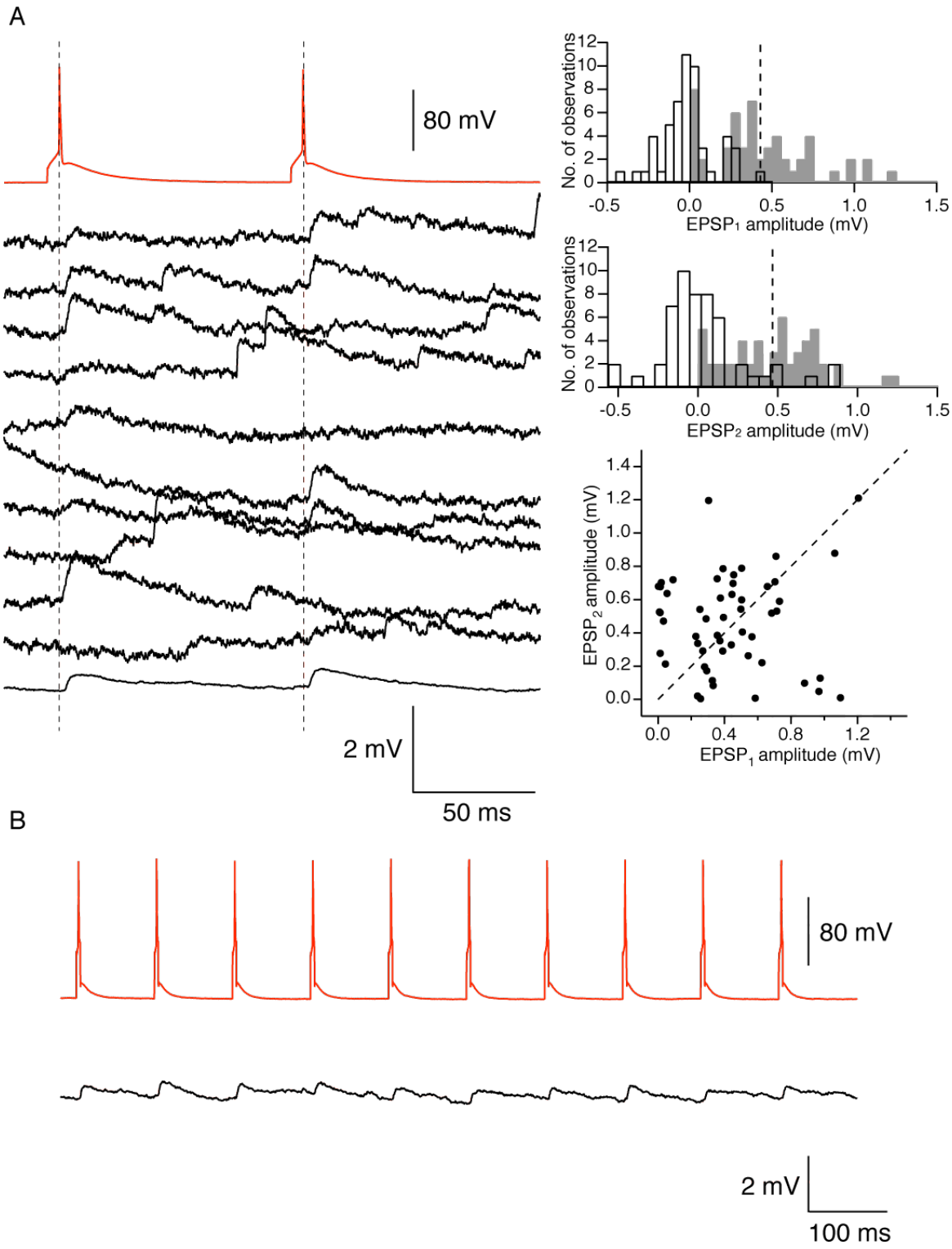


Fig. 3.8 Short-term plasticity of the L4-L4 connection shown in Fig. 3.7. A, Left, Ten consecutive EPSPs (middle) recorded in a postsynaptic L4 spiny neuron elicited by two APs (top) at 100 ms interval in a presynaptic L4 spiny neuron. The mean EPSP waveform is shown at the bottom. Right, Corresponding EPSP amplitude histograms for the first (top, black open bars are for noise) and second (middle) EPSPs. The mean value of EPSP amplitude is denoted by the dashed vertical line. Comparison of the second and first EPSPs is shown at the bottom. B, Train of ten presynaptic APs at 10 Hz (top trace) and the mean EPSP waveform (black trace).

to the small sample size, we could not evaluate the difference among these four types of connections here. In a previous study (Feldmeyer, Egger et al. 1999) it was shown that there was no statistically significant difference in the properties of the different connection types.

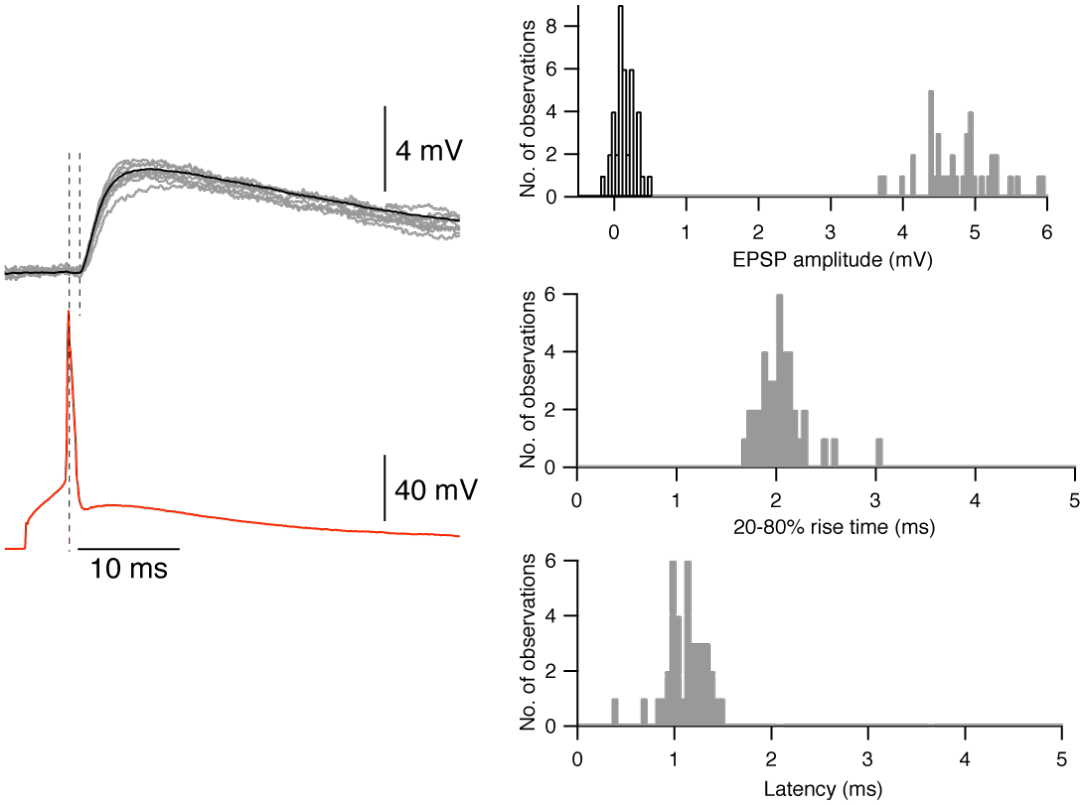


Fig. 3.9 Properties of EPSPs in the other direction of the same pair as in Fig. 3.7. Left, A presynaptic AP (red trace) and 10 consecutive EPSPs (grey traces) superimposed with the mean EPSP waveform (black trace) are shown. Right, EPSP amplitude (top, black open bars are for noise), 20-80% rise time (middle) and latency (bottom) histograms for this connection.

Figs. 3.7-3.10 show a representative example of an excitatory connection between two L4 SS neurons. This pair of neurons was reciprocally coupled. In one direction, it had a weak synapse with small mean EPSP amplitude (0.35 mV) and in the other direction, the synapse was strong with a large mean EPSP amplitude (4.71 mV). The characteristics of the average EPSP waveforms for the weak and the strong synapses are as follows: 20-80% rise time (1.58 *vs.* 2.02 ms) and latency (2.04 *vs.* 1.12 ms). The weak connection showed a weak short-term facilitation with a PPR of 1.12 at an interstimulus interval (ISI) of 100 ms, while the strong connection exhibited short-term depression with a PPR = 0.89. The failure rate and the CV for the weak and strong connections are 22.6% *vs.*

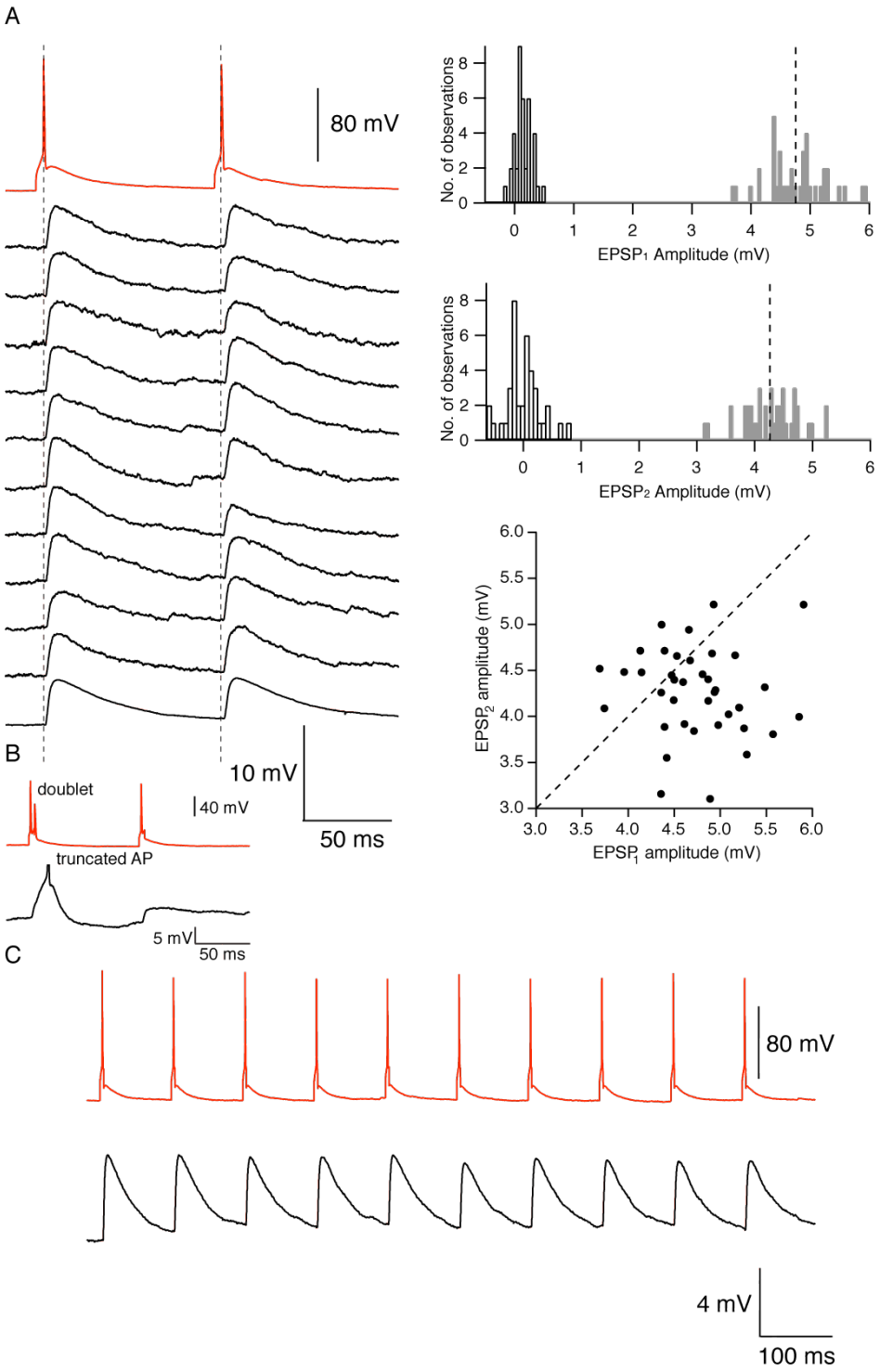


Fig. 3.10 Short-term plasticity of the connection shown in Fig. 3.9. A, Left, Ten consecutive EPSPs (middle) recorded in a postsynaptic L4 spiny neuron elicited by two APs (top) at 100 ms interval in a presynaptic L4 spiny neuron. The mean EPSP waveform is shown at the bottom. Right, Corresponding EPSP amplitude histograms for the first (top, black open bars are for noise) and second (middle) EPSPs. The mean value of EPSP amplitude is denoted by the dashed vertical line. Comparison of the second and first EPSPs is shown at the bottom. B, An example sweep shows that a burst of two closely timed presynaptic APs is enough to induce the firing in the postsynaptic neuron. C, Train of ten presynaptic APs at 10 Hz (top trace) and the mean EPSP waveform (black trace).

0.0% and 0.68 *vs.* 0.11, respectively. For the strong connection, if the postsynaptic neuron was depolarised from the resting membrane potential (V_{rest}) (around -70 mV) to -60 mV by injecting positive current to the soma, the first brief burst of two closely timed presynaptic APs could initiate

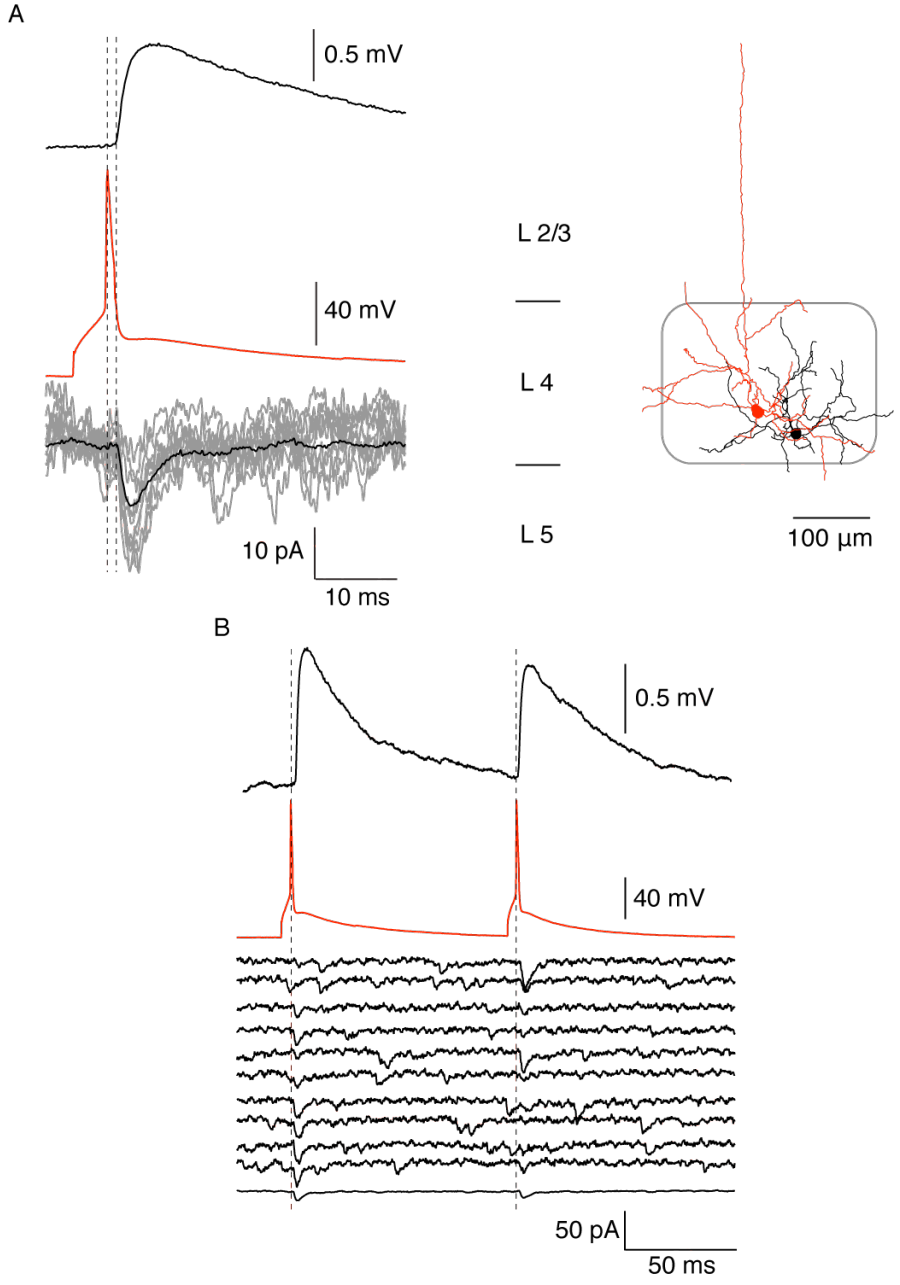


Fig. 3.11 EPSC properties and short-term plasticity of a L4-L4 connection (BC 080609 BC). A, Left, A presynaptic AP (red trace), the mean EPSP waveform (top) and 10 consecutive EPSCs (grey traces) superimposed with the mean EPSC waveform (black trace) are shown. Right, Neurolucida reconstruction of the pair shown on the left. Pre- and post-somatodendritic structures are shown in red and black, respectively B, Ten consecutive EPSCs (middle) recorded in a postsynaptic L4 spiny neuron elicited by two APs (top) at 100 ms interval in a presynaptic L4 spiny neuron. The mean EPSP and EPSC waveforms are shown on the top and at the bottom, respectively.

the firing in the postsynaptic neuron while the second single presynaptic AP failed to do so (see Fig. 3.10b). In younger rats (around 13 days old), even a single presynaptic AP could also initiate postsynaptic firing (Egger, Feldmeyer et al. 1999; Feldmeyer, Egger et al. 1999), which was not observed for other intralaminar excitatory connections (*e.g.*, L2/3-L2/3 (Feldmeyer, Lubke et al. 2006), L5-L5 (Markram, Lubke et al. 1997) and L6-L6 (Beierlein and Connors 2002) connections).

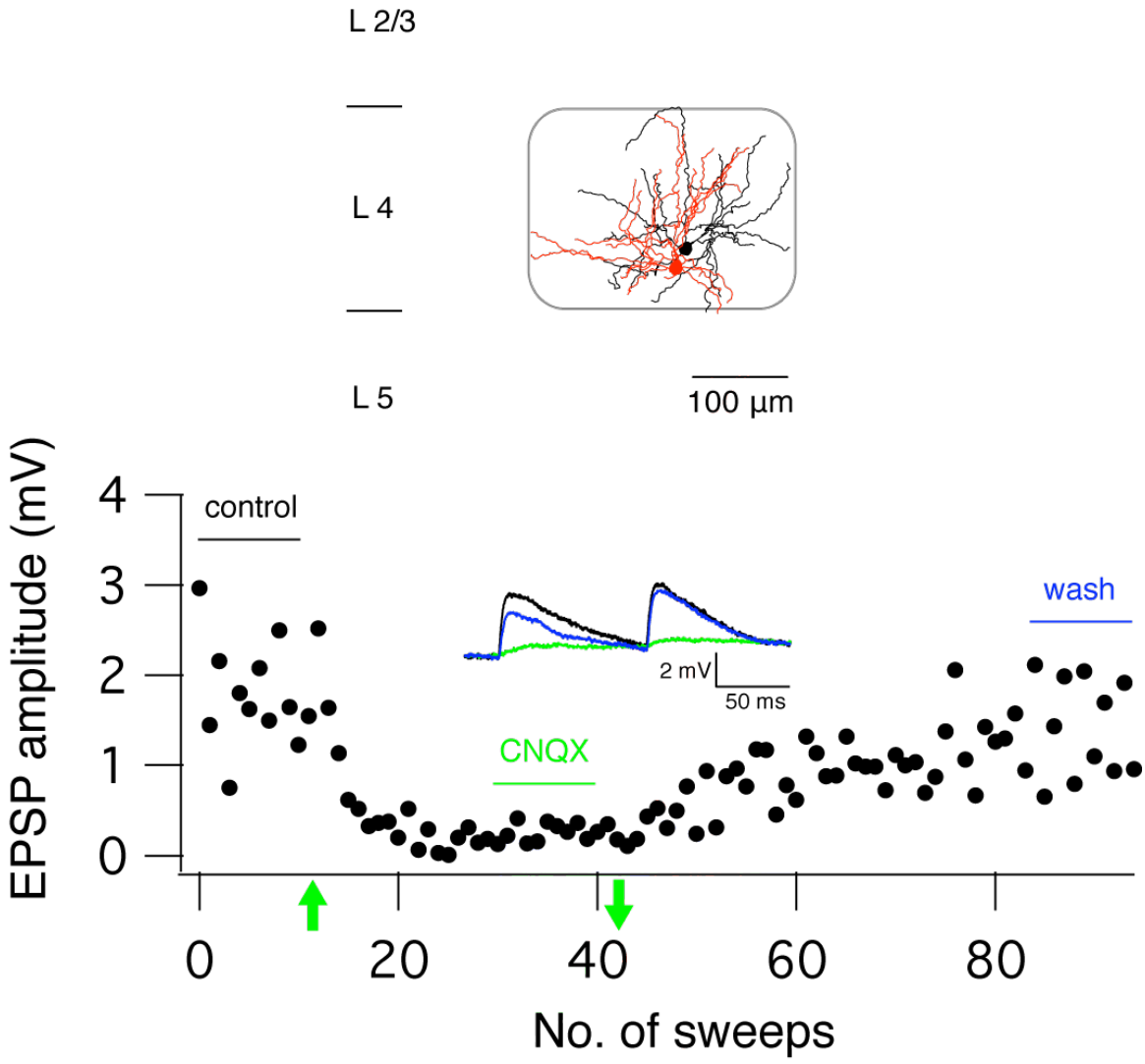


Fig. 3.12 Pharmacological properties of a L4-L4 connection (BC 070510 CD). Top, Neurolucida reconstruction of the pair for pharmacological analysis. Pre- and post-somatodendritic structures are shown in red and black, respectively Bottom, Time course of EPSP amplitude during pharmacological treatment. Inset, mean EPSP waveforms from control (black trace), with 10 µM CNQX (green trace) and after wash (blue trace) are shown superimposed aligned with respect to the peak time of presynaptic APs. Each sweep was collected at 20 s intervals.

For another L4-L4 pair, in addition to EPSPs, excitatory postsynaptic currents (EPSCs) were also measured by clamping the postsynaptic neuron to -70 mV (see Fig. 3.11). The amplitude of the mean EPSP for this pair is 0.98 mV and the 20-80 rise time and latency are 1.30 ms and 0.83 ms, respectively. It showed short-term depression with the PPR = 0.83. The mean EPSC of this pair was characterised by a amplitude of -11.5 pA, a 20-80% rise time of 0.66 ms, a latency of 1.20 ms and a PPR of 0.69.

Fig. 3.12 demonstrates the result of a pharmacological experiment on another L4-L4 connection. The addition of the AMPA receptor antagonist CNQX (10 μM) into the perfusion solution resulted in a partial block of the EPSP. The amplitude under control conditions was 1.80 mV (black curve in Fig. 3.12); in 10 μM CNQX only a small slow component remained (amplitude 0.31 mV, green curve in Fig. 3.12). After wash-out of CNQX, the EPSP partially recovered (amplitude = 1.30 mV, blue curve in Fig. 3.12). Therefore, at the resting potential of postsynaptic neuron, a large portion of the EPSP is mediated by AMPA receptors on the postsynaptic densities in L4-L4 excitatory connections; the remaining component is likely carried by NMDA receptors.

3.2.2 L6A-L6A pairs

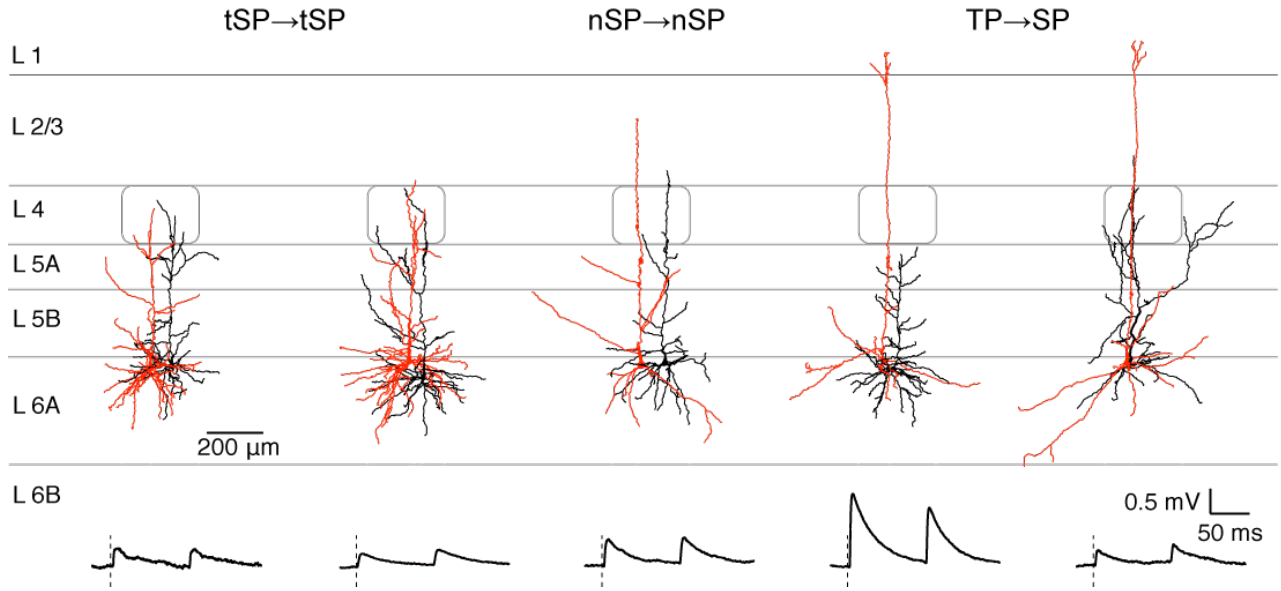


Fig. 3.13 Summary of L6A-L6A excitatory connection phenotypes. Top, three L6A-L6A excitatory connection phenotypes: tufted short pyramid-tufted short pyramid (tSP-tSP), nontufted short pyramid-nontufted short pyramid (nSP-nSP) and tall pyramid-short pyramid (TP-SP). Pre- and post-somatodendritic structures are shown in red and black, respectively. Layer (grey lines) and barrel (grey contours) borders are also shown. Bottom, the corresponding mean EPSP waveforms.

L6A-L6A excitatory connections have not been studied in detail and there are only few reports available describing the properties of L6A-L6A connections (Beierlein and Connors 2002; Mercer, West et al. 2005; West, Mercer et al. 2006). It has been shown that the connectivity between L6A excitatory neurons is relatively low (less than 10%) compared to other intralaminar excitatory connections in the rat barrel cortex, *e.g.*, L4-L4, L5-L5 and L2/3-L2/3 connections. Furthermore, previous sutides demonstrated that L6A CC neurons preferentially send excitatory synapses to other L6A CC and CT neurons while sparsely receiving excitatory connections from other L6A CT neurons (Mercer, West et al. 2005). On the contrary, L6A CT neurons rarely send excitatory synapses to other L6A CC and CT neurons, but prefer to form excitatory connections with inhibitory interneurons in layer 6A (West, Mercer et al. 2006). In contrast to previous studies, we obtained a relatively high connection probability between L6A excitatory neurons: out of 17 potential connections tested, five L6A-L6A excitatory connections were found; there were no

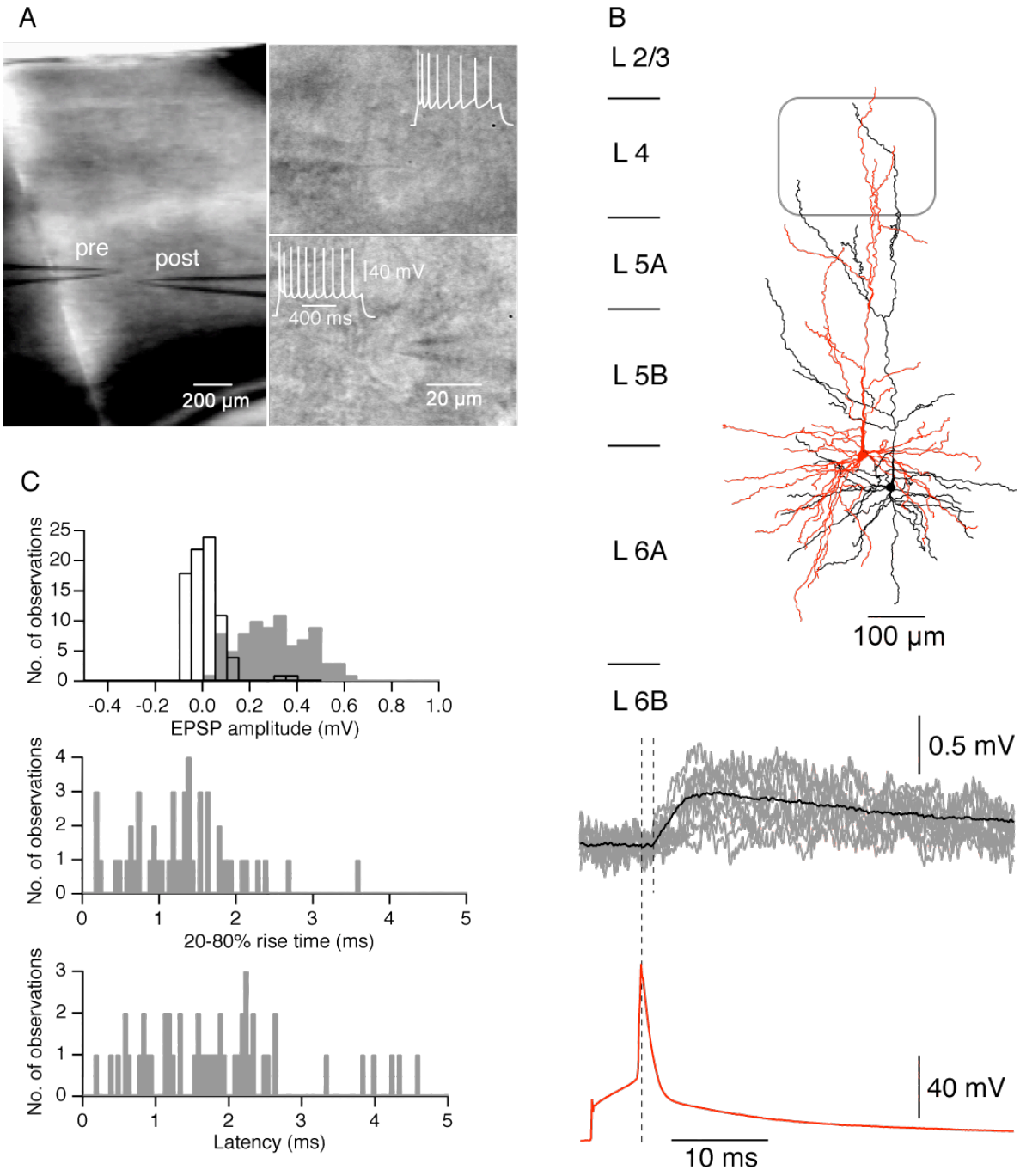


Fig. 3.14 Representative example of a L6A-L6A excitatory connection (BC 151209 AB). A, Left, IR-DIC image of the slice. The pipettes mark the positions of the pre- and postsynaptic L6A pyramidal cells. Right, High-magnification images of the pre- (top) and postsynaptic (bottom) neurons. Insets, the corresponding firing patterns of pre- and postsynaptic neurons. B, Neurolucida reconstruction of the pair shown in A. Pre- and post-somatodendritic structures are shown in red and black, respectively C, Left, EPSP amplitude (top, black open bars are for noise), 20-80% rise time (middle) and latency (bottom) histograms for this connection. Right, A presynaptic AP (red trace) and 10 consecutive EPSPs (grey traces) superimposed with the mean EPSP waveform (black trace) are shown.

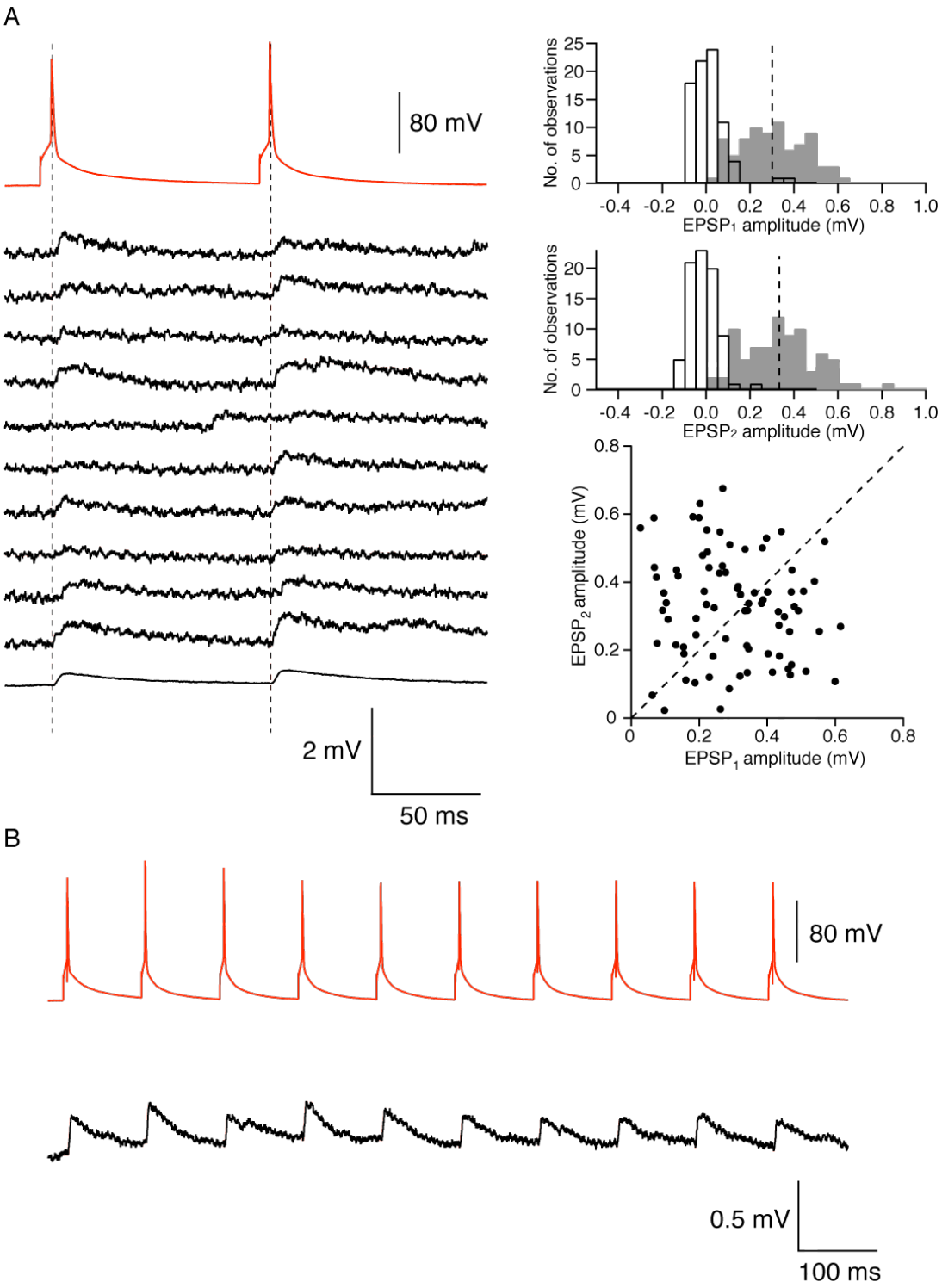


Fig. 3.15 Short-term plasticity of the connection shown in Fig. 3.14. A, Left, Ten consecutive EPSPs (middle) recorded in a postsynaptic L6A pyramidal cell elicited by two APs (top) at 100 ms interval in a presynaptic L6A pyramidal cell. The mean EPSP waveform is shown at the bottom. Right, Corresponding EPSP amplitude histograms for the first (top, black open bars are for noise) and second (middle) EPSPs. The mean value of EPSP amplitude is indicated by the dashed vertical line. Comparison of the second and first EPSPs is shown at the bottom. B, Train of ten presynaptic APs at 10 Hz (top trace) and the mean EPSP waveform (black trace).

reciprocal connections. Therefore, the connectivity ratio is about 29%, a value similar to that for L4-L4 excitatory connection given above. Due to the diversity of excitatory neurons in layer 6A, there are many possible types of L6A-L6A excitatory connections. Here, we found three: tufted short pyramid-tufted short pyramid (tSP-tSP), nontufted short pyramid-nontufted short pyramid (nSP-nSP) and tall pyramid-short pyramid (TP-SP) (see Fig. 3.13). We did not find any significant difference among the three L6A-L6A connection types, which may result from the small sample size for any specific connection type.

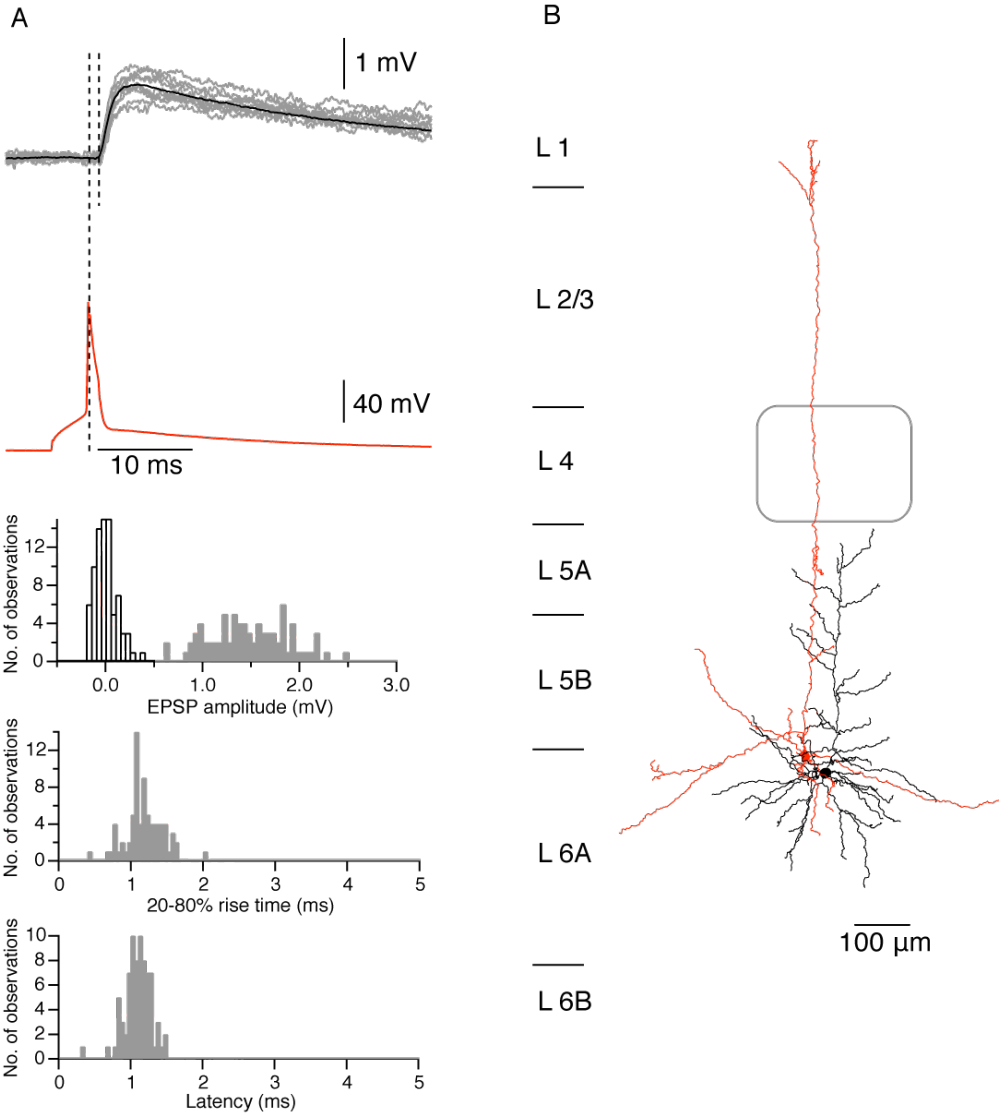


Fig. 3.16 Properties of EPSPs in a L6A-L6A connection (BC 270509 CD). A, Top, A presynaptic AP (red trace) and 10 consecutive EPSPs (grey traces) superimposed with the mean EPSP waveform (black trace) are shown. Bottom, EPSP amplitude (top, black open bars are for noise), 20-80% rise time (middle) and latency (bottom) histograms for this connection. B, Neurolucida reconstruction of the pair shown in A. Pre- and post-somatodendritic structures are shown in red and black, respectively

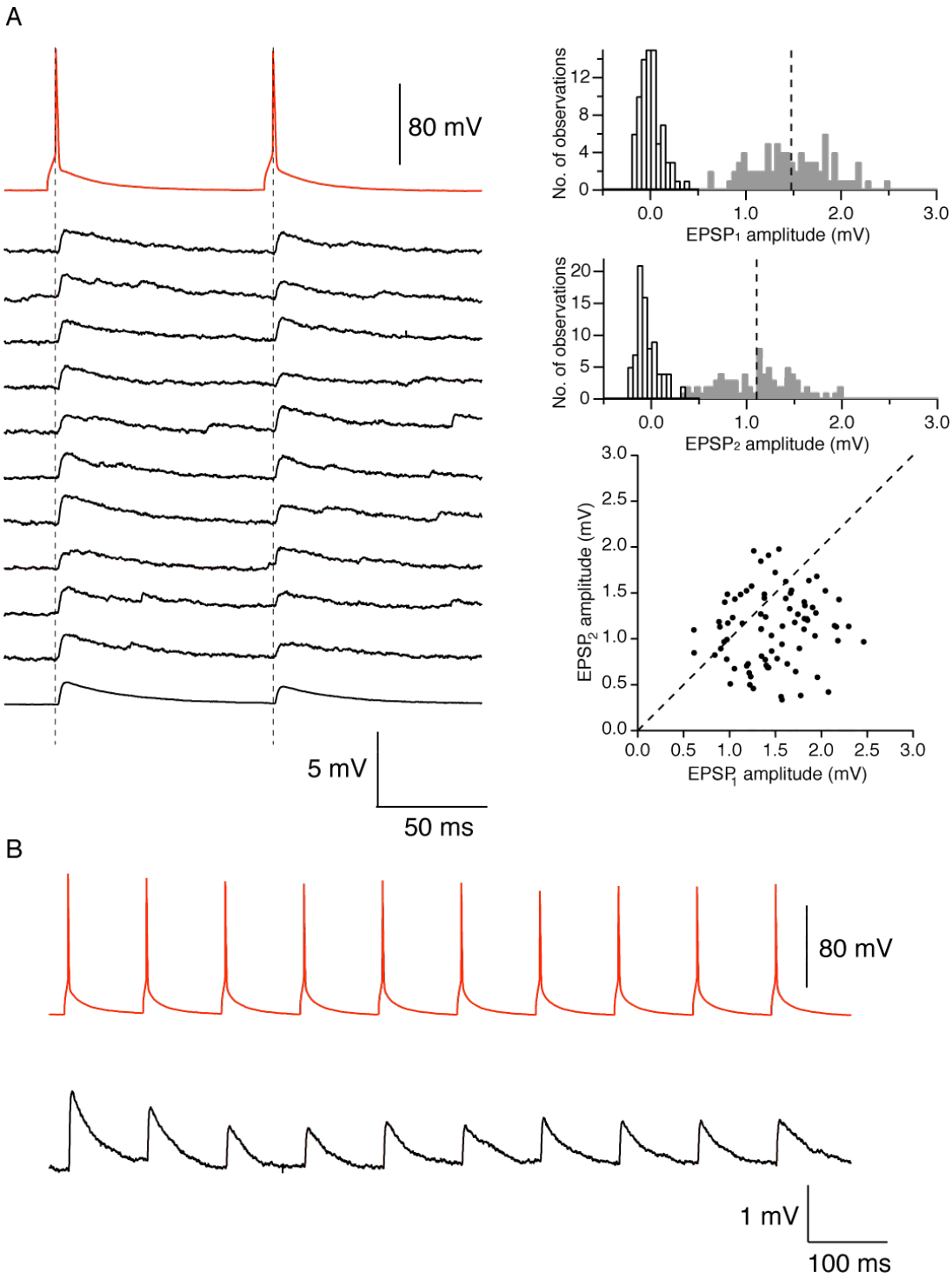


Fig. 3.17 Short-term plasticity of the connection shown in Fig. 3.16. A, Left, Ten consecutive EPSPs (middle) recorded in a postsynaptic L6A pyramidal cell elicited by two APs (top) at 100 ms interval in a presynaptic L6A pyramidal cell. The mean EPSP waveform is shown at the bottom. Right, Corresponding EPSP amplitude histograms for the first (top, black open bars are for noise) and second (middle) EPSPs. The mean value of EPSP amplitude is denoted by the dashed vertical line. Comparison of the second and first EPSPs is shown at the bottom. B, Train of ten presynaptic APs at 10 Hz (top trace) and the mean EPSP waveform (black trace).

A representative example of a L6A-L6A excitatory connection is shown in Figs. 3.14 and 3.15. This pair showed EPSPs with a relatively small mean amplitude (0.27 mV), a 20-80% rise time of 2.27 ms and latency of 1.21 ms. This weak L6A-L6A connection exhibited short-term facilitation with PPR = 1.11 at an ISI of 100 ms. Its failure rate and CV are 13.6% and 0.49, respectively. Figs. 3.16 and 3.17 show the result from another L6A-L6A pair in which a tall pyramid formed an excitatory connection with a short pyramid in layer 6A. The characteristics of the mean EPSP in this pair are as follows: amplitude (1.46 mV), 20-80% rise time (1.14 ms) and latency (1.14 ms). This strong connection demonstrated short-term depression with PPR = 0.74. In the same pair, EPSCs were also recorded at -70 mV under voltage clamp (see Fig. 3.18). The mean EPSC has an amplitude of -27.7 pA, a 20-80% rise time of 0.86 ms, a latency of 1.28 ms and a PPR of 0.70.

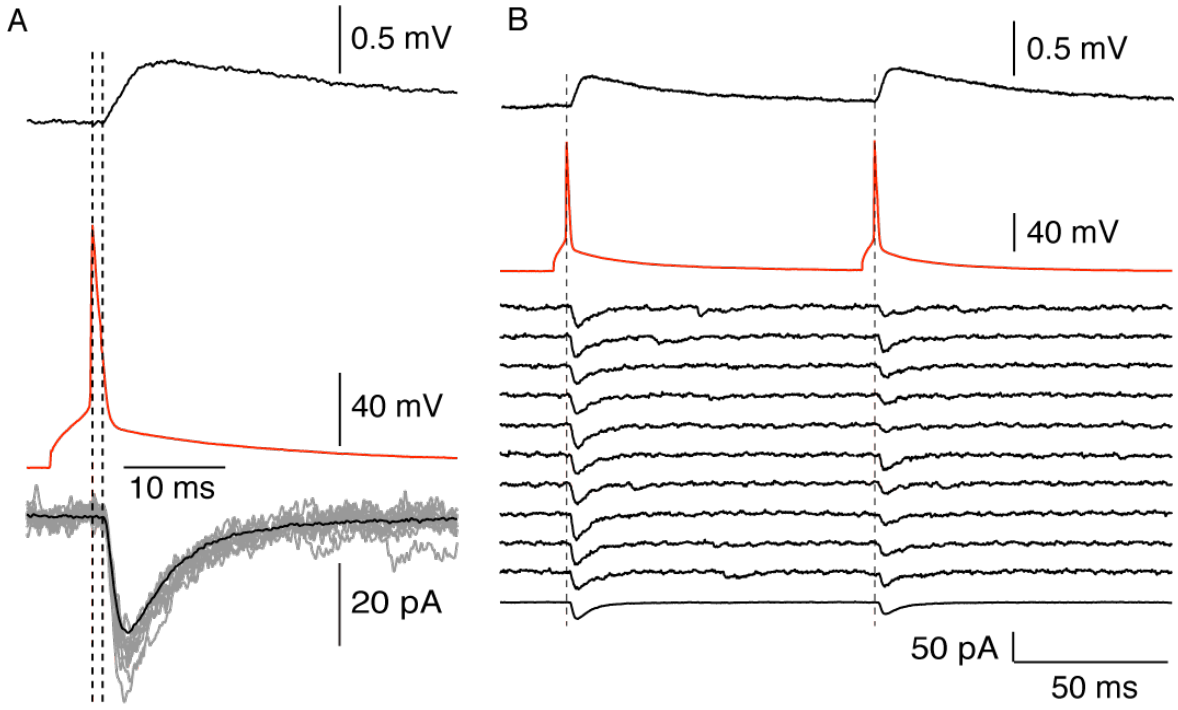


Fig. 3.18 EPSC properties and short-term plasticity of the connection shown in Fig. 3.16. A, Left, a presynaptic AP (red trace), the mean EPSP waveform (top) and 10 consecutive EPSCs (grey traces) superimposed with the mean EPSC waveform (black trace) are shown. B, Ten consecutive EPSCs (middle) recorded in a postsynaptic L6A pyramidal cell elicited by two APs (top) at 100 ms interval in a presynaptic L6A pyramidal cell. The mean EPSP and EPSC waveforms are shown at the top and at the bottom, respectively.

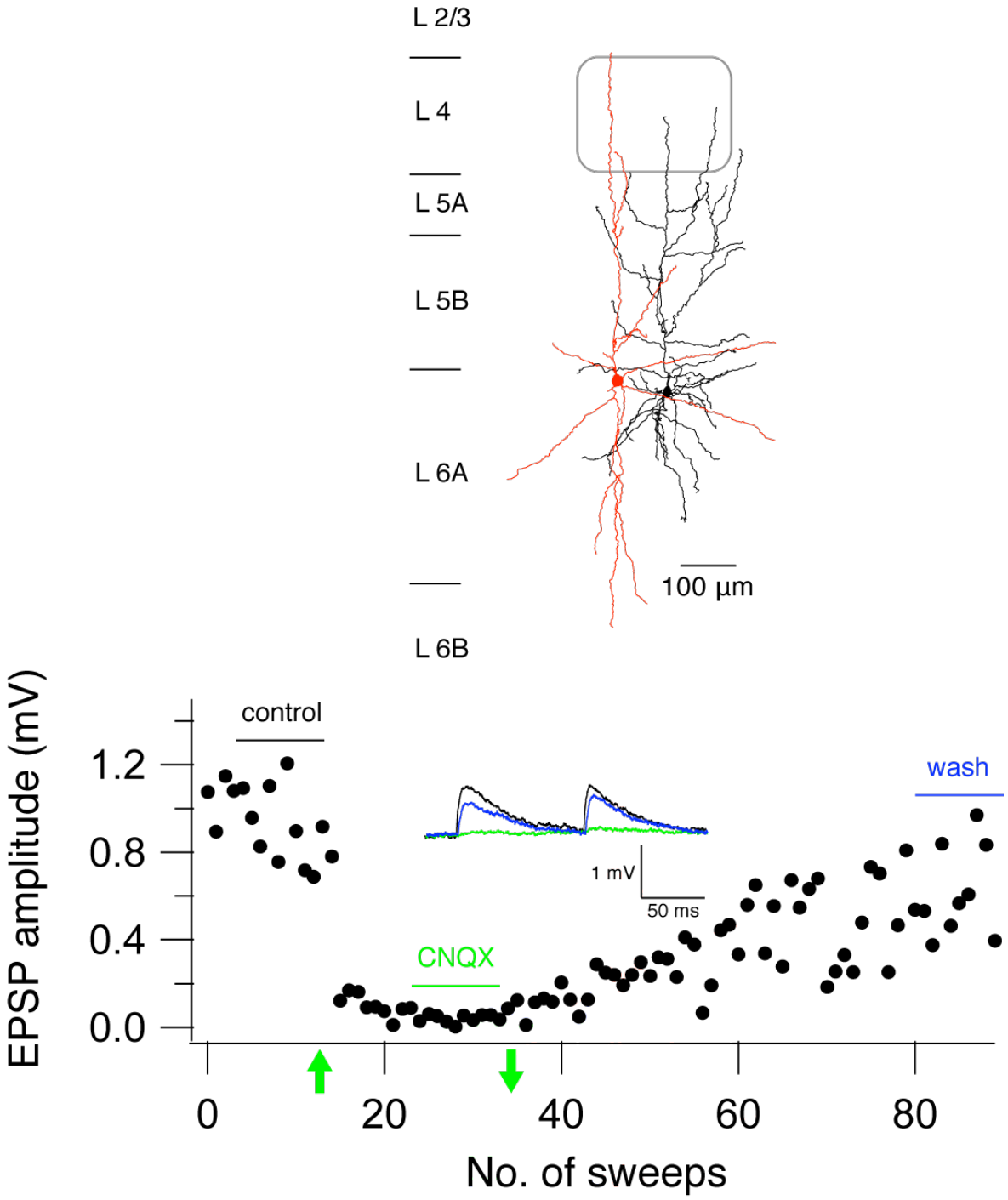


Fig. 3.19 Pharmacological properties of a L6A-L6A connection (BC 300410 DE). Top, Neurolucida reconstruction of the pair for pharmacological analysis. Pre- and post-somatodendritic structures are shown in red and black, respectively Bottom, Time course of EPSP amplitude during pharmacological treatment. Inset, mean EPSP waveforms from control (black trace), with 10 µM CNQX (green trace) and after wash (blue trace) are shown superimposed aligned with respect to the peak time of presynaptic APs. Each sweep was collected at 20 s intervals.

Another L6A-L6A pair was used to study the pharmacological properties of this connection type (see Fig. 3.19). It was shown that during the application of the AMPA receptor blocker CNQX (10

μM), the EPSP in the control condition (amplitude = 0.96 mV, black curve in Fig. 3.19) was largely blocked, with a small slow component remaining (amplitude = 0.07 mV, green curve in Fig. 3.19). After wash-out, the EPSP amplitude partially recovered (amplitude = 0.60 mV, blue curve in Fig. 3.19). Therefore, at the resting potential of the postsynaptic neuron, the EPSP is mediated largely by AMPA receptors, similar to that of L4-L4 excitatory connections shown above.

3.2.3 Summary of data

In summary, ten L4-L4 pairs and five L6A-L6A pairs were recorded for this work. The sample size of these intralaminar excitatory connections is relatively small because they were recorded mainly for comparison with interlaminar L4-L6A excitatory connections (given below). Despite the small sample size, some general principles were discovered that are in accordance with previously published data.

Table 3.1. EPSP characteristics of L4-L4 excitatory connections.

	Amplitude (mV)	20-80% rise time (ms)	Latency (ms)	Paired-pulse ratio	Failure rate (%)	Coefficient of variation
Mean	1.02	1.59	1.17	0.92	12.3	0.41
SD	1.33	0.49	0.41	0.14	13.3	0.18
Range	0.30 - 4.71	0.80 - 2.48	0.72 - 2.04	0.68 - 1.12	0.0 - 39.6	0.11 - 0.68
n	10	10	10	10	9	9

Table 3.2. Passive properties of postsynaptic L4 spiny neurons.

	V_{rest} (mV)	Input resistance (MΩ)	Time constant (ms)
Mean	-76.8	201.0	16.8
SD	4.0	71.8	3.7
Range	-83.0 - -69.0	87.4 - 335.6	12.6 - 23.5
n	10	10	10

Table 3.3. EPSP characteristics of L6A-L6A excitatory connections.

	Amplitude (mV)	20-80% rise time (ms)	Latency (ms)	Paired-pulse ratio	Failure rate (%)	Coefficient of variation
Mean	0.58	1.38	1.69	0.98	17.5	0.53
SD	0.50	0.59	0.65	0.15	15.0	0.23
Range	0.27 - 1.46	0.72 - 2.27	1.14 - 2.70	0.74 - 1.12	0.0 - 37.5	0.28 - 0.91
n	5	5	5	5	5	5

Table 3.4. Passive properties of postsynaptic L6A pyramidal cells.

	V_{rest} (mV)	Input resistance (MΩ)	Time constant (ms)
Mean	-74.4	128.5	20.1
SD	2.1	42.1	4.1
Range	-77.0 - -72.0	81.8 - 182.9	15.6 - 24.2
n	5	5	5

Tables 3.1, 3.2 and 3.3, 3.4 summarise the parameters of EPSP characteristics and passive properties of postsynaptic neurons for L4-L4 and L6A-L6A excitatory connections, respectively.

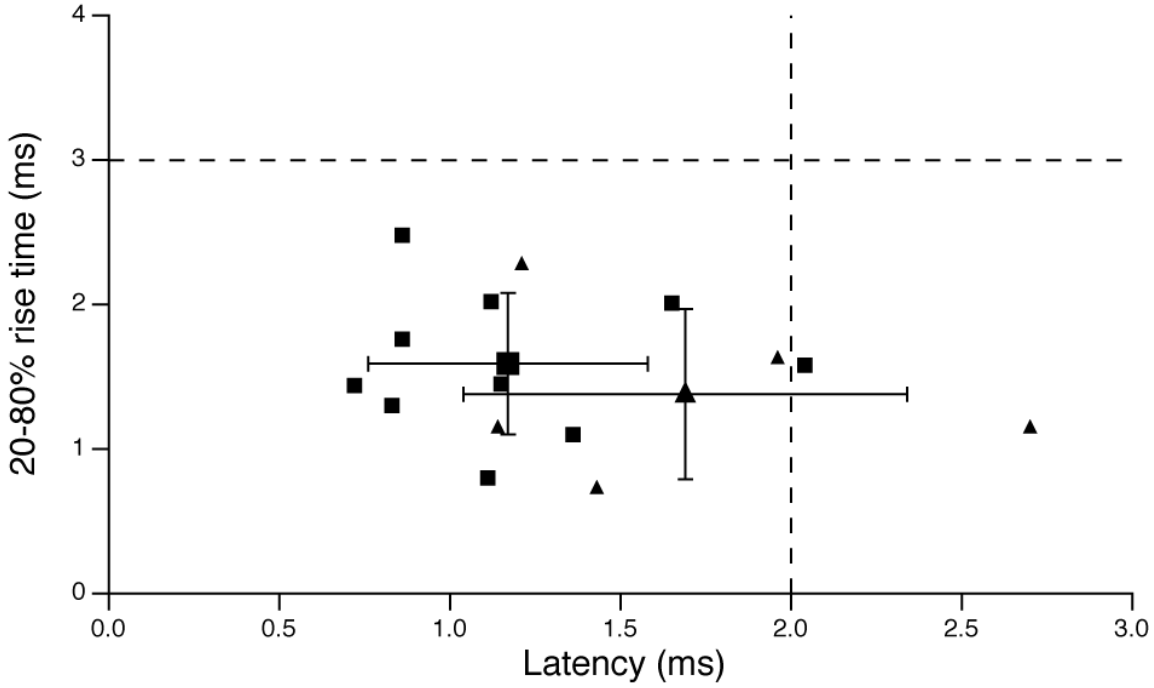


Fig. 3.20 Summary plot of 20-80% rise time versus latency for L4-L4 and L6A-L6A excitatory connections. Black triangles and squares represent the data from individual L4-L4 and L6A-L6A pairs, respectively. Larger black triangle and square with error bars stand for the mean and standard deviation value of L4-L4 and L6A-L6A connections, respectively.

The plots of 20-80% rise time versus latency for individual L4-L4 and L6A-L6A connections and their respective means ± SD are shown in Fig. 3.20. Most of these pairs showed a fast rise time (1.59 ± 0.49 ms, range 0.80 - 2.48 ms for L4-L4 connections and 1.39 ± 0.59 ms, range 0.72 - 2.27

ms for L6A-L6A connections) and short latency (1.17 ± 0.41 ms, range 0.72 - 2.04 ms for L4-L4 connections and 1.69 ± 0.65 ms, range 1.14 - 2.70 ms for L6A-L6A connections).

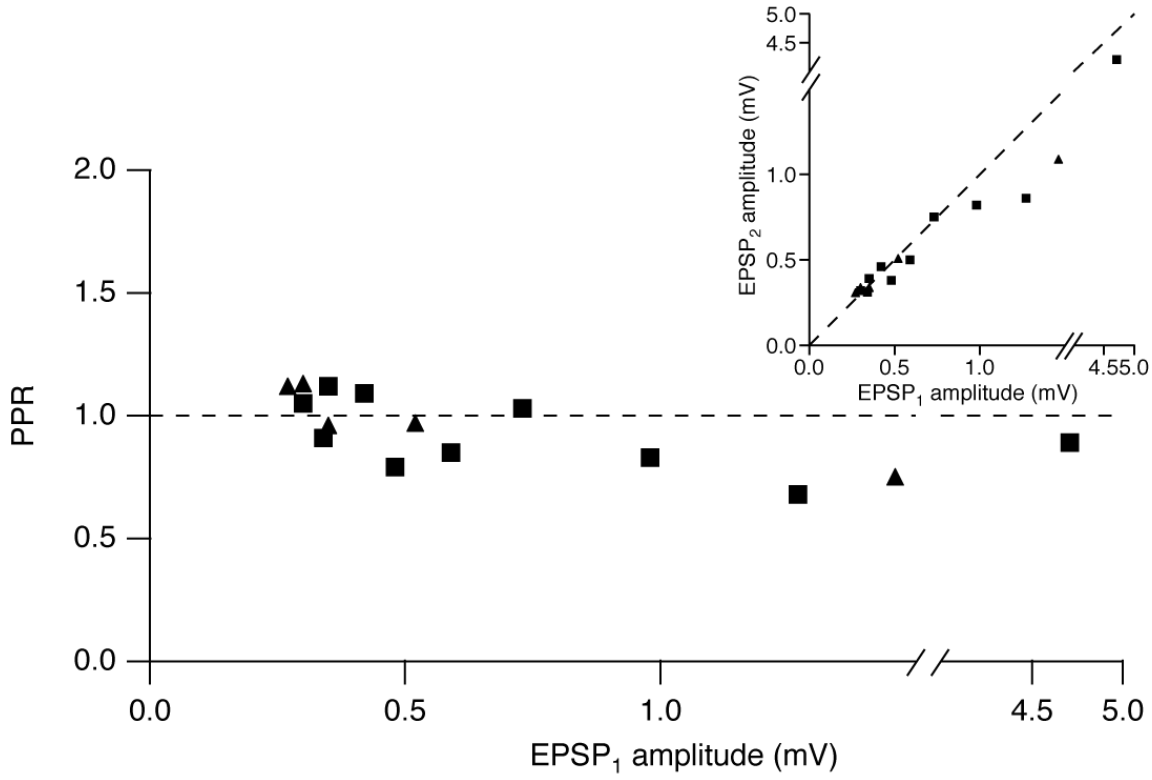


Fig. 3.21 Summary plot of paired-pulse ratio (PPR) versus the 1st EPSP amplitude for L4-L4 and L6A-L6A excitatory connections. Black triangles and squares represent the data from individual L4-L4 and L6A-L6A pairs, respectively. Inset, Plot of the 2nd versus the 1st EPSP amplitude.

For short-term plasticity, there is a general tendency for both L4-L4 and L6A-L6A pairs: weak connections tended to show (a weak) short-term facilitation while strong ones demonstrated short-term depression but the linear correlations between PPR and the 1st EPSP amplitude are not statistical significant for both L4-L4 ($r = -0.24$, $P = 0.75$) and L6A-L6A ($r = -0.91$, $P = 0.98$) connections (see Fig. 3.21).

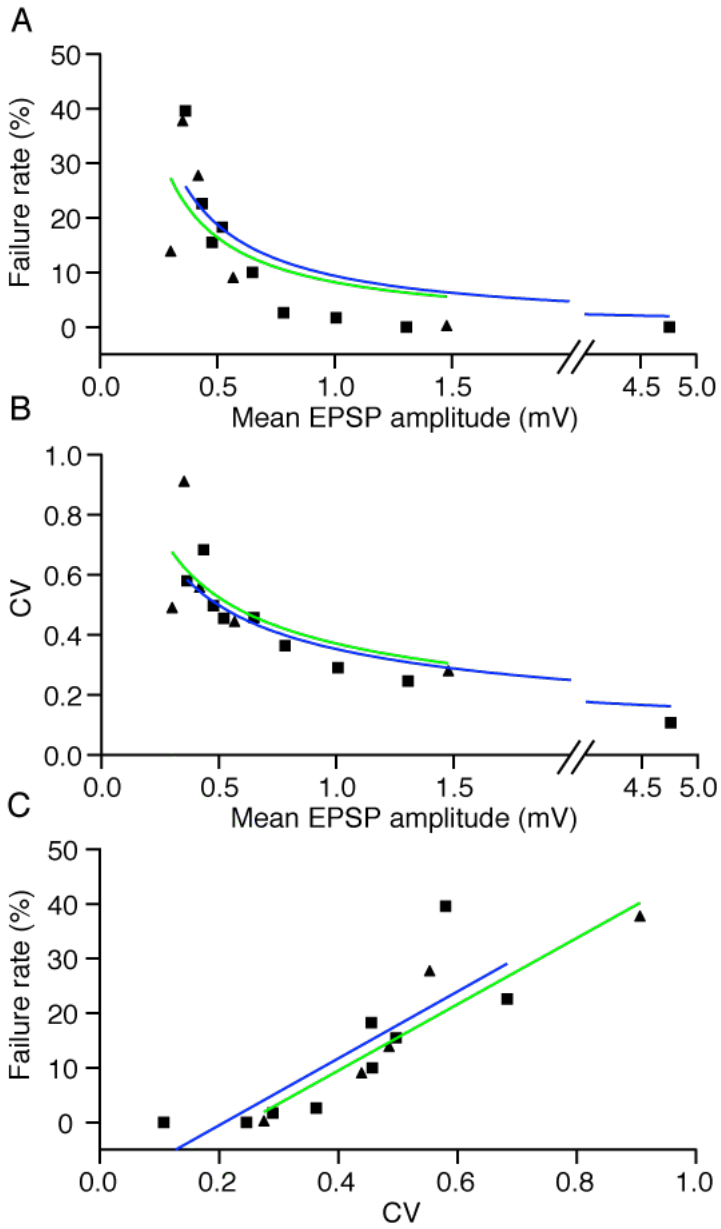


Fig. 3.22 Summary of the relationship between synaptic properties for L4-L4 and L6A-L6A excitatory connections. A, Plot of failure rate versus mean EPSP amplitude. B, CV versus mean EPSP amplitude. C, Failure rate versus CV. Black triangles and squares represent the data from individual L4-L4 and L6A-L6A pairs, respectively. Best hyperbolic or linear fits for L4-L4 (blue lines) and L6A-L6A (green lines) connections are also shown.

The failure rate and the CV are closely related to the mean EPSP amplitude: connections with a small EPSP amplitude show a high failure rate and CV while those with a large EPSP amplitude show a low failure rate and CV. The failure rate and the CV are linearly correlated for both L4-L4 ($r = 0.82$, $P = 3.59\times10^{-3}$) and L6A-L6A ($r = 0.94$, $P = 7.86\times10^{-3}$) connections as shown in Fig. 3.22.

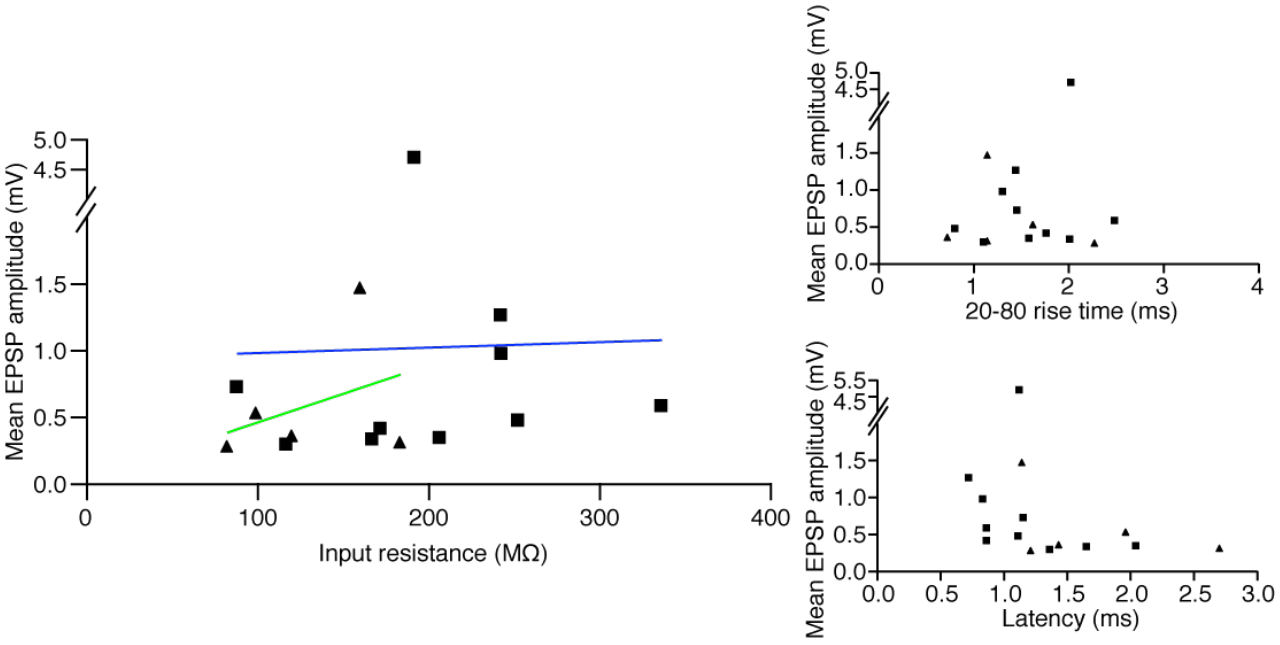


Fig. 3.23 Summary plot of mean EPSP amplitude versus input resistance, 20-80% rise time or latency for L4-L4 and L6A-L6A excitatory connections. Black triangles and squares represent the data from individual L4-L4 and L6A-L6A pairs, respectively. Best linear fits for L4-L4 (blue lines) and L6A-L6A (green lines) connections are also shown.

A weak but statistically not significant correlation between the mean EPSP amplitude and the input resistance of postsynaptic neuron for L4-L4 ($r = 0.02$, $P = 0.48$) and L6A-L6A ($r = 0.36$, $P = 0.28$) connections was found. Furthermore, the mean EPSP amplitude decreased roughly with an increasing 20-80% rise time and latency (see Fig. 3.23).

3.3 Monosynaptic L4-L6A excitatory connections

For all pairs between L4 spiny neurons and L6A pyramidal cells (n = 19), the presynaptic neuron was located in the L4 barrel and the postsynaptic cell in the region of layer 6A directly below the L4 neuron, *i.e.,* in the same barrel column. The L6A pyramidal cells were readily identified as excitatory neurons since they displayed a characteristic regular firing pattern with a spike doublet or triplet at the beginning of the action potential train and spike frequency adaptation (Connors and Gutnick 1990); this was subsequently confirmed by *post hoc* histological processing. The connectivity between L4 spiny neurons and L6A pyramidal cells was found to be extremely low on one hand but relatively high on the other hand: In 2576 potential connections tested in the 'loose-seal' searching mode, we found only 40 synaptic connections. Thus the probability to find a connection was only 1.6%. However, when only the 305 potential connections tested in search for the 40 established pairs were taken into account, the connectivity ratio was 13.1% (*i.e.*, one in eight tested neurons was connected). In nearly half of the 40 synaptic connections found in the searching mode, the presynaptic L4 neurons were successfully repatched and recorded in the whole-cell mode. Altogether, nineteen L4-to-L6A excitatory connections were measured and then processed for physiological (n = 19) or morphological (n = 18) analysis. The direct distance between L4 and L6A somata ranged from 416 to 567 μm with average 526 ± 37 μm (n = 19).

3.3.1 Three connection phenotypes

Morphologically, in 7 of 18 pairs, the presynaptic L4 neuron was a spiny stellate, while in the remaining 11 pairs, the presynaptic neuron was a star pyramid. In 3 of 18 pairs, the postsynaptic L6A neuron was a tall pyramidal neuron, while in the remaining 15 pairs, the postsynaptic neuron was a short pyramidal neuron. Electrophysiologically, in 12 of 19 L4-L6A connections, synaptic transmission showed 'slow' EPSPs with a slow rising phase and long latency. The remaining 7 connections demonstrated 'fast' EPSPs with a fast rising phase and short latency. Therefore,

combining morphological properties of presynaptic neurons with physiological characteristics of EPSPs, we could divide all the electrophysiologically and morphologically identified eighteen L4-L6A excitatory connections into three categories as follows: a spiny stellate as the presynaptic L4 neuron (SS), a star pyramid as the presynaptic L4 neuron with a fast EPSP (fSP), a presynaptic L4 star pyramid with a slow EPSP (sSP). Furthermore, by examining the dendritic structure and axonal projection pattern of the postsynaptic L6A pyramidal cell, these connections could be further hierarchically subdivided into subgroups (see Fig. 3.24).

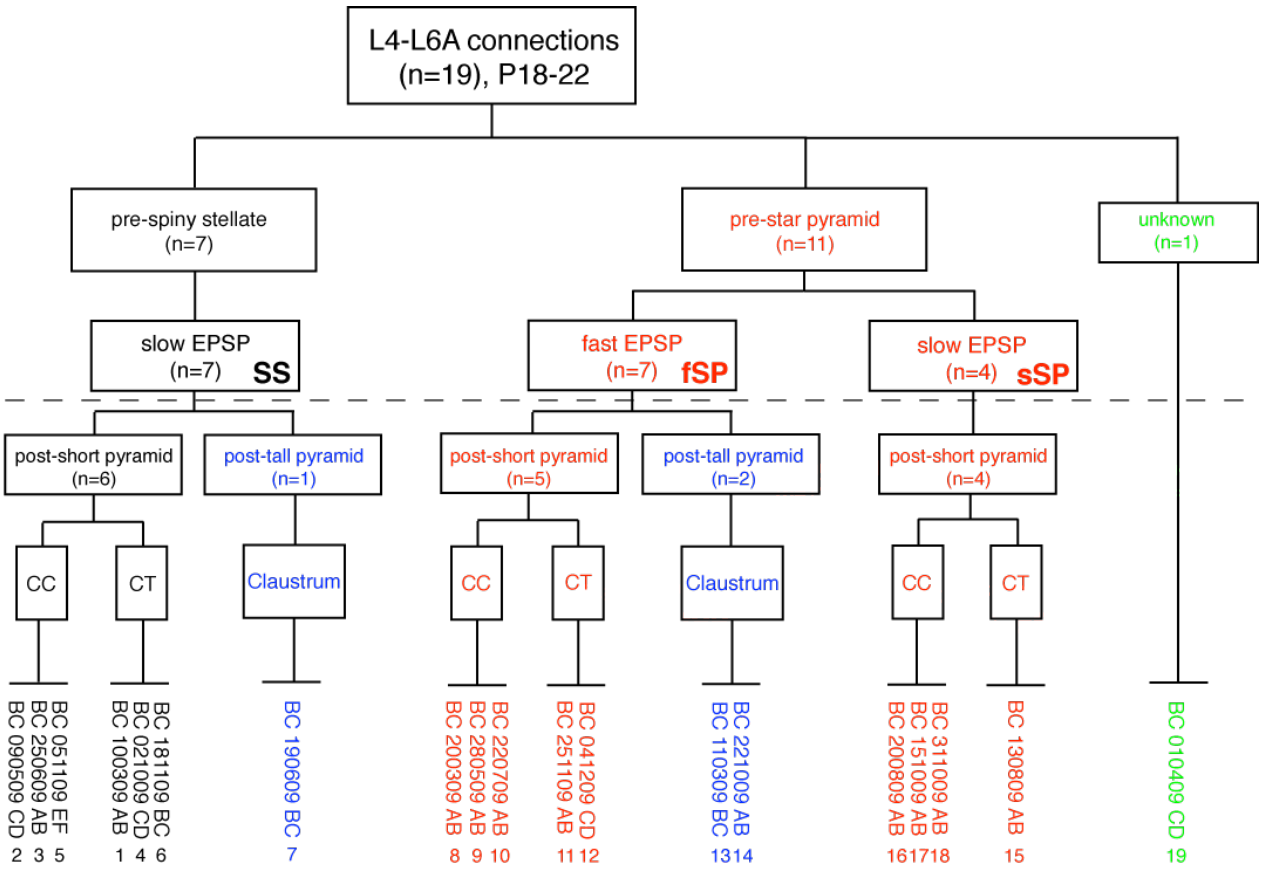


Fig. 3.24 Dendrogram of L4-to-L6A excitatory connections. All the L4-L6A excitatory connections are hierarchically subdivided into subgroups based on their pre- and postsynaptic neuron type and synaptic physiology. Abbreviations: P, postnatal day; SS, spiny stellate; fSP, star pyramid with fast synapse: sSP, star pyramid with slow synapse; CC, corticocortical-like; CT, corticothalamic-like; Claustrum, claustrum projecting-like.

3.3.2 L4 spiny stellate-L6A pyramidal cell pairs

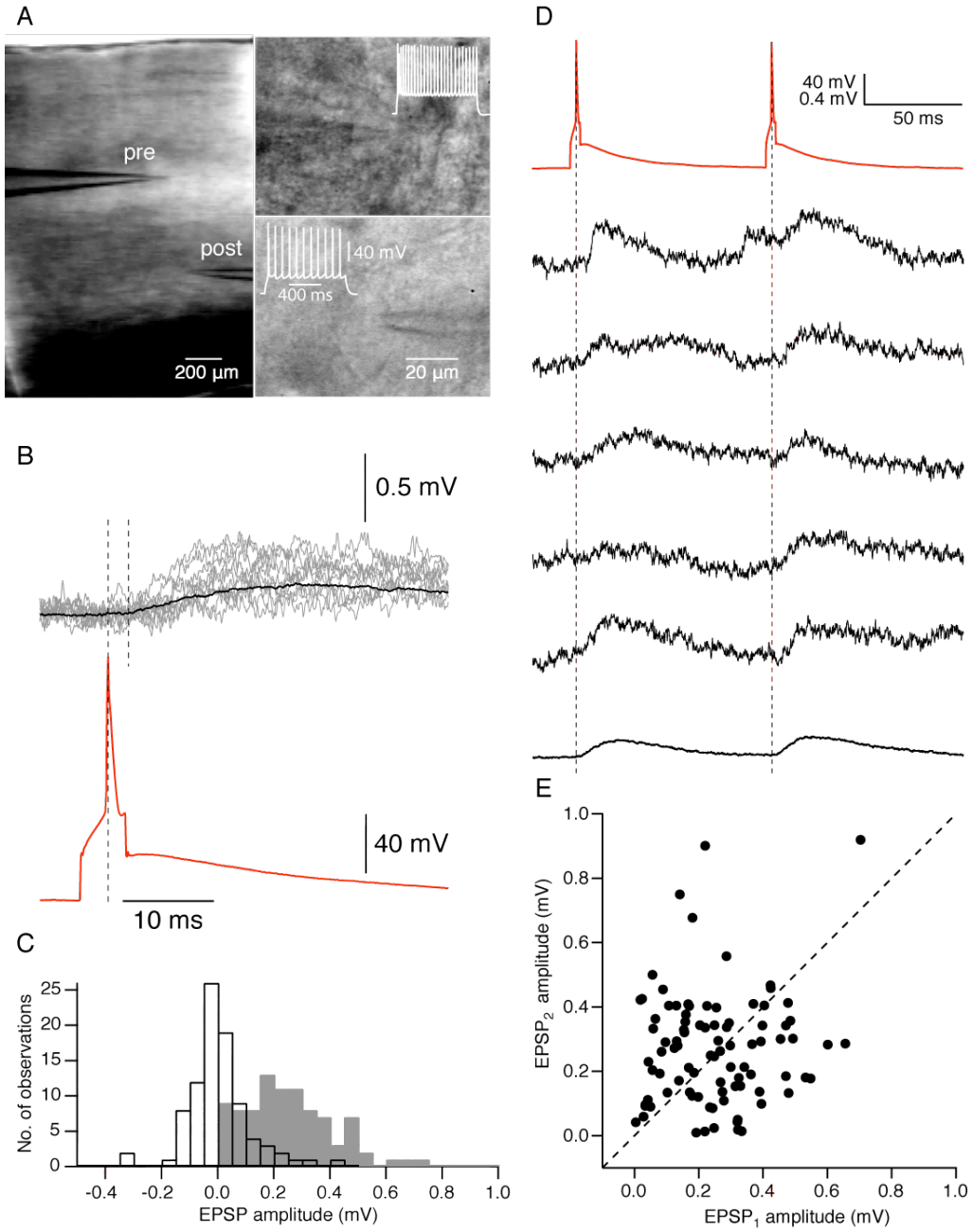


Fig. 3.25 Representative example of a L4 spiny stellate-L6A pyramidal cell pair (BC 090509 CD). A, Left, IR-DIC image of the slice. The pipettes mark the positions of the presynaptic L4 spiny neuron and the postsynaptic L6A pyramidal cell. Right, High-magnification images of the presynaptic L4 spiny stellate neuron (top) and the postsynaptic L6A pyramidal cell (bottom). Insets, the corresponding firing patterns of pre- and postsynaptic neurons (white traces). B, A presynaptic AP (red trace) and 10 consecutive EPSPs (grey traces) superimposed with the mean EPSP waveform (black trace) are shown. C, EPSP amplitude histogram for this connection (black open bars are for noise). D, Five consecutive EPSPs (middle) recorded in a postsynaptic L6A pyramidal cell elicited by two APs (top) at 100 ms interval in a presynaptic L4 spiny stellate neuron. The mean EPSP waveform is shown at the bottom. E, Comparison of the second and first EPSPs.

Seven L4-L6A SS pairs were recorded. A representative example of a L4-L6A SS connection is shown in Fig. 3.25. This connection had a small mean EPSP (amplitude = 0.22 mV) with a slow rise time (20-80% rise time = 9.15 ms) and relatively long latency (latency = 2.31 ms). The failure rate and CV for this connection are 43.3% and 0.63, respectively. This pair exhibited weak short-term facilitation at an ISI of 100 ms with a PPR = 1.08. Fig. 3.26 shows the microphotographs of the

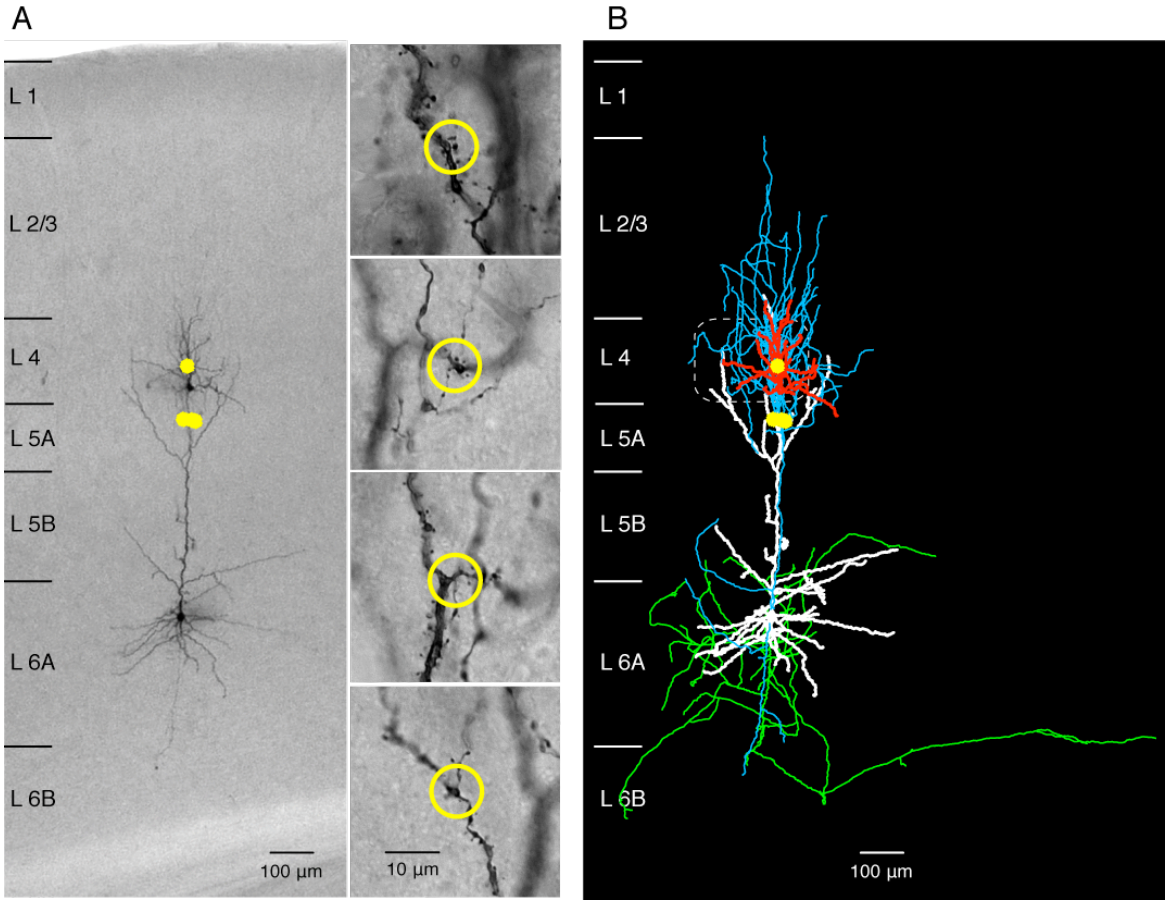


Fig. 3.26 Photomicrographs of the stained slice and its Neurolucida reconstructions (BC 090509 CD). A, Left, Half-tone photomicrograph of a biocytin-filled pair between a spiny stellate neuron in layer 4 and a pyramidal cell in layer 6A. Light-microscopically identified putative synaptic contacts are marked by filled yellow circles. Right, Higher magnification half-tone photomicrographs of four putative synaptic contacts marked by open yellow circles. All contacts were established on the tuft of the apical dendrite of the L6A pyramidal cell by three *en passant* and one *terminal* axonal bouton(s). B, 2D projection of 3D Neurolucida reconstruction. The axonal arbor (blue) and the somatodendritic arbor (red) of the L4 spiny stellate neuron and the axonal arbor (green) and the somatodendritic domain (white) of the L6A pyramidal cell are shown. The barrel is indicated by a dashed contour. Light-microscopically identified putative synaptic contacts are marked by filled yellow circles.

stained slice of this cell pair and four putative synaptic contacts at the higher magnification. The Neurolucida reconstruction of this cell pair is also shown (see Fig. 3.26B). The presynaptic neuron is a L4 SS neuron with its soma being located near the centre in the horizontal direction and near the lower border in the vertical direction with respect to the barrel. The dendritic branches of L4 SS neuron were largely confined to the barrel border and displayed a nearly symmetric orientation in the horizontal direction and an asymmetric orientation towards the barrel centre in the vertical direction. The axon of L4 SS neuron was largely confined to the barrel column with most arbors

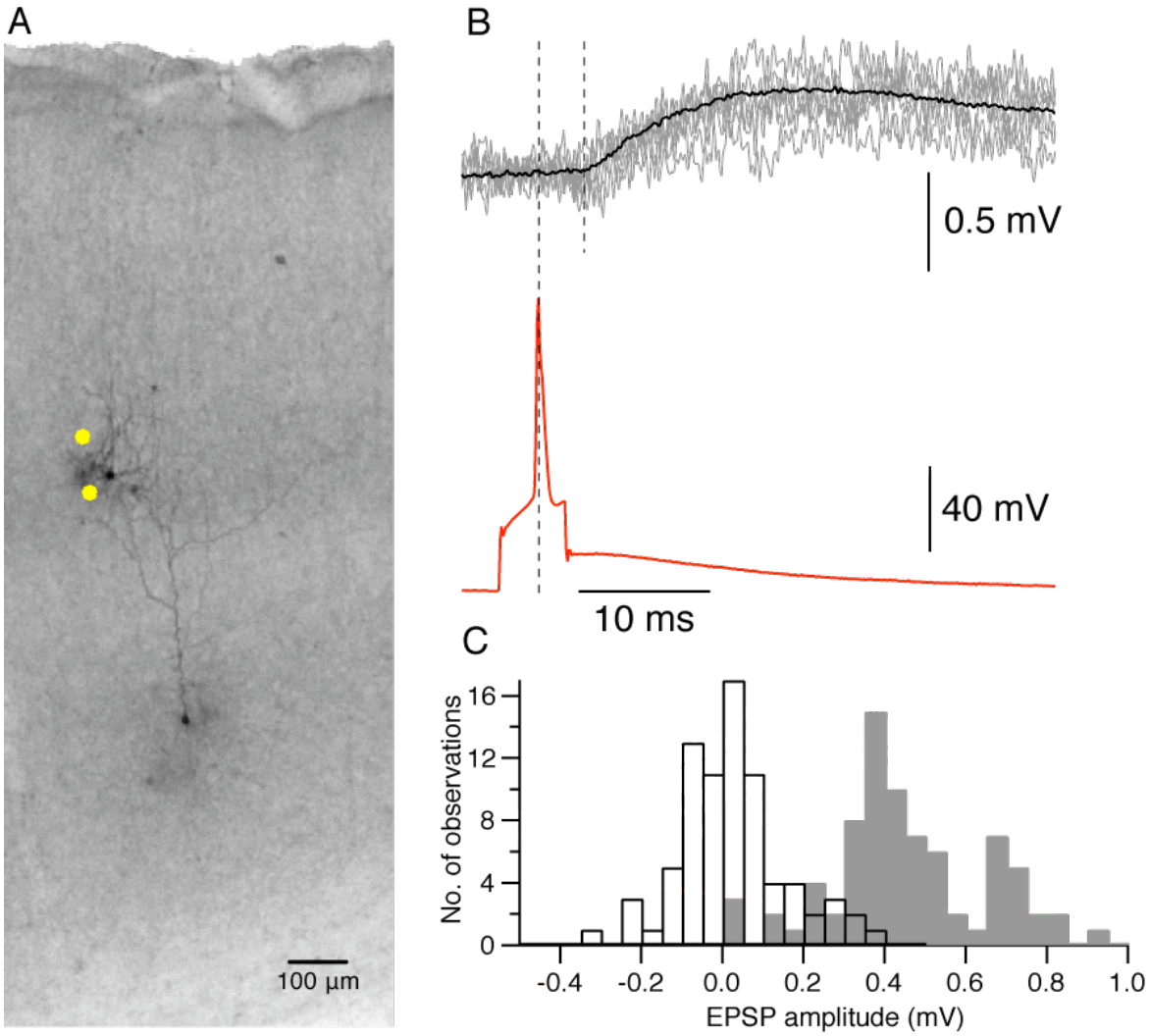


Fig. 3.27 Another example of L4 spiny stellate-L6A pyramidal neuron connection (BC 100309 AB). A, Half-tone photomicrograph of the stained slice. Light-microscopically identified putative synaptic contacts are marked by filled yellow circles. B, A presynaptic AP (red trace) and 10 consecutive EPSPs (grey traces) superimposed with the mean EPSP waveform (black trace) are shown. C, EPSP amplitude histogram for this connection (black open bars are for noise).

being located in layers 4 and 2/3 and one branch descending vertically to the layer 6B with sparse bifurcations. The postsynaptic neuron is a L6A short pyramidal cell with its soma being located

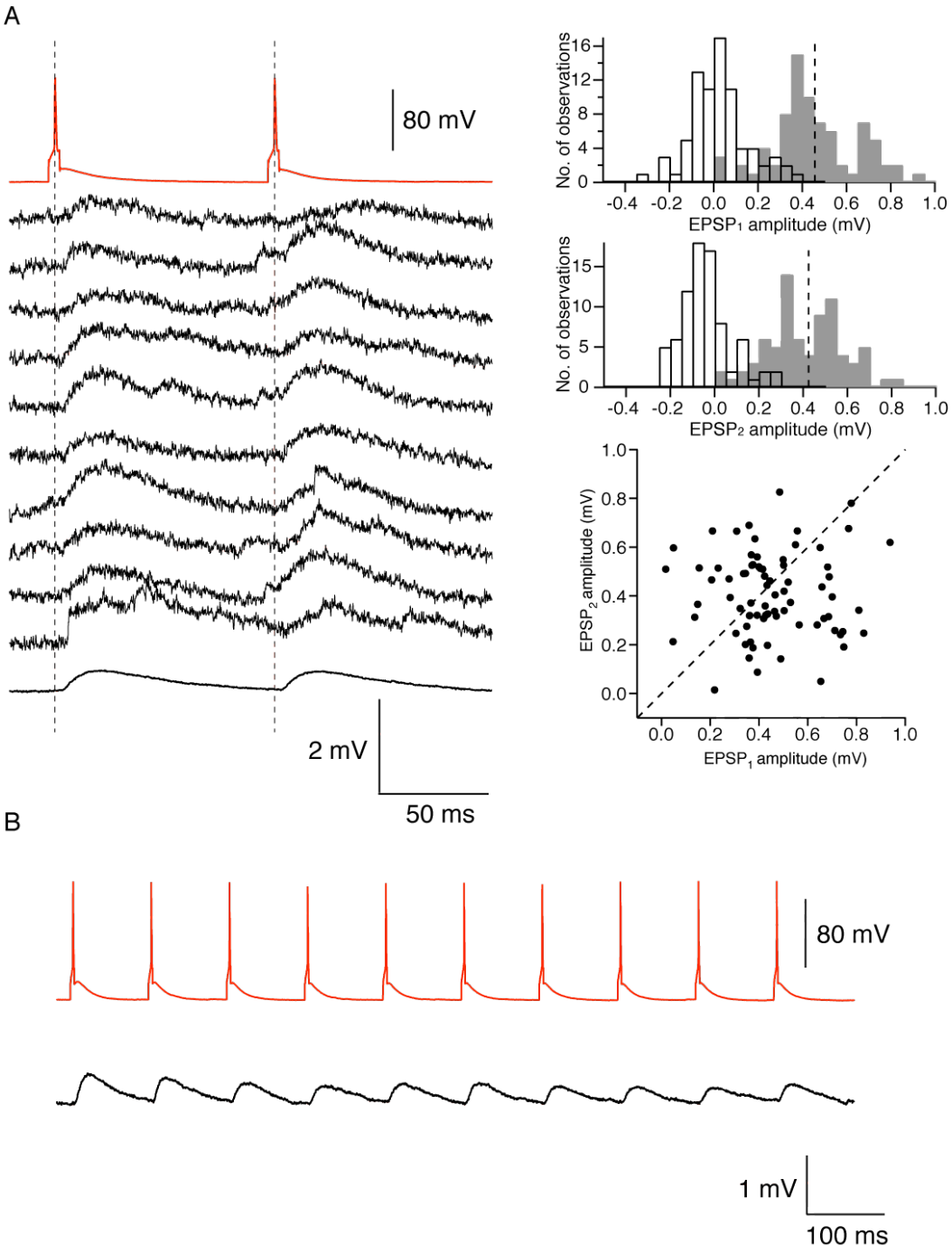


Fig. 3.28 Short-term plasticity of the connection shown in Fig. 3.27. A, Left, Ten consecutive EPSPs (middle) recorded in a postsynaptic L6A pyramidal cell elicited by two APs (top) at 100 ms interval in a presynaptic L4 spiny stellate neuron. The mean EPSP waveform is shown at the bottom. Right, Corresponding EPSP amplitude histograms for the first (top, black open bars are for noise) and second (middle) EPSPs. Comparison of the second and first EPSPs is shown at the bottom. B, Train of ten presynaptic APs at 10 Hz (top trace) and the mean EPSP waveform (black trace).

directly below the presynaptic L4 soma. The dendrite branches of L6A short pyramid were columnar and had two domains: one was located near the soma in layer 6A (basal dendrites) and the other in the distal part of the apical dendrite in layer 4 (apical tuft dendrites). The axon of L6A short pyramid was exclusively located in infragranular layers 5B and 6 with some long horizontal branches. Therefore, this L6A short pyramidal cell is probably a L6A CC neuron (*cf*. (Zhang and Deschenes 1997; Kumar and Ohana 2008)). All of four putative synaptic contacts identified under the light microscope for this pair are established on the apical tuft dendrite of the L6A pyramidal

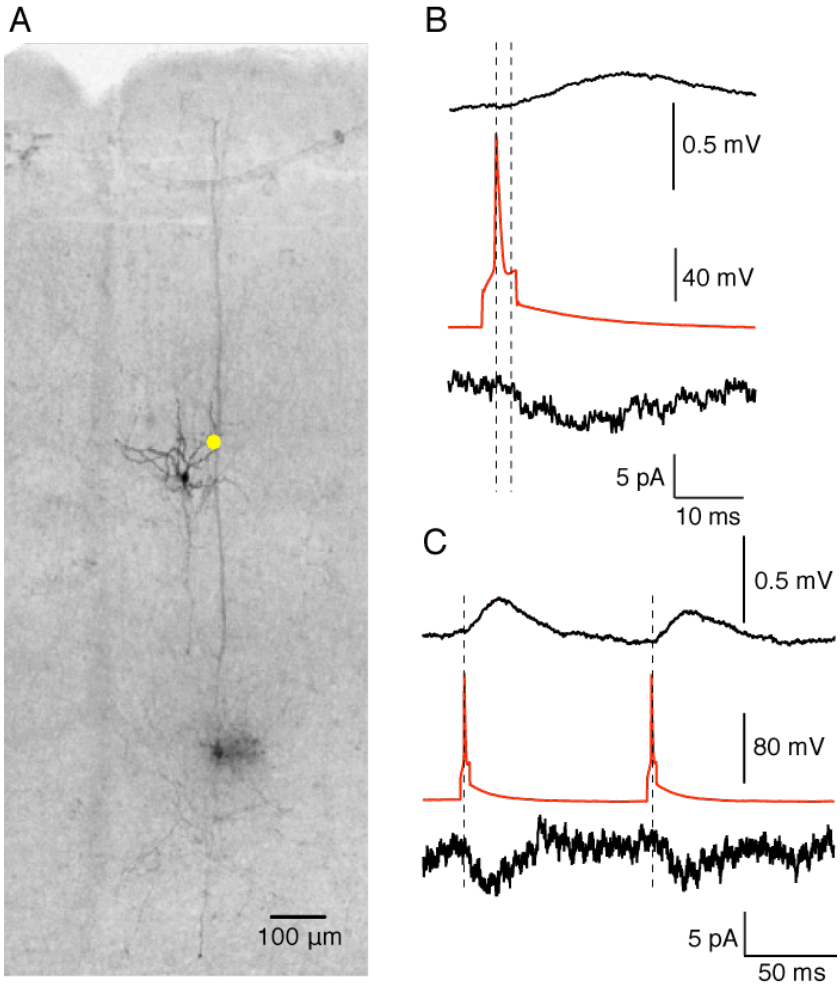


Fig. 3.29 EPSC properties and short-term plasticity of a L4-L6A SS connection (BC 190609 BC). A, Half-tone photomicrograph of the stained slice. A light-microscopically identified putative synaptic contact is marked by a filled yellow circle. B, A presynaptic AP (red trace), the mean EPSP waveform (top) and the mean EPSC waveform (bottom) are shown. C, The mean EPSC waveform (bottom) recorded in a postsynaptic L6A pyramidal cell elicited by two APs (top) at 100 ms interval in a presynaptic L4 spiny stellate neuron. The mean EPSP waveform is shown on the top.

cell. The synapse-to-soma distances of four putative synaptic contacts are 632.6, 512.6, 506.0 and 494.1 µm, respectively. The mean synapse-to-soma distance is 536.3 µm.

Another L4-L6A SS pair with a stronger synapse is shown in Figs. 3.27 and 3.28. The mean EPSP characteristics of this connection are as follows: amplitude = 0.42 mV, 20-80% rise time = 6.70 ms and latency = 3.97 ms. The failure rate and CV for this connection are 10.1% and 0.44, respectively. This pair displayed short-term depression with PPR = 0.91 at an ISI of 100 ms. There are two

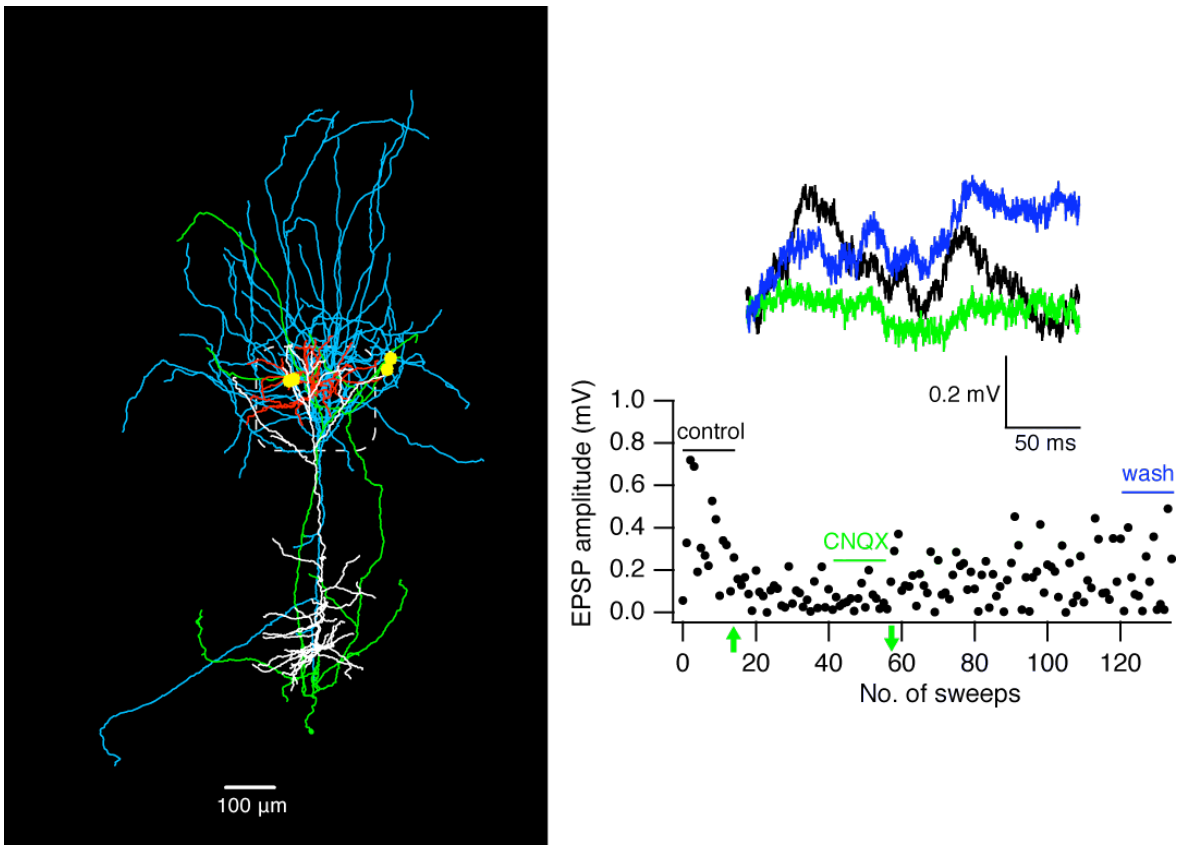


Fig. 3.30 Pharmacological properties of a L4-L6A SS connection (BC 021009 CD). Left, 2D projection of 3D Neurolucida reconstruction. The axonal arbor (blue) and the somatodendritic arbor (red) of the L4 spiny stellate neuron and the axonal arbor (green) and the somatodendritic arbor (white) of the L6A pyramidal cell are shown. The barrel is indicated by a dashed contour. Light-microscopically identified putative synaptic contacts are marked by filled yellow circles. Right, Time course of EPSP amplitude during pharmacological treatment. Inset, mean EPSP waveforms from control (black trace), with 10 µM CNQX (green trace) and after wash (blue trace) are shown superimposed aligned with respect to the peak time of presynaptic APs. Each sweep was collected at 20 s intervals.

putative synaptic contacts which are located exclusively on the apical tuft of the postsynaptic L6A pyramidal cell. The synapse-to-soma distances for them are 629.5 and 520.9 μm, respectively.

EPSCs were recorded at -70 mV under voltage clamp in another L4-L6A SS connection between a L4 SS and a L6A tall pyramidal cell (see Fig. 3.29). The mean EPSC (amplitude = -4.3 pA) exhibited a very slow time course, in accordance with that of the mean EPSP (amplitude = 0.19 mV) with a 20-80% rise time of 7.93 ms, a latency of 2.16 ms and a PPR = 0.90. One putative synaptic contact was light microscopically identified; it is located on the distal apical oblique dendrite with a synapse-to-soma distance of 595.9 μm. Due to the distal location of this synaptic contact, the distal part of the apical dendrite could not be completely clamped to the voltage as expected (Schaefer, Helmstaedter et al. 2003). Therefore, the mean EPSC amplitude measured here is likely to be significantly underestimated.

In another L4-L6 SS pair (shown in Fig. 3.30) the pharmacological profile of the synaptic response was investigated. The mean EPSP of this pair showed also a slow rise time (20-80% rise time = 6.67 ms) and a long latency (latency = 4.98 ms). Four putative synaptic contacts were discovered in this connection which are all located in the apical tuft of the postsynaptic L6A pyramidal cell, the synapse-to-soma distances for them are 801.1, 764.6, 679.2 and 668.7 μm, respectively. During the application of the AMPA receptor blocker CNQX (10 μM), the EPSP in the control condition (amplitude = 0.21 mV, black curve in Fig. 3.30) was largely blocked with a barely detectable slow component left (green curve in Fig. 3.30). After a prolonged wash-out of CNQX for more than ten minutes, the EPSP amplitude partially recovered (amplitude = 0.17 mV, blue curve in Fig. 3.30). This suggested that, at the resting membrane potential of the postsynaptic synaptic L6A pyramidal cell, the L4-to-L6A synaptic transmission is mainly mediated by AMPA receptors.

3.3.3 L4 star pyramid-L6A pyramidal cell pairs with fast synapses

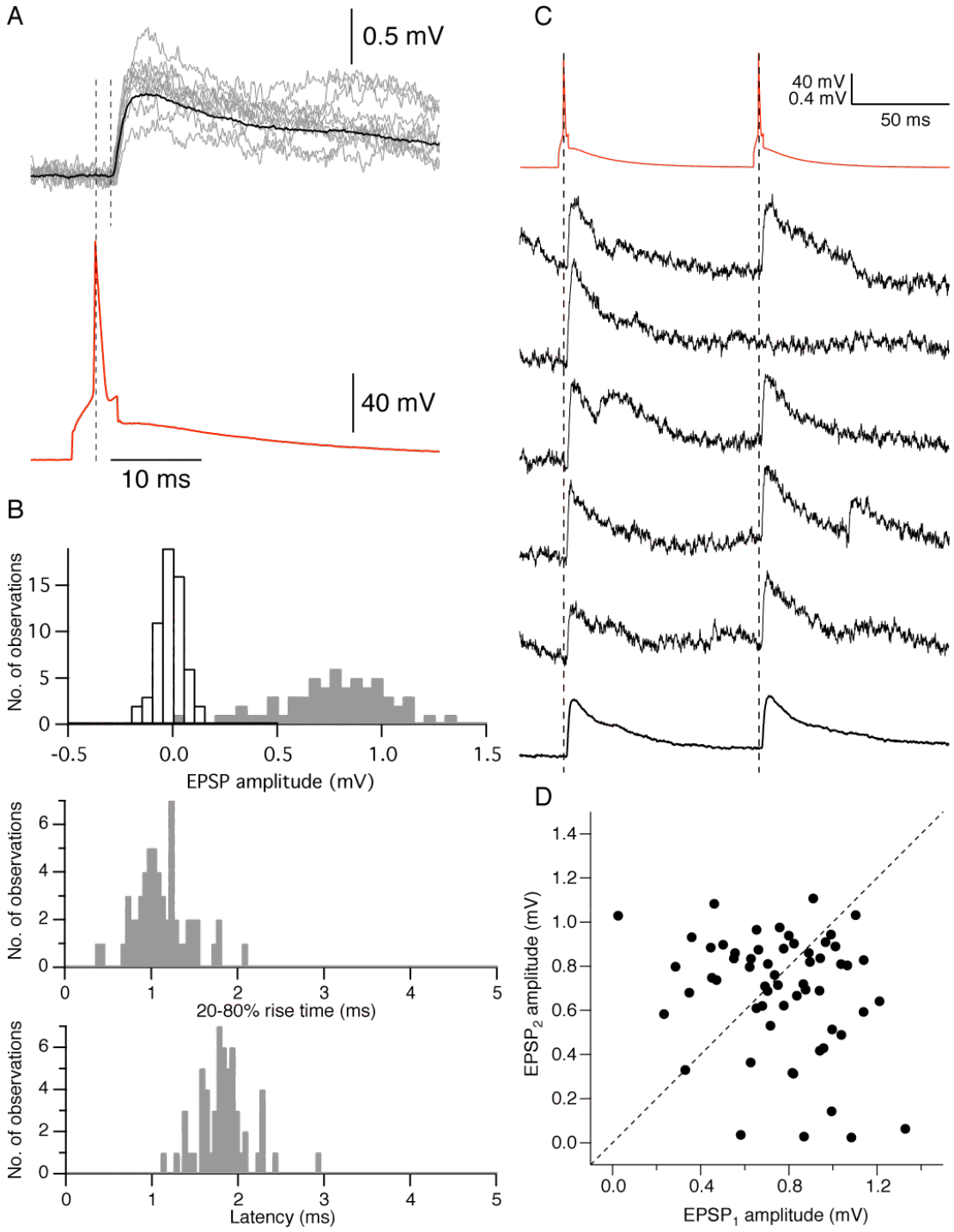


Fig. 3.31 Representative example of a L4 star pyramid-L6A pyramidal cell pair with fast EPSP (BC 220709 AB). A, A presynaptic AP (red trace) and 10 consecutive EPSPs (grey traces) superimposed with the mean EPSP waveform (black trace) are shown. B, EPSP amplitude (black open bars are for noise), 20-80% rise time and latency histograms for this connection. C, Five consecutive EPSPs (middle) recorded in a postsynaptic L6A pyramidal cell elicited by two APs (top) at 100 ms interval in a presynaptic L4 star pyramidal neuron. The mean EPSP waveform is shown at the bottom. D, Comparison of the second and first EPSPs.

Seven connections of the L4-L6A fSP phenotype were found. A representative example of such a L4-L6A fSP pair is shown in Fig. 3.31. This connection had a relatively large mean EPSP amplitude (0.74 mV) with a fast 20-80% rise time of 1.07 ms and short latency of 1.87 ms. This pair exhibited

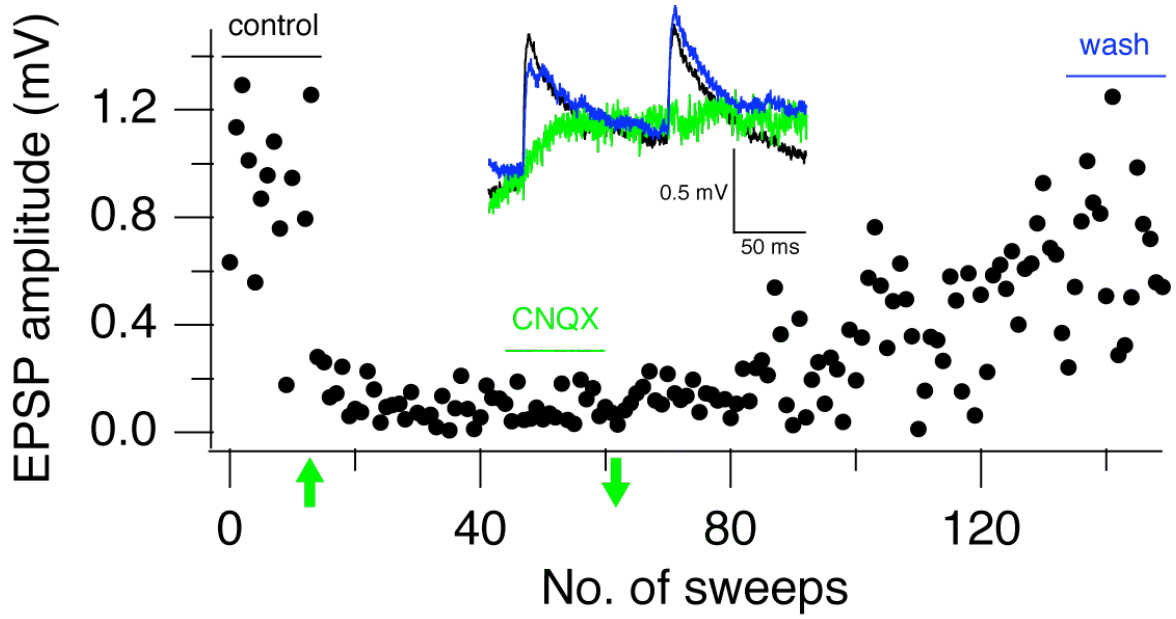


Fig. 3.32 Pharmacological properties of the connection shown in Fig. 3.31. Time course of EPSP amplitude during pharmacological treatment. Inset, mean EPSP waveforms from control (black trace), in the presence of 10 μM CNQX (green trace) and after wash (blue trace) are shown superimposed aligned with respect to the peak time of presynaptic APs. Each sweep was collected at 20 s intervals.

a weak short-term depression at an ISI of 100 ms with a PPR of 0.92. The microphotographs of the stained slice for this cell pair and two putative synaptic contacts at the higher magnification are presented in Fig. 2.4 given before. The Neurolucida reconstruction of this cell pair is also shown there. The presynaptic neuron is a L4 SP neuron with its soma located near the centre of the barrel. The basal dendrites of the L4 SP neuron were largely confined to the barrel border and displayed a nearly symmetric orientation. The apical dendrite projected out of barrel towards the pial surface and reached the middle of layer 2/3. The axon of L4 SP neuron was largely confined to the barrel column with most collaterals being sparsely distributed in layers 4 and 2/3 and one branch descending vertically to layer 6B with some bifurcations. The postsynaptic neuron is a L6A short pyramidal cell with its soma located directly below the presynaptic L4 soma. The dendritic

branches of the L6A short pyramidal cell were columnar and had two domains: one was located near the soma in layer 6A (basal dendrites) and the other in the distal part of the apical dendrite in layer 5A just below L4 barrel (apical tuft dendrites). Between these two dendritic domains, there were several apical oblique dendrites. The axon of L6A short pyramidal cell was mainly located in infragranular layers 5B and 6 with several long horizontal branches. In addition, there were some axonal collaterals which project up to layer 4. Therefore, this L6A short pyramidal cell is probably a L6A CC neuron (*cf.* (Zhang and Deschenes 1997; Kumar and Ohana 2008)). Two putative synaptic

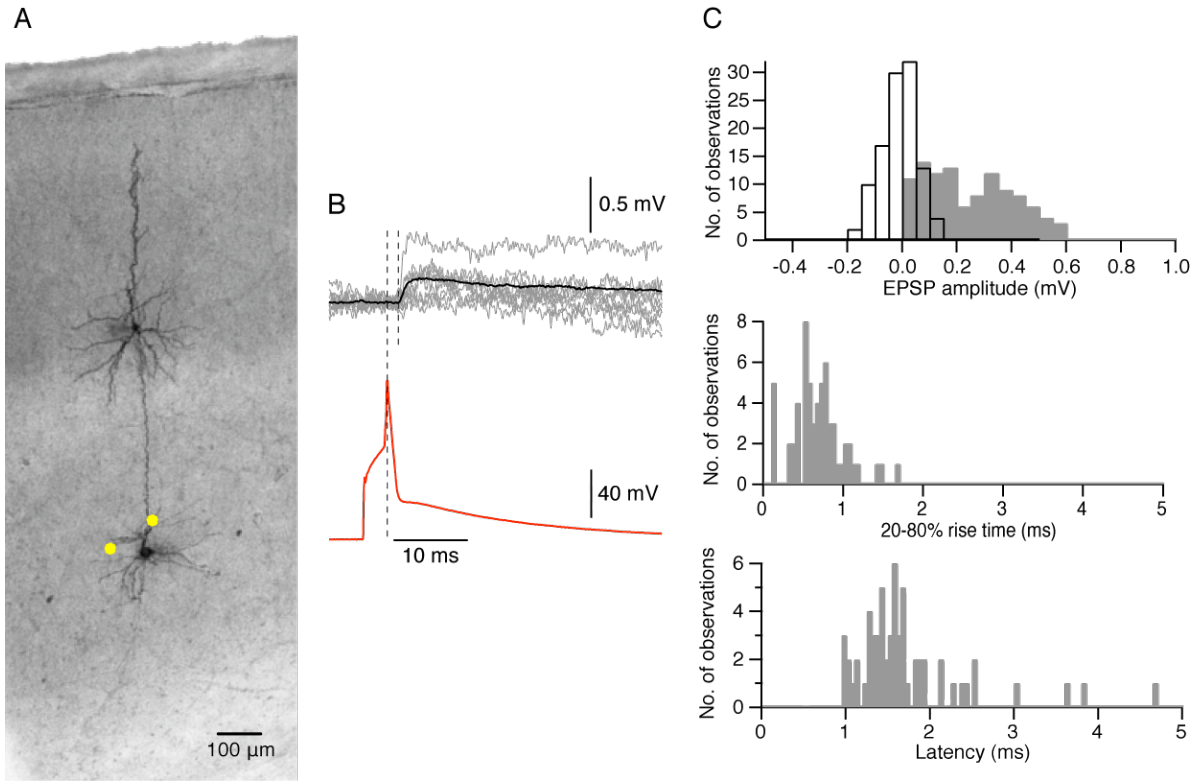


Fig. 3.33 Another example of L4 star pyramid-L6A pyramid connection with fast EPSP (BC 251109 AB). A, Half-tone photomicrograph of the stained slice. Light-microscopically identified putative synaptic contacts are marked by filled yellow circles. B, A presynaptic AP (red trace) and 10 consecutive EPSPs (grey traces) superimposed with the mean EPSP waveform (black trace) are shown. C, EPSP amplitude (black open bars are for noise), 20-80% rise time and latency histograms for this connection.

contacts were identified under the light-microscope. One synapse was located in the basal dendrite near the soma of the postsynaptic L6A pyramidal cell, while the other was found in an apical oblique dendrite close to the soma. The synapse-to-soma distances of these two synapses are 83.8 and 50.3 µm, respectively. The mean synapse-to-soma distance for this pair is 67.1 µm.

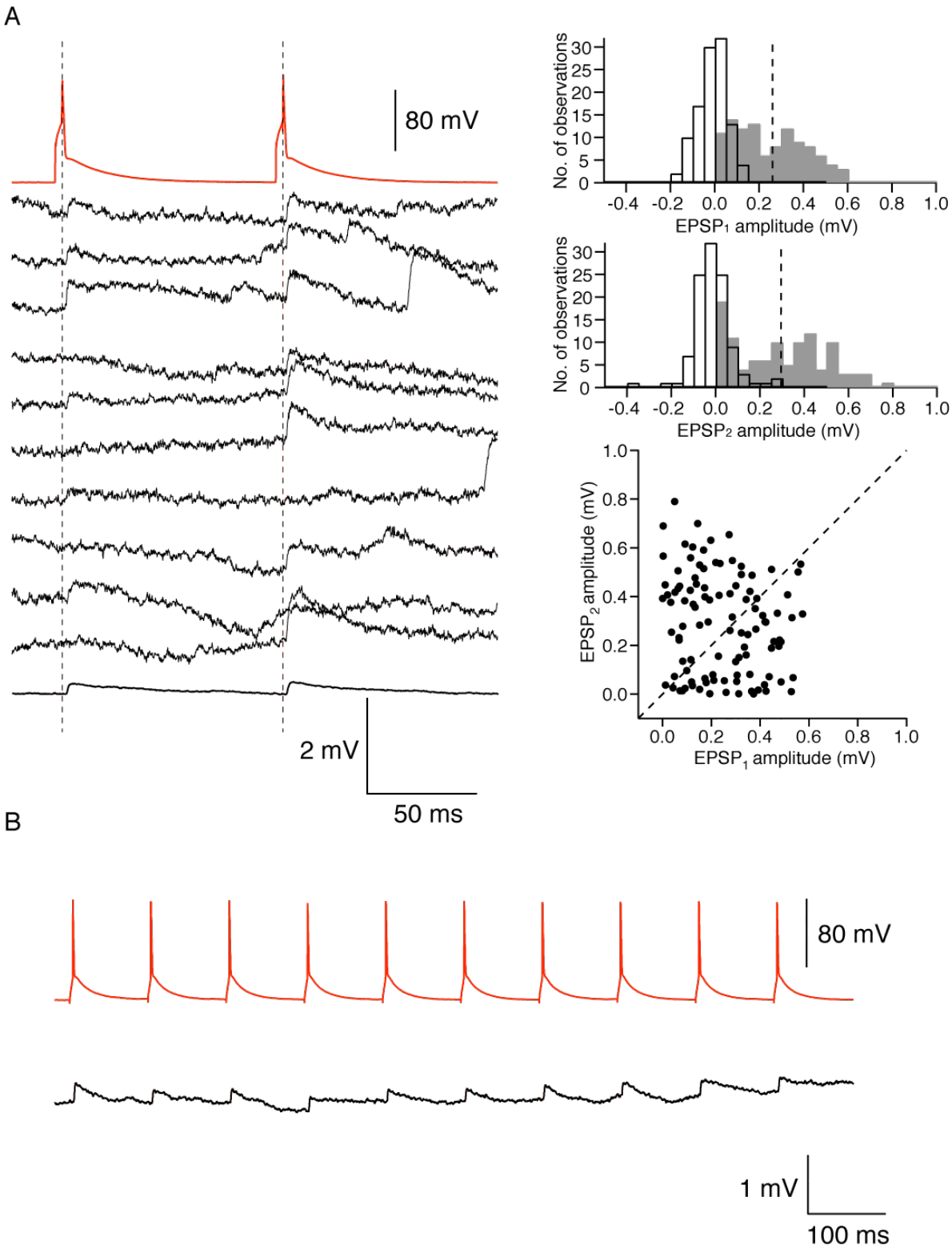


Fig. 3.34 Short-term plasticity of the connection shown in Fig. 3.33. A, Left, Ten consecutive EPSPs (middle) recorded in a postsynaptic L6A pyramidal cell elicited by two APs (top) at 100 ms interval in a presynaptic L4 star pyramidal neuron. The mean EPSP waveform is shown at the bottom. Right, Corresponding EPSP amplitude histograms for the first (top, black open bars are for noise) and second (middle) EPSPs. Comparison of the second and first EPSPs is shown at the bottom. B, Train of ten presynaptic APs at 10 Hz (top trace) and the mean EPSP waveform (black trace).

A pharmacological experiment was done in this L4-L6A fSP pair. Figure 3.32 demonstrates the pharmacological results. The mean EPSP measured in the control condition (amplitude = 0.81 mV, black curve in Fig. 3.32) was largely eliminated by the addition of CNQX (10 µM) to the external solution (amplitude = 0.12 mV, green curve in Fig. 3.32). After a prolonged wash-out, the EPSP was nearly recovered to the control level (amplitude = 0.61 mV, blue curve in Fig. 3.32).

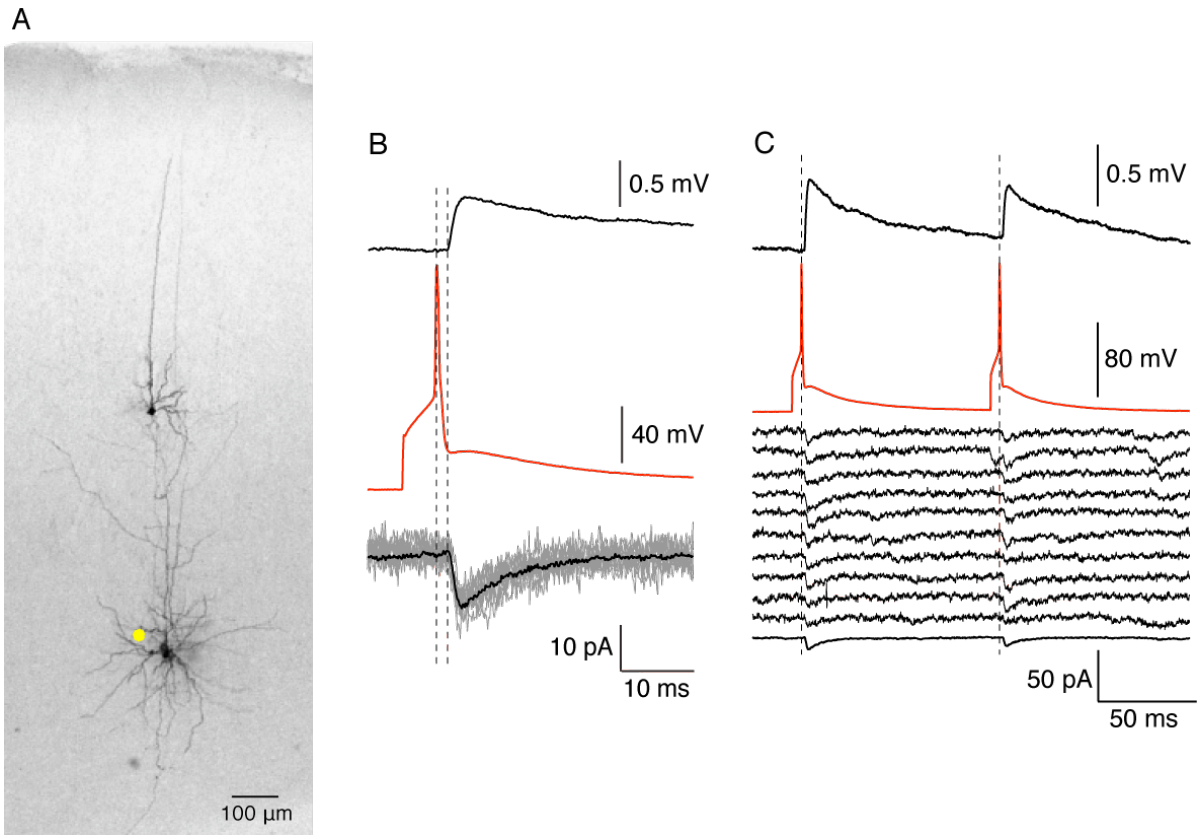


Fig. 3.35 EPSC properties and short-term plasticity of a L4-L6A fSP connection (BC 280509 AB). A, Half-tone photomicrograph of the stained slice. A light-microscopically identified putative synaptic contact is marked by a filled yellow circle. B, A presynaptic AP (red trace), the mean EPSP waveform (top) and 10 consecutive EPSCs (grey traces) superimposed with the mean EPSC waveform (black trace) are shown. C, Ten consecutive EPSCs (middle) recorded in a postsynaptic L6A pyramidal cell elicited by two APs (red trace) at 100 ms interval in a presynaptic L4 star pyramidal neuron. The mean EPSP and EPSC waveforms are shown on the top and at the bottom, respectively.

Another relatively weak L4-L6 fSP connection is shown in Figs. 3.33 and 3.34. The parameters of the mean EPSP for this pair are as follows: amplitude = 0.21 mV, 20-80% rise time = 0.82 ms and latency = 1.56 ms. Two putative synaptic contacts were identified for this connection. Both of them

are located on the basal dendrites near the soma of postsynaptic L6A pyramidal cell. The synapse-to-soma distances are 158.9 and 74.8 µm, respectively. At an ISI of 100 ms the EPSPs at this connection displayed short-term facilitation with PPR of 1.19.

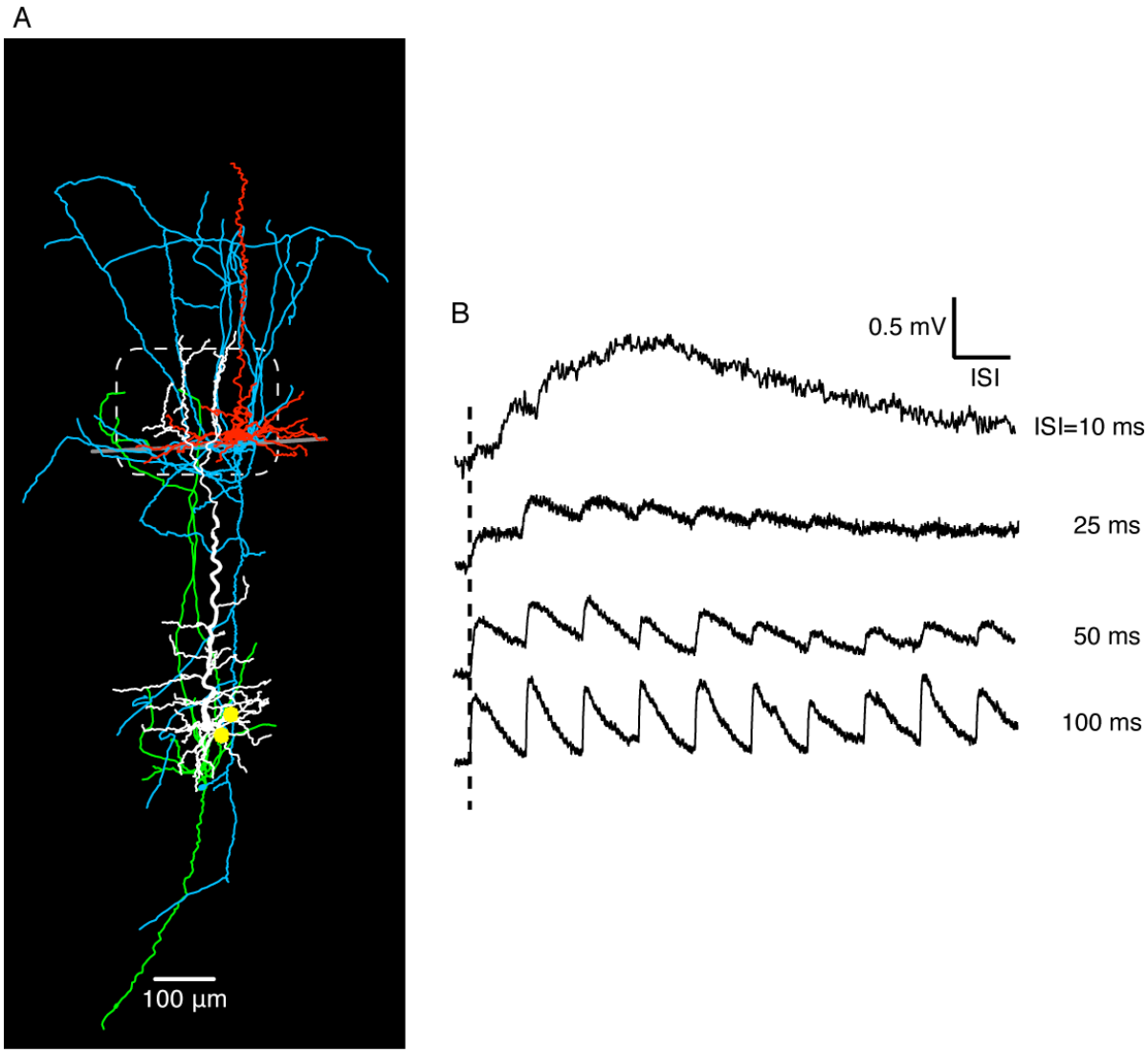


Fig. 3.36 Frequency effect on the short-term plasticity of a L4-L6A fSP connection (BC 041209 CD). A, 2D projection of 3D Neurolucida reconstruction. The axonal arbor (blue) and the somatodendritic arbor (red) of the L4 star pyramidal neuron and the axonal arbor (green) and the somatodendritic arbor (white) of the L6A pyramidal cell are shown. The barrel is indicated by a dashed contour. Light-microscopically identified putative synaptic contacts are marked by filled yellow circles. B, Trains of ten consecutive EPSPs evoked at various interstimulus intervals (ISIs) as indicated on the right.

In another L4-L6A fSP pair EPSCs were recorded and are shown in Fig. 3.35. The average EPSC of this pair had an amplitude of -10.6 pA, a 20-80% rise time of 0.62 ms, a latency of 1.86 ms and a PPR of 0.76. The corresponding mean EPSP characteristics are as follows: amplitude = 0.56 mV,

20-80% rise time = 0.84 ms, latency = 1.58 ms and PPR = 0.73. Only one putative synaptic contact was identified in this connection, and this contact was located in the apical oblique dendrite with 130.3 μm far away from the postsynaptic L6A soma.

The frequency effect on the short-term dynamics of EPSP was studied in another L4-L6 fSP connection (Fig. 3.36). When the firing frequency in the presynaptic neuron was increased from 10 Hz to 100 Hz, the EPSP amplitude in the postsynaptic L6A pyramidal cell exhibited marked depression, while the summation of subsequent EPSPs became more pronounced. Two putative synaptic contacts which are located in the basal dendrites near the postsynaptic soma were identified for this pair. The synapse-to-soma distances of these two synaptic contacts are 55.2 and 40.3 μm, respectively.

3.3.4 L4 star pyramid-L6A pyramidal cell pairs with slow synapses

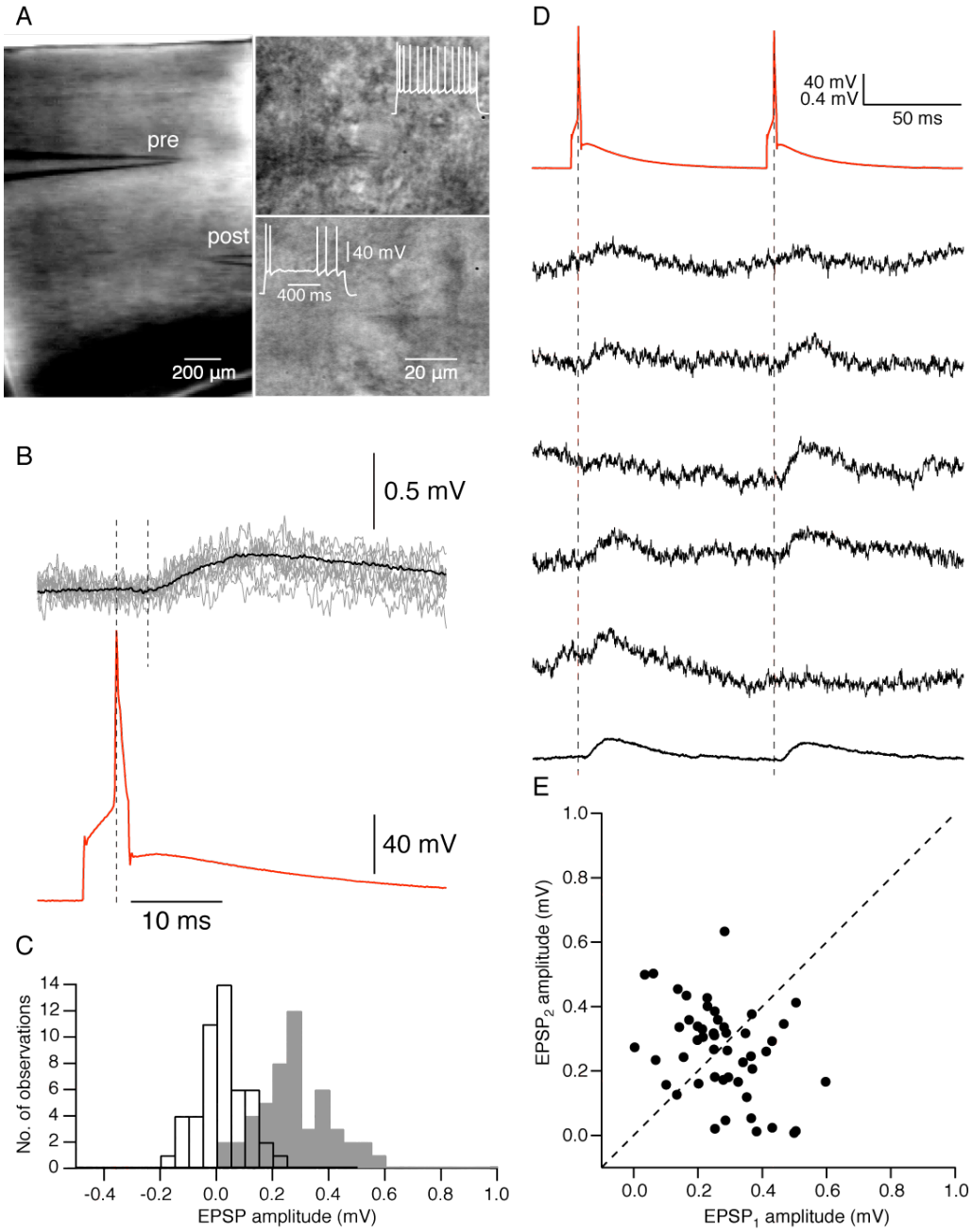


Fig. 3.37 Representative example of a L4 star pyramid-L6A pyramidal cell pair with slow EPSP (BC 130809 AB). A, Left, IR-DIC image of the slice. The pipettes mark the positions of the presynaptic L4 spiny neuron and the postsynaptic L6A pyramidal cell. Right, High-magnification images of the presynaptic L4 star pyramidal neuron (top) and the postsynaptic L6A pyramidal cell (bottom). Insets, the corresponding firing patterns of pre- and postsynaptic neurons. B, A presynaptic AP (red trace) and 10 consecutive EPSPs (grey traces) superimposed with the mean EPSP waveform (black trace) are shown. C, EPSP amplitude histogram for this connection (black open bars are for noise). D, Five consecutive EPSPs (middle) recorded in a postsynaptic L6A pyramidal cell elicited by two APs (top) at 100 ms interval in a presynaptic L4 star pyramidal neuron. The mean EPSP waveform is shown at the bottom. E, Comparison of the second and first EPSPs.

Four L4-L6A sSP connections were found. A representative example of a L4-L6A sSP pair is shown in Fig. 3.37. This pair had a mean EPSP amplitude of 0.23 mV with a 20-80% rise time of 4.98 ms and a latency of 4.92 ms. When two presynaptic APs with an ISI of 100 ms were initiated, the EPSP recorded in the postsynaptic L6A neuron showed paired pulse depression with a PPR of 0.94. The failure rate and CV for this pair are 22.0% and 0.47, respectively. Photographs of the stained slice and two putative synaptic contacts at higher magnification and the Neurolucida reconstruction

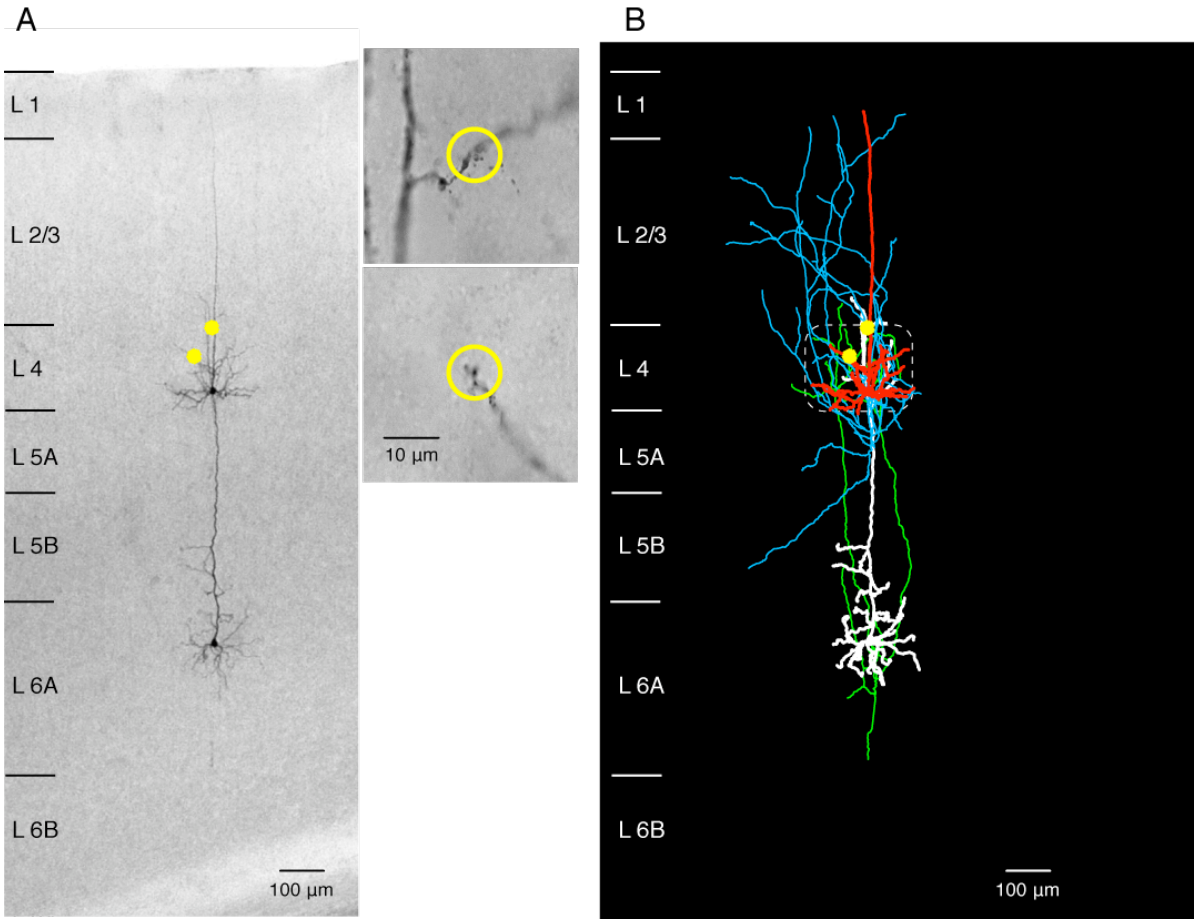


Fig. 3.38 Photomicrographs of the stained slice and its Neurolucida reconstructions (BC 130809 AB). A, Left, Half-tone photomicrograph of a biocytin-filled pair between a star pyramidal neuron in layer 4 and a pyramidal cell in layer 6A. Light-microscopically identified putative synaptic contacts are marked by filled yellow circles. Right, Higher magnification half-tone photomicrographs of two putative synaptic contacts marked by open yellow circles. They are all established on the apical tuft dendrite of the L6A pyramidal cell. B, 2D projection of 3D Neurolucida reconstruction. The axonal (blue) and the somatodendritic arbor (red) of the L4 star pyramidal neuron and the axonal (green) and the somatodendritic arbor (white) of the L6A pyramidal cell are shown. The barrel is indicated by a dashed contour. Light-microscopically identified putative synaptic contacts are marked by filled yellow circles.

of this cell pair are shown in Fig. 3.38. The presynaptic neuron is a L4 SP neuron with its soma being located near the barrel centre in the horizontal direction and near the L4/L5A border in the vertical direction. The basal dendrites of the L4 SP neuron are largely confined to the barrel border and display a nearly symmetric orientation in the horizontal direction. The apical dendrite projected out of the barrel towards the pial surface and reached layer 1 without forming a tuft. The axon of the L4 SP neuron was largely confined to the barrel column with most of its collaterals being sparsely distributed in layers 4 and 2/3 and one descending branch being truncated in the layer 5A/layer 5B border during the slice preparation. The postsynaptic neuron is a L6A short pyramid with its soma being located directly below the presynaptic L4 soma. The dendrite branches of L6A short pyramidal cells were columnar and had two domains: one was located near the soma in L6A (basal dendrites) and the other in the distal part of the apical dendrite in L4 barrel (apical tuft dendrites). The axon of L6A short pyramid was largely columnar organised with vertically oriented axonal collaterals that terminated at the layer 4/layer 2/3 border, where they gave rise to several short branches in the L4 home barrel. In addition, there is a descending axonal branch with nearly no bifurcation in infragranular layers. Therefore, this L6A short pyramid is likely to be a L6A CT

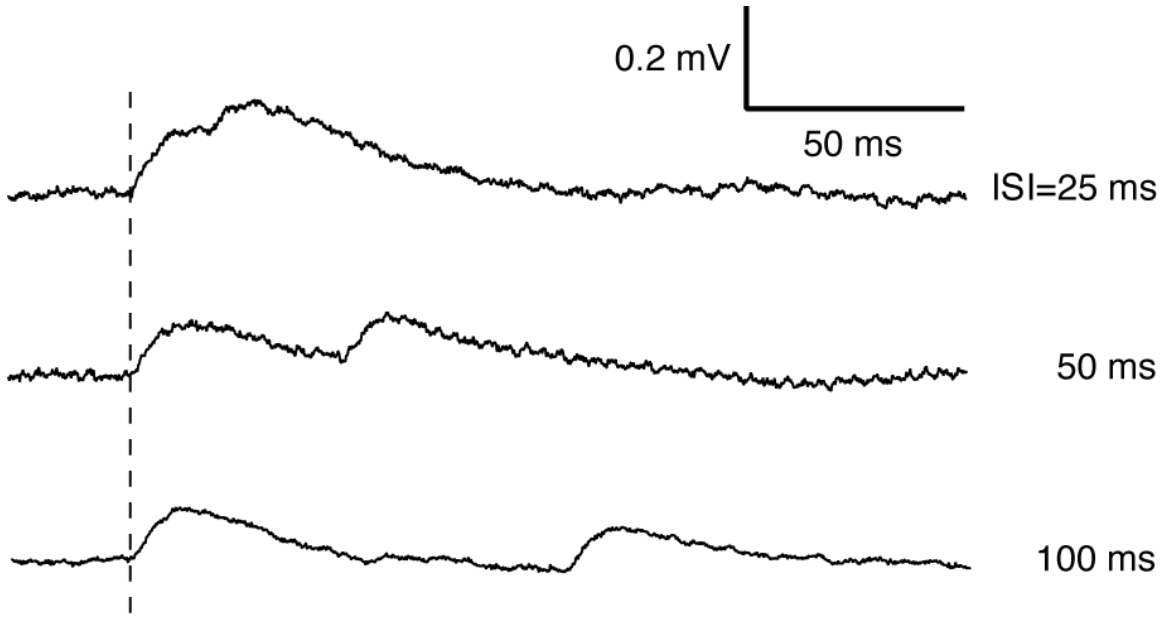


Fig. 3.39 Frequency effect on the short-term plasticity of the connection shown in Fig. 3.37. Trains of two consecutive EPSPs were evoked at various interstimulus intervals (ISIs) as indicated on the right.

neuron (*cf.* (Zhang and Deschenes 1997; Kumar and Ohana 2008)). Two putative synaptic contacts, which were located on the apical tuft of the postsynaptic L6A pyramidal cell, were found for this pair. The synapse-to-soma distances for these two synapses are 731.9 and 674.4 µm, respectively. The mean synapse-to-soma distance for this connection is 703.2 µm.

The frequency dependence of the short-term dynamics of the EPSP was also studied in this pair. When two presynaptic APs with decreasing ISI were elicited (corresponding to an increasing firing frequency in the presynaptic neuron), the postsynaptic EPSPs exhibited a paired-pulse depression while a marked summation appeared at the same time (see Fig. 3.39).

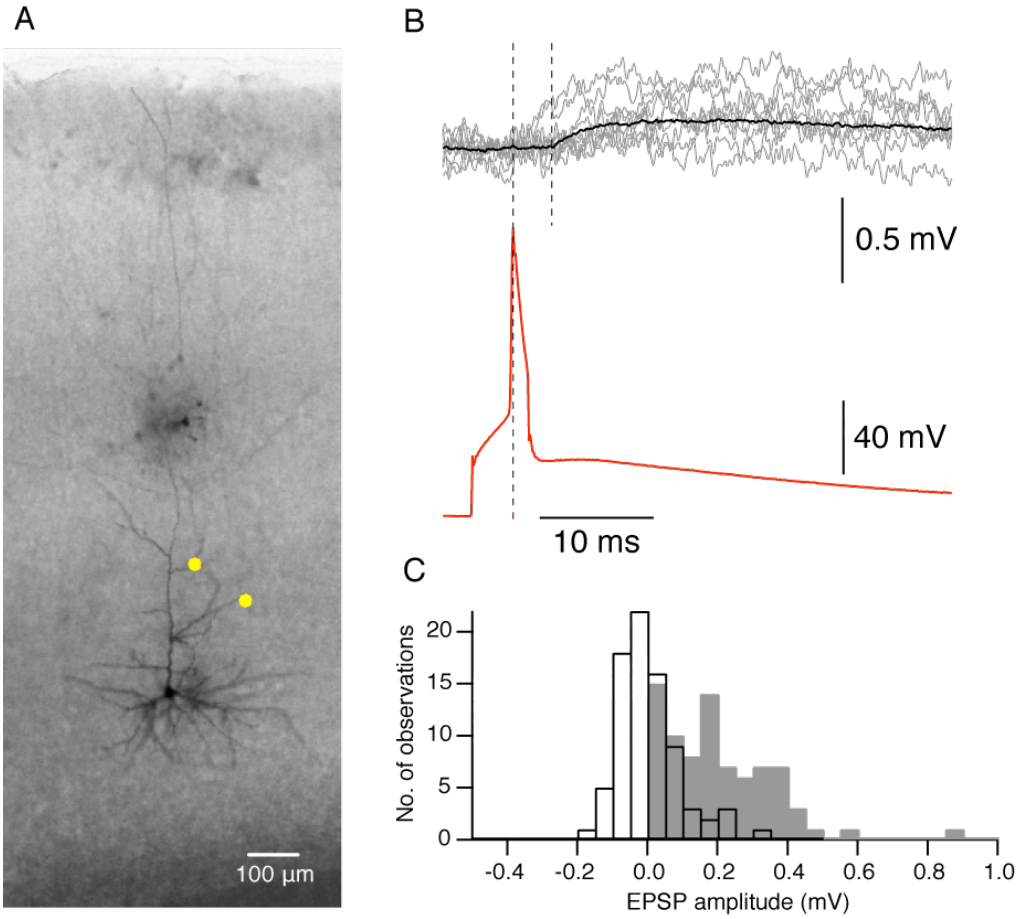


Fig. 3.40 Another example of L4 star pyramid-L6A pyramid connection with slow EPSP (BC 151009 AB). A, Half-tone photomicrograph of the stained slice. Light-microscopically identified putative synaptic contacts are marked by filled yellow circles. B, A presynaptic AP (red trace) and 10 consecutive EPSPs (grey traces) superimposed with the mean EPSP waveform (black trace) are shown. C, EPSP amplitude histogram for this connection (black open bars are for noise).

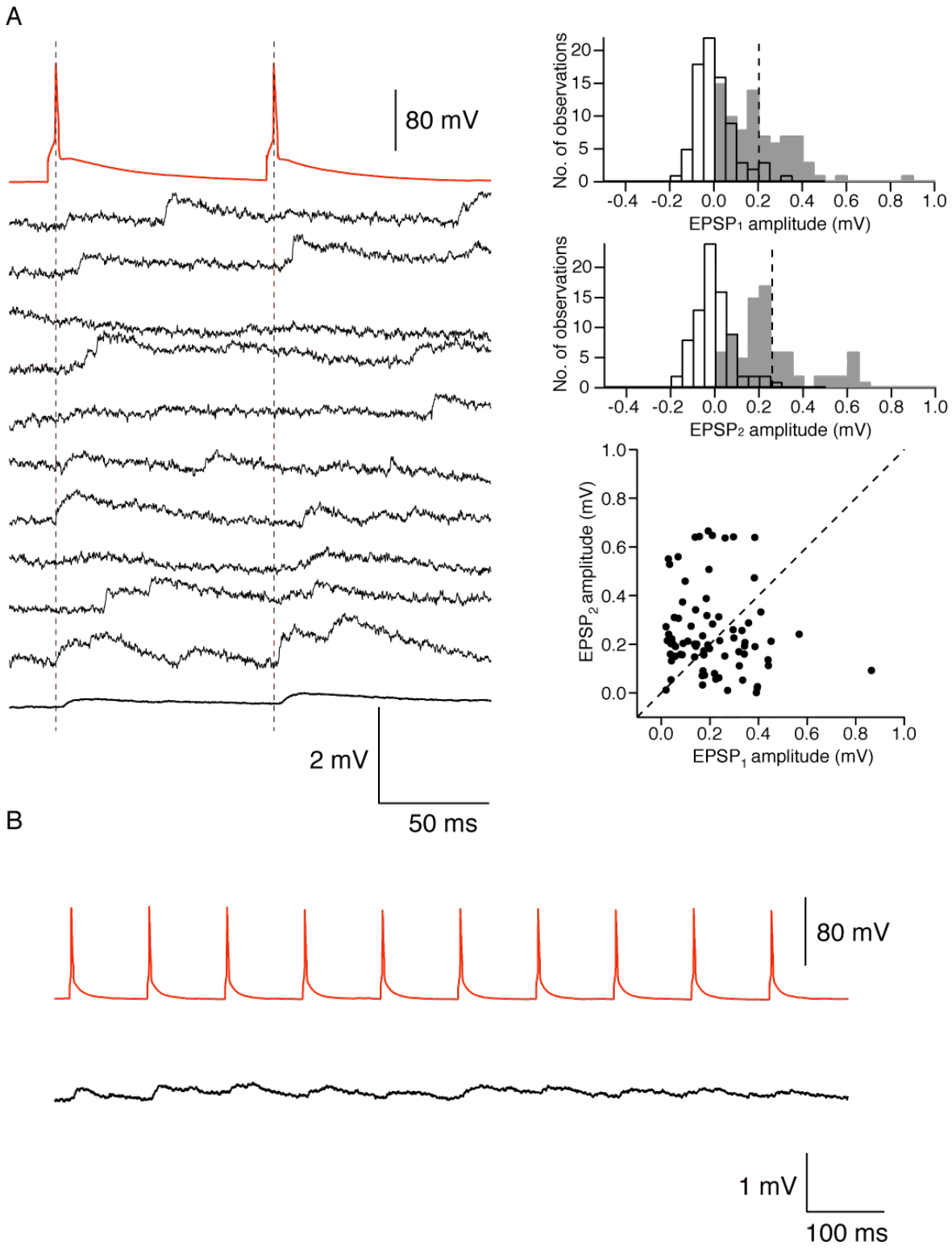


Fig. 3.41 Short-term plasticity of the connection shown in Fig. 3.40. A, Left, Ten consecutive EPSPs (middle) recorded in a postsynaptic L6A pyramidal cell elicited by two APs (top) at 100 ms interval in a presynaptic L4 star pyramidal neuron. The mean EPSP waveform is shown at the bottom. Right, Corresponding EPSP amplitude histograms for the first (top, black open bars are for noise) and second (middle) EPSPs. Comparison of the second and first EPSPs is shown at the bottom. B, Train of ten presynaptic APs at 10 Hz (top trace) and the mean EPSP waveform (black trace).

Another L4-L6A sSP connection with weak synaptic coupling is shown in Figs. 3.40 and 3.41. The mean EPSP of this pair showed the amplitude (0.16 mV), 20-80% rise time (3.31 ms), latency (3.29 ms), and demonstrated short-term facilitation with a PPR = 1.37. Morphologically, two putative synaptic contacts for this connection were identified with synapse-to-soma distances of 359.9 and 310.2 μm, respectively. The mean synapse-to-soma distance for this pair is 335.1 μm.

3.3.5 Summary of data

In summary, seven L4-L6A SS, seven L4-L6 fSP and four L4-L6A sSP connections were measured. The electrophysiological and morphological data extracted from these L4-L6A pairs were analysed. Some general conclusions similar to (or different from) that of intralaminar L4-L4 and L6A-L6A excitatory connections are given as shown below.

Table 3.5. EPSP characteristics of L4-L6A SS excitatory connections.

	Amplitude (mV)	20-80% rise time (ms)	Latency (ms)	Paired-pulse ratio	Failure rate (%)	Coefficient of variation
Mean	0.29	6.70	3.77	0.95	25.0	0.50
SD	0.16	2.08	1.57	0.28	16.4	0.11
Range	0.12 - 0.55	2.94 - 9.15	2.16 - 6.14	0.45 - 1.24	10.1 - 46.7	0.40 - 0.65
n	6	6	6	6	6	6

Table 3.6. Passive properties of postsynaptic L6A pyramidal cells.

	V_{rest} (mV)	Input resistance (MΩ)	Time constant (ms)
Mean	-71.7	128.7	17.2
SD	1.8	36.2	2.5
Range	-74.0 - -69.0	61.8 - 168.8	13.8 - 21.1
n	6	6	6

Table 3.7. EPSP characteristics of L4-L6A fSP excitatory connections.

	Amplitude (mV)	20-80% rise time (ms)	Latency (ms)	Paired-pulse ratio	Failure rate (%)	Coefficient of variation
Mean	0.37	1.48	1.65	1.12	21.0	0.59
SD	0.23	0.87	0.20	0.23	22.1	0.22
Range	0.07 - 0.74	0.82 - 3.05	1.37 - 1.87	0.73 - 1.38	1.7 - 62.6	0.33 - 0.83
n	7	7	7	7	6	6

Table 3.8. Passive properties of postsynaptic L6A pyramidal cells.

	V_{rest} (mV)	Input resistance (MΩ)	Time constant (ms)
Mean	-72.9	193.4	26.4
SD	3.2	87.7	11.2
Range	-79.0 - -70.0	105.4 - 306.6	16.6 - 44.5
n	7	7	7

Table 3.9. EPSP characteristics of L4-L6A sSP excitatory connections.

	Amplitude (mV)	20-80% rise time (ms)	Latency (ms)	Paired-pulse ratio	Failure rate (%)	Coefficient of variation
Mean	0.26	5.42	3.70	0.97	27.8	0.61
SD	0.16	1.67	0.82	0.28	16.5	0.14
Range	0.16 - 0.50	3.31 - 7.18	3.21 - 4.92	0.70 - 1.37	8.3 - 46.9	0.47 - 0.75
n	4	4	4	4	4	4

Table 3.10. Passive properties of postsynaptic L6A pyramidal cells.

	V_{rest} (mV)	Input resistance (MΩ)	Time constant (ms)
Mean	-75.0	175.8	24.0
SD	1.8	61.7	7.5
Range	-77.0 - -73.0	134.5 - 267.7	15.8 - 32.8
n	4	4	4

Table 3.11. Synapse-to-soma distances of L4-L6A excitatory connections.

	L4-L6A SS dist. (μm)	L4-L6A fSP dist. (μm)	L4-L6A sSP dist. (μm)
Mean	590.6	86.4	524.2
SD	136.9	54.1	166.8
Range	275.2 - 801.1	24.7 - 183.5	310.2 - 731.9
n	15	13	6

Tables 3.5, 3.6 and 3.7, 3.8 and 3.9, 3.10 give detailed parameters of the EPSP characteristics and passive properties of postsynaptic L6A pyramidal cells for L4-L6A SS, fSP and sSP excitatory connections, respectively. Table 3.11 summarises the synapse-to-soma distances for three connection phenotypes.

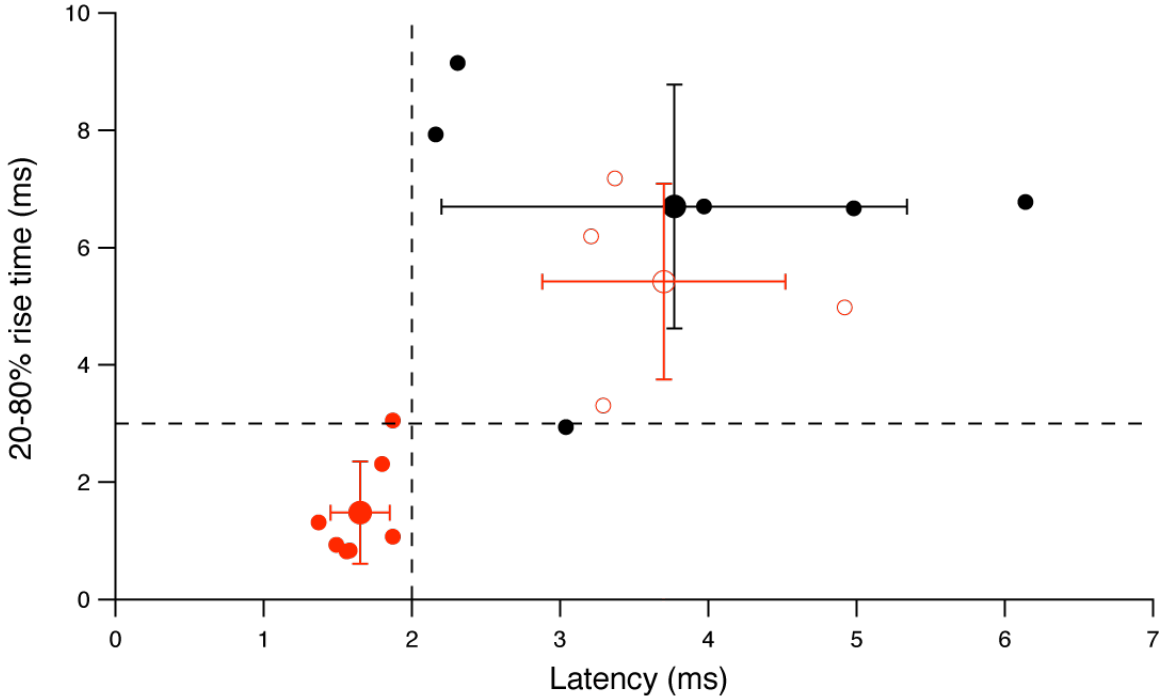


Fig. 3.42 Summary plot of 20-80% rise time versus latency for three types of L4-to-L6A excitatory connections. Black filled dots, red filled dots and red open dots represent the data from individual L4-L6A SS, L4-L6A fSP and L4-L6A sSP pairs, respectively. Larger dots with error bars stand for the mean and standard deviation value of the corresponding L4-L6A connection phenotypes.

Fig. 3.42 gives the plots of 20-80% rise time versus latency for three L4-L6A connection groups. For L4 SS-L6A connections, all pairs demonstrated slow 20-80% rise time (6.70 ± 2.08 ms, range 2.94 - 9.15 ms, n = 6) and long latency (3.77 ± 1.57 ms, range 2.16 - 6.14, n = 6). L4 sSP-L6A connections showed the similar distribution pattern with 20-80% rise time (5.42 ± 1.67 ms, range 3.31 - 7.18 ms, n = 4) and latency (3.70 ± 0.82 ms, range 3.21 - 4.92 ms, n = 4). On the contrary, L4 fSP-L6A connections had a fast 20-80% rise time (1.48 ± 0.87 ms, range 0.82 - 3.05 ms, n = 7) and a short latency (1.65 ± 0.20 ms, range 1.37 - 1.87 ms, n = 7).

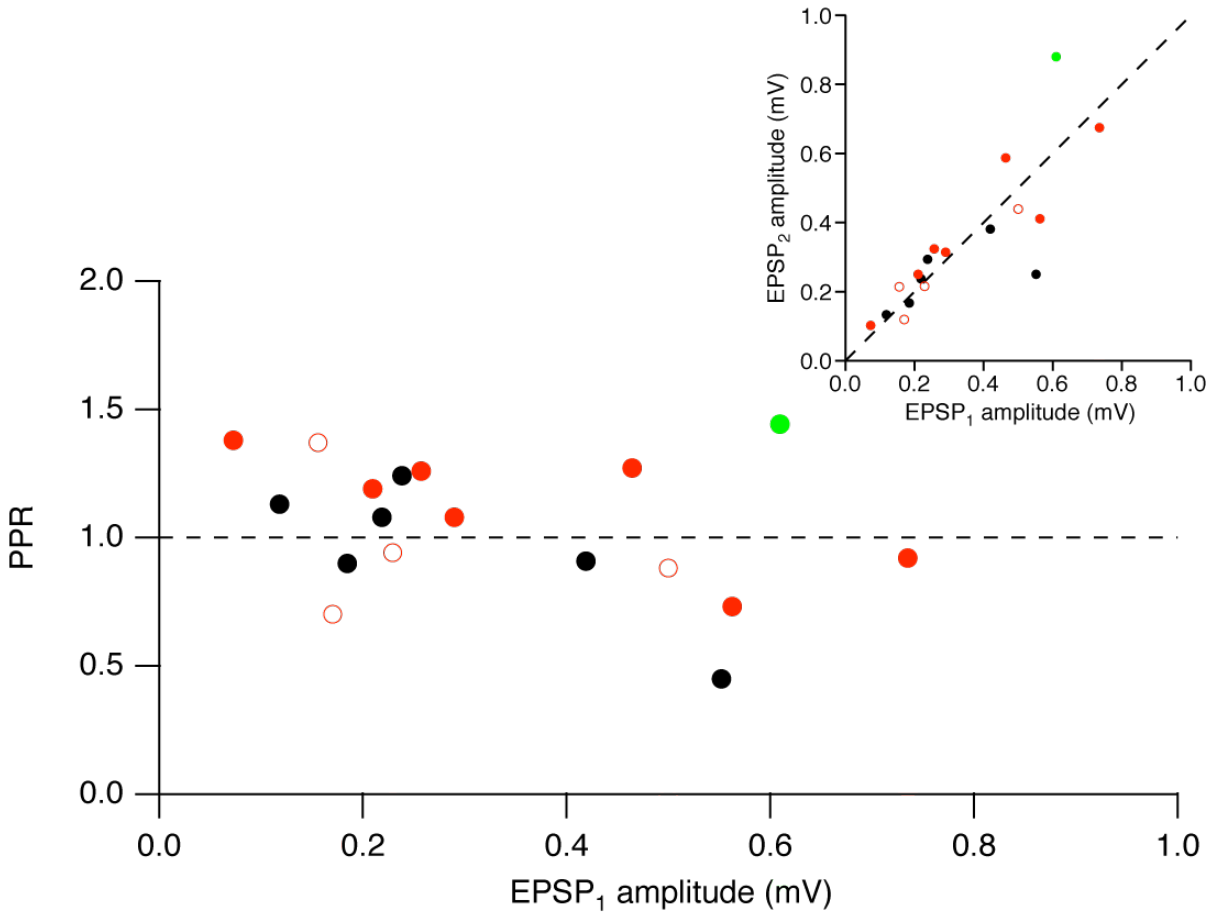


Fig. 3.43 Summary plot of paired-pulse ratio (PPR) versus the 1st EPSP amplitude for three types of L4-to-L6A excitatory connections. Black filled dots, red filled dots and red open dots represent the data from individual L4 SS-L6A, L4 fSP-L6A and L4 sSP-L6A pairs, respectively. The green filled dot is for a morphologically unidentified L4-L6A pair. Inset, Plot of the 2nd EPSP amplitude versus the 1st EPSP amplitude.

With respect to short-term synaptic plasticity, there is a general rule for all of three types of L4-L6A connections: weak connections tended to show short-term facilitation while strong ones exhibit short-term depression (see Fig. 3.43). However, the linear correlation between PPR and the 1st EPSP amplitude is not statistical significant ($r = -0.33$, $P = 0.91$).

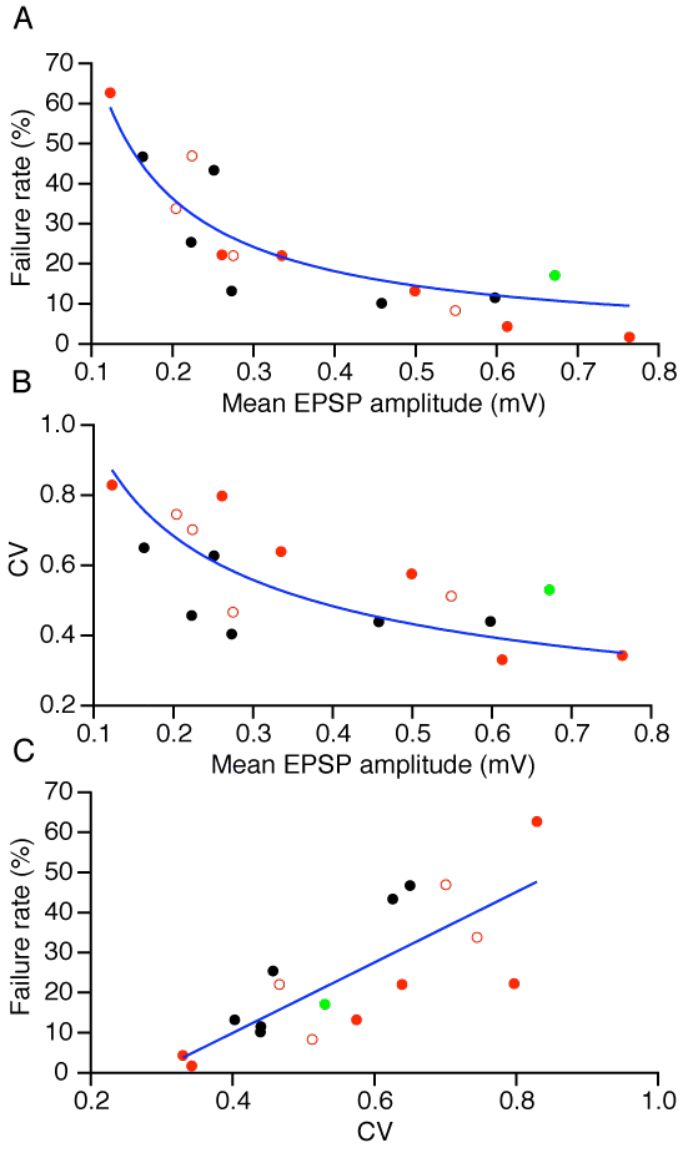


Fig. 3.44 Summary of the relationship between synaptic properties for three types of L4-to-L6A excitatory connections. A, Plot of failure rate versus mean EPSP amplitude. B, CV versus mean EPSP amplitude. C, Failure rate versus CV. Black filled dots, red filled dots and red open dots represent the data from individual L4-L6A SS, L4-L6A fSP and L4-L6A sSP pairs, respectively. The green filled dot is for a morphologically unidentified L4-L6A pair. Best hyperbolic or linear fits (blue lines) are also shown.

The failure rate and the CV are closely correlated to the mean EPSP amplitude: connections with small EPSP amplitude demonstrated high failure rate and CV, whereas ones with large EPSP amplitude showed low failure rate and CV. The failure rate and the CV are linearly correlated ($r = 0.78$, $P = 1.01 \times 10^{-4}$), as shown in Fig. 3.44.

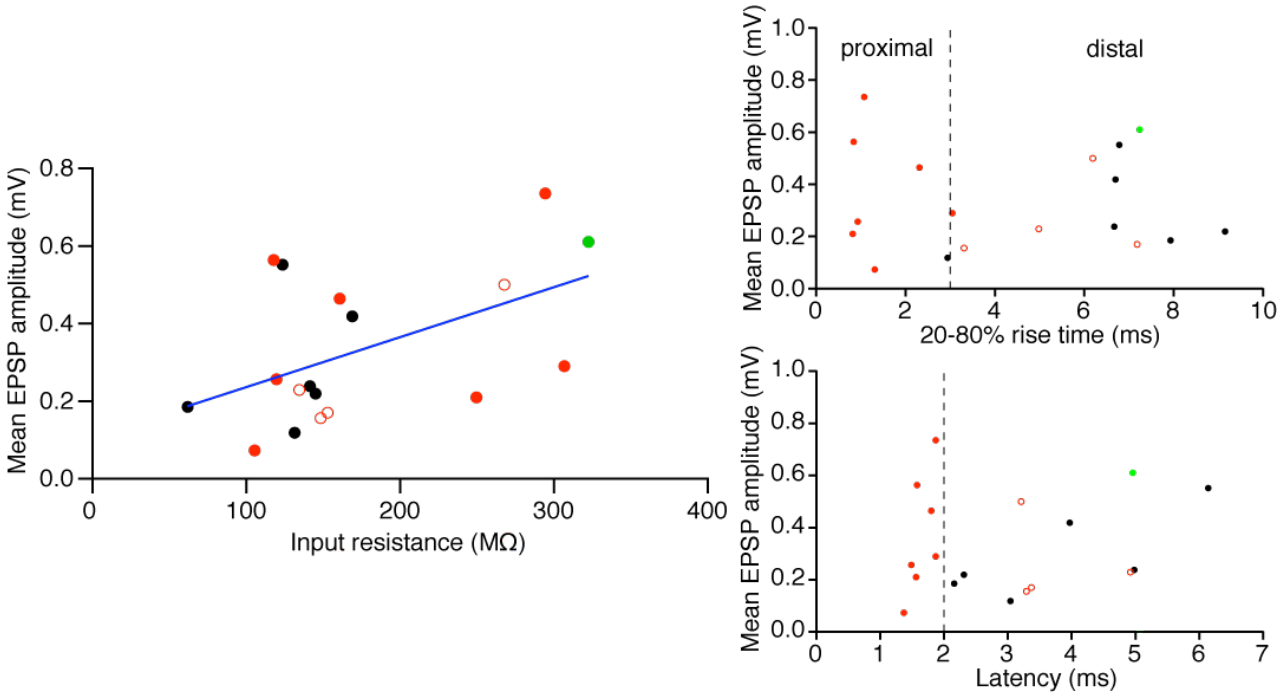


Fig. 3.45 Summary plot of mean EPSP amplitude versus input resistance, 20-80% rise time or latency for three types of L4-to-L6A excitatory connections. Black filled dots, red filled dots and red open dots represent the data from individual L4-L6A SS, L4-L6A fSP and L4-L6A sSP pairs, respectively. The green filled dot is for a morphologically unidentified L4-L6A pair. Best linear fit (blue line) is also shown in the left panel.

A statistically significant correlation (r = 0.51, P = 0.01) between the mean EPSP amplitude and the input resistance of postsynaptic neuron was found in L4-L6A connections. An interesting phenomenon was discovered: with increasing 20-80% rise time and latency, the mean EPSP amplitude first decreased and then increased (see Fig. 3.45). This means that, from the somatic point of view, the distal and proximal inputs in L4-L6A excitatory connections contributed nearly equally to the postsynaptic firing in L6A pyramidal cells if only the EPSP amplitude being considered, which is different from that described in other short-range (*e.g.*, L4-L4 and L6A-L6A connections given above) and long-range (*e.g.*, L2/3-L5 connections in rat barrel cortex (Williams and Stuart 2002)) excitatory connections.

Five representative pairs from each of three L4-L6A connection phenotypes were chosen to demonstrate the axonal and dendritic morphologies of pre- and postsynaptic neurons and the

synaptic patterns. Furthermore, the presynaptic axonal and postsynaptic dendritic density maps and the innervation domain were calculated based on the data from these pairs. Figs. 3.46, 3.47 and 3.48 summarise the results.

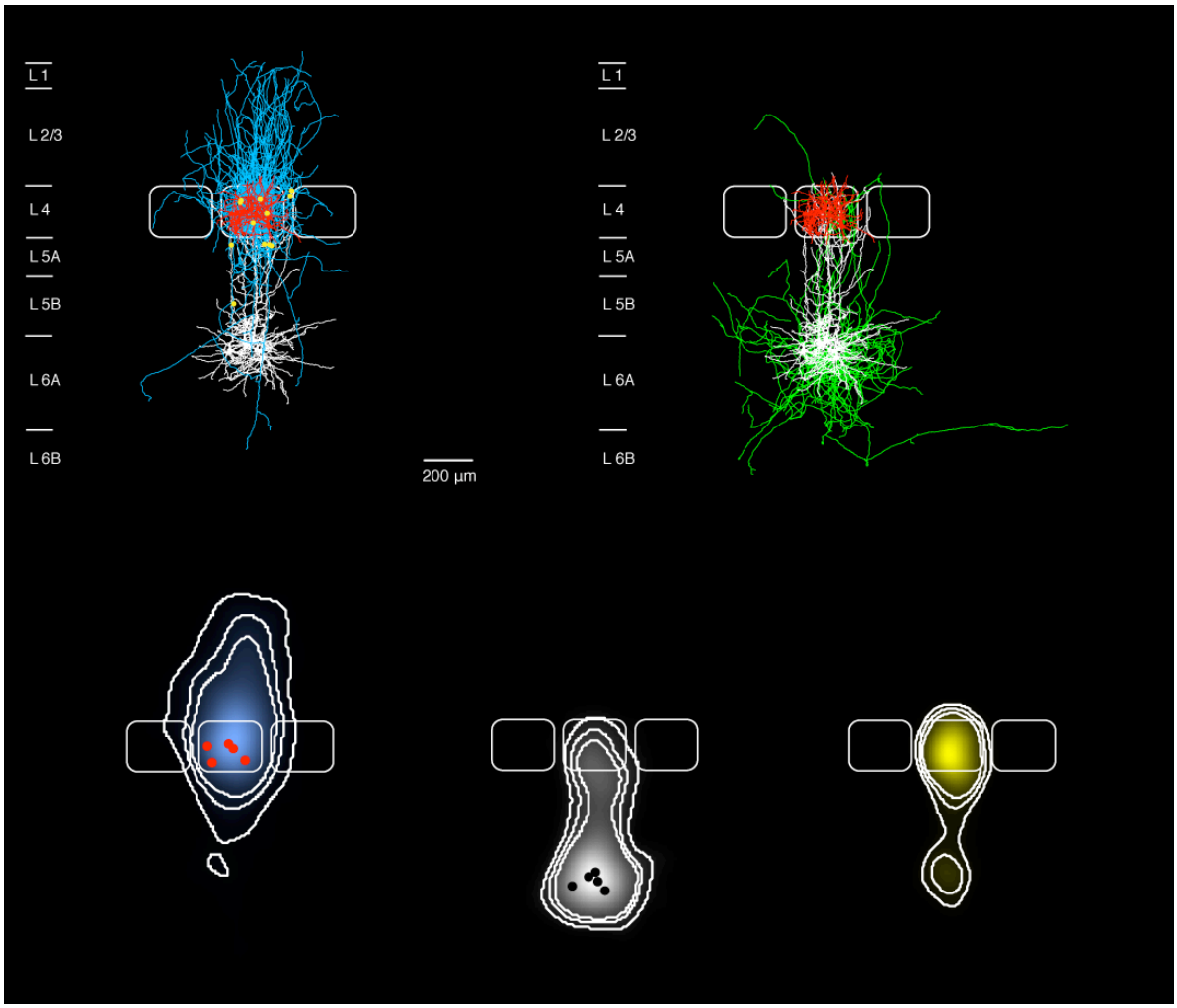


Fig. 3.46 Overlay and density maps of L4-to-L6A SS connections. Top left, Barrel-centered overlay of five synaptically coupled L4-L6A SS pairs. The average barrel in the centre is outlined in white; two neighbouring barrels are added symbolically. Putative synaptic contacts (yellow filled dots) are also shown. Top right, Superposition of Neurolucida reconstructions of the postsynaptic L6A pyramidal cell axons from the same L4-L6A pairs as on the left, aligned with respect to the barrel centre. The somatodendritic arbors of the postsynaptic L6A pyramidal cells (white) and that of the presynaptic L4 spiny stellate neurons (red) are also shown. Bottom, 2D maps of axonal (left) and dendritic (middle) length density of synaptically coupled L4 spiny stellate neurons and L6A pyramidal cells, respectively. The predicted innervation domain (right) of L6A dendrites by L4 axons is given by the product of the L4 axonal density and the L6A dendritic density. Contours (thick white lines) enclosing 70, 80 and 90% of the integrated density are shown superimposed. Positions of L4 spiny stellate neuron somata (red dots), L6A pyramidal cell somata (black dots), and outlines of barrels (thinner white lines) are indicated symbolically.

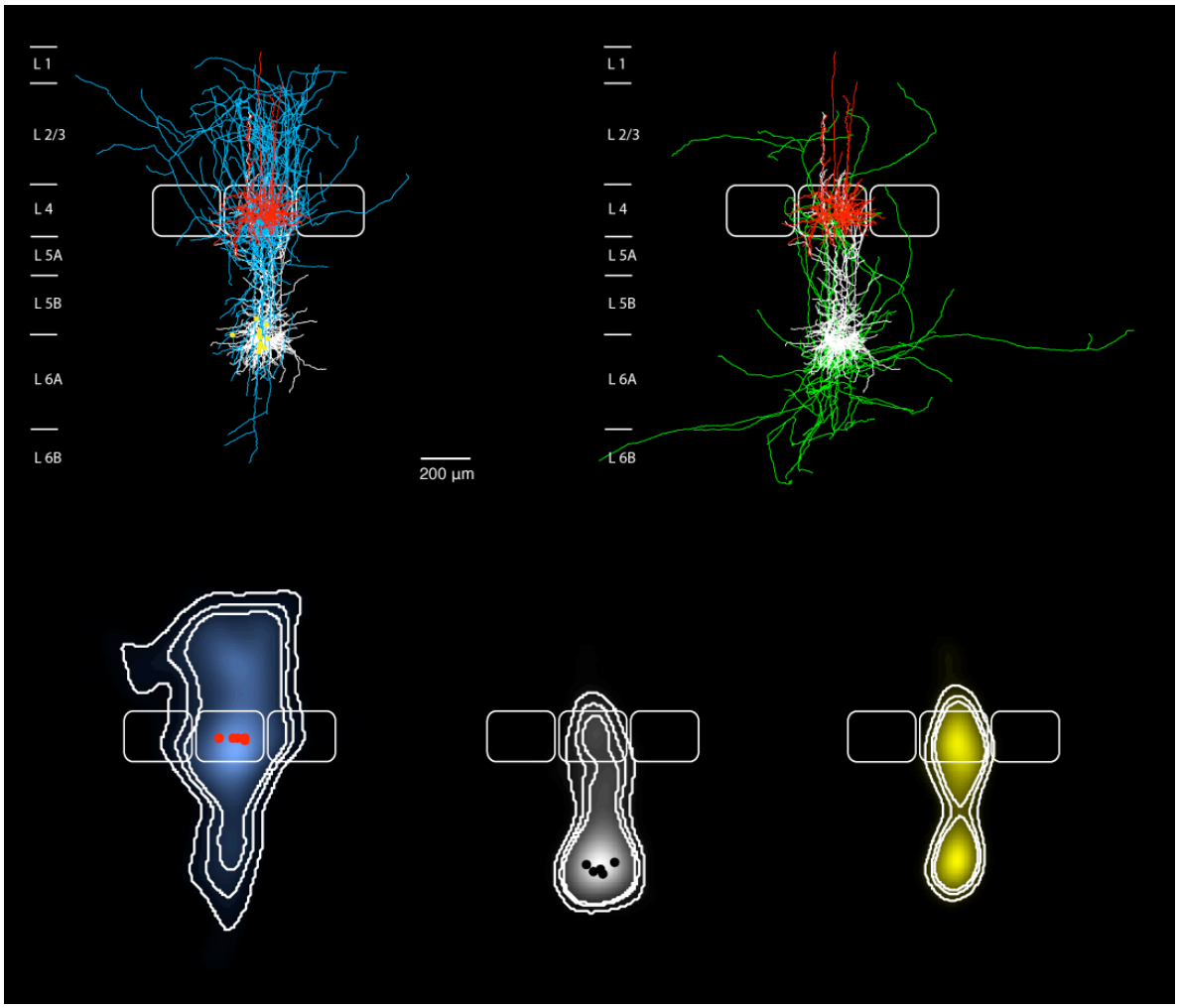


Fig. 3.47 Overlay and density maps of L4-to-L6A fSP connections. Same as in Fig. 3.46 but for five synaptically coupled L4-L6A fSP pairs.

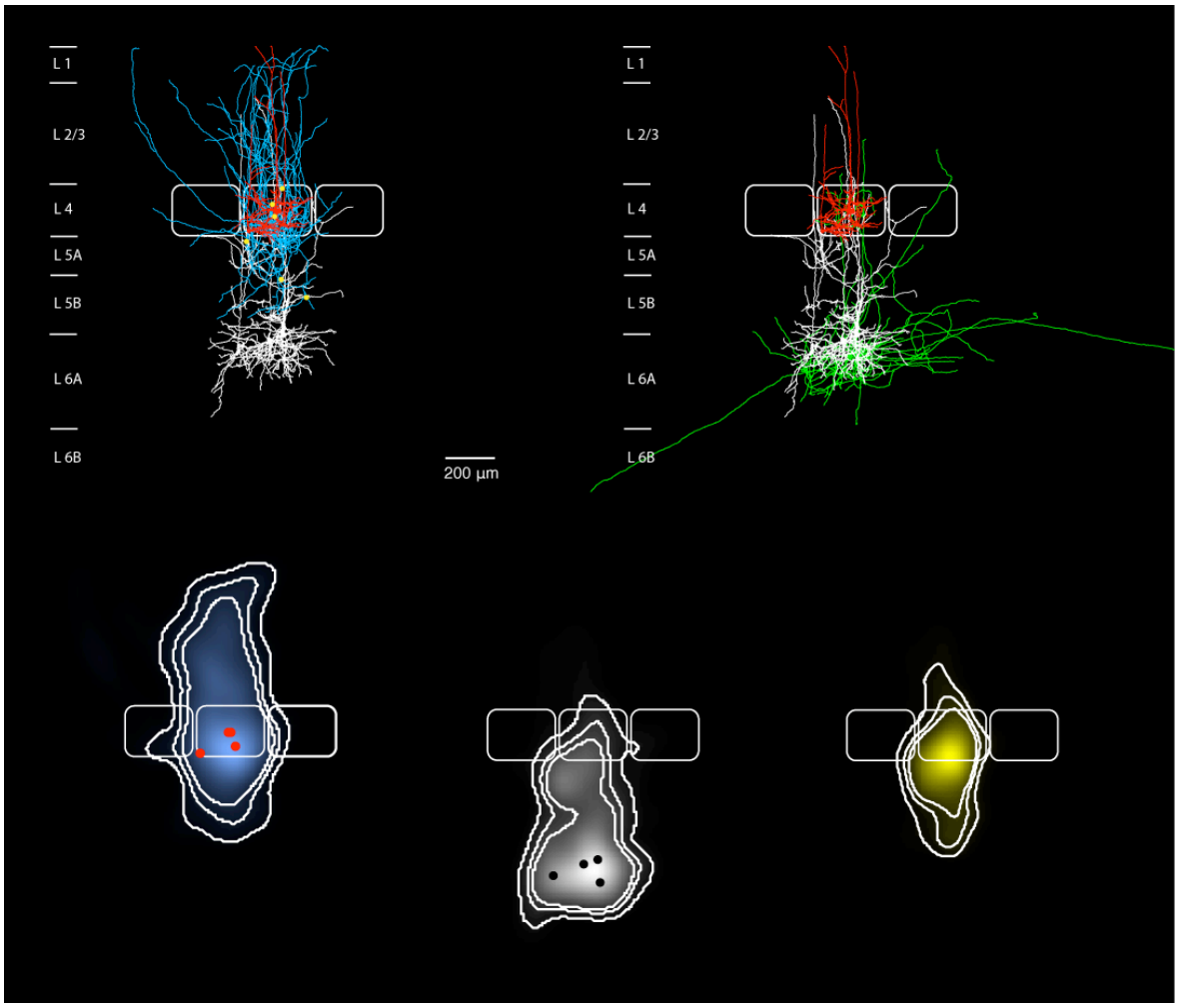


Fig. 3.48 Overlay and density maps of L4-to-L6A sSP connections. Same as in Fig. 3.46 but for four synaptically coupled L4-L6A sSP pairs.

3.4 Several interesting findings

3.4.1 Tight correlation between geometric and functional properties

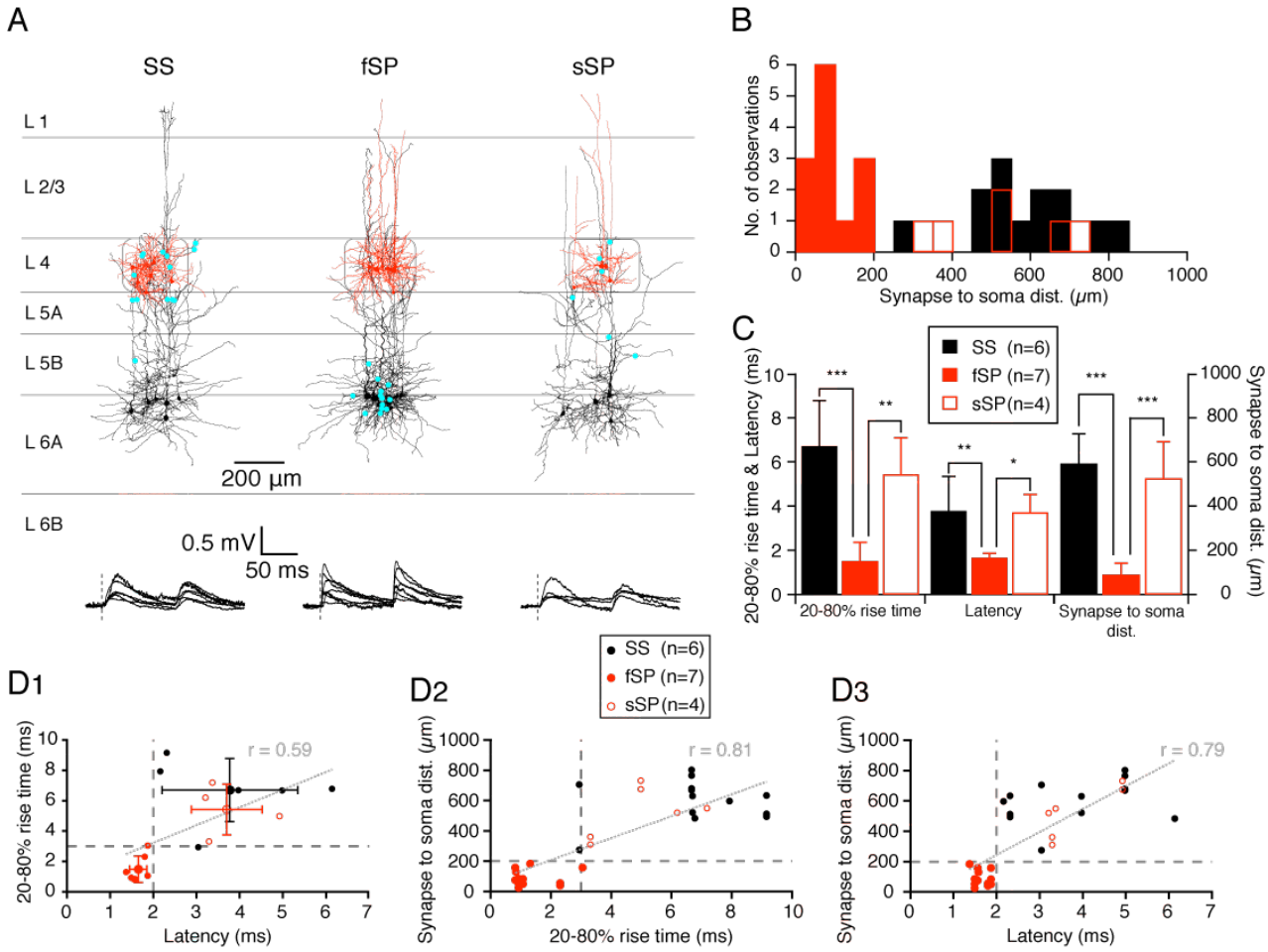


Fig. 3.49 Geometric and functional properties of L4-to-L6A excitatory connections. A, Top, Pre- and postsynaptic somatodendritic structures of the three types of L4-L6A excitatory connections, *i.e.,* SS, fSP, and sSP. The somatodendritic domains of L4 spiny neurons and L6A pyramidal cells are shown in red and black, respectively. Light-microscopically identified putative synaptic contacts are marked by filled light-blue circles. Here, L4 spiny neurons and L6A pyramidal cells were aligned with respect to the barrel centre. Bottom, Overlay of mean EPSPs of individual L4-L6A pairs within their corresponding groups. Each mean EPSP was aligned with respect to the peak time of presynaptic AP (vertical dashed line). B, Distribution of synapse-to-soma distances for the three L4-L6A excitatory connection phenotypes. C, Comparison of 20-80% rise time, latency, and synapse-to-soma distance. *p < 0.05, **p < 0.01, ***p < 0.001, Tukey's test for statistical comparisons of multiple groups. D, D1, Plots of 20-80% rise time versus latency of mean EPSPs for three types of L4-L6A connections. The rise time correlates well with the latency in L4-L6A connections (best linear fit, grey dotted line, r = 0.59). Vertical and horizontal grey dashed lines are drawn just for eye. D2, D3, Plots of synapse-to-soma distance versus 20-80% rise time and latency of mean EPSPs, respectively. Best linear fit (grey dotted line) and r are also shown.

Fig. 3.49A shows the pre- and postsynaptic somatodendritic morphologies of the three types of L4-L6A excitatory connections. The overlay of the mean EPSP waveforms for the individual connections in each of the three categories and the corresponding putative synaptic contacts are also shown. For the three connection types, the distributions of putative synaptic contacts are clearly different: for all SS and the sSP connections, putative synaptic contacts are almost exclusively located on the distal apical tuft dendrites of L6A pyramidal cells. For fSP connections, synaptic contacts are exclusively located on the proximal basal and proximal apical oblique dendrites. Note that the synapse distribution on the apical dendrite is more dispersed for sSP connections than for SS connections. The distribution of geometric distances from putative synaptic contacts to postsynaptic L6A somata for three types of L4-L6A connections is shown in Fig. 3.49B. The distribution for fSP connections is clearly separated from those of the SS and sSP connections. A comparison of the rise time, latency, and synapse-to-soma distance among the three L4-L6A connection types is shown in Fig. 3.49C. For SS, fSP, and sSP connections, the 20-80% rise time, latency, and synapse-to-soma distance are 6.7 ± 2.1 ms (n = 6), 1.5 ± 0.9 ms (n = 7), and 5.4 ± 1.7 ms (n = 4); 3.8 ± 1.6 ms (n = 6), 1.7 ± 0.2 ms (n = 7), and 3.7 ± 0.8 ms (n = 4); 591 ± 137 μm (n = 6), 86 ± 54 μm (n = 7), and 524 ± 167 μm (n = 4), respectively. No obvious differences in the EPSP amplitude (P = 0.56, one-way ANOVA), paired-pulse ratio (P = 0.48), failure rate (P = 0.85), or coefficient of variation (P = 0.56) were observed for the three connection types. Furthermore, the resting membrane potential (P = 0.15), input resistance (P = 0.25), and time constant (P = 0.16) of the postsynaptic L6 pyramidal cells are also not significantly different. Plots of rise time versus latency between all L4-L6A pairs reveal two clusters: one with a fast rise time (< 3 ms) and a short latency (< 2 ms) while the other has a slow rise time (> 3 ms) and a long latency (> 2 ms) (Fig. 3.49D1). The 2nd cluster can be further divided into two subtypes based on the presynaptic cell type: spiny stellate *vs*. star pyramid. For comparison, ten L4-L4 (two are reciprocally connected) and five

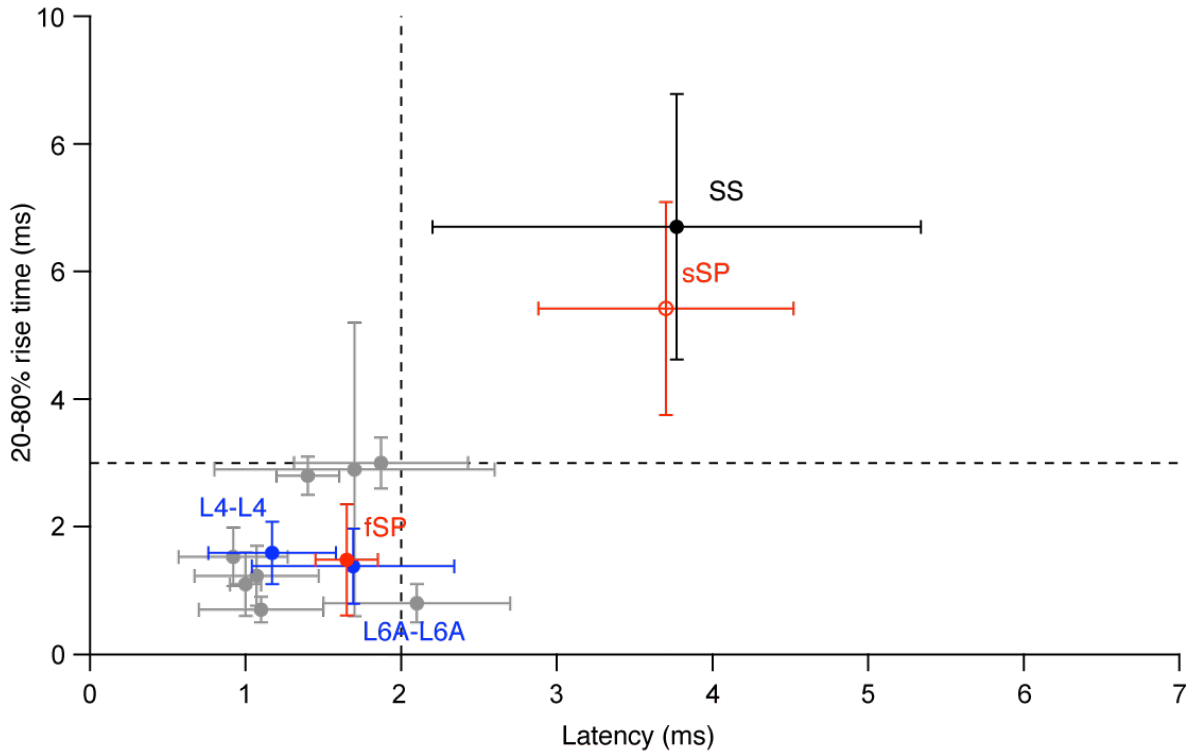


Fig. 3.50 Comparison with other corticocortical excitatory connections in the rat barrel cortex. For L4-L6A connections, they are divided into three phenotypes (SS, fSP, and sSP). Blue dots with whiskers represent L4-L4 and L6A-L6A connections obtained in this study. Other corticocortical excitatory connections in the barrel cortex of rats (grey dots with whiskers) given previously include intralaminar connections (L4-L4 (Feldmeyer, Egger et al. 1999), L2/3-L2/3 (Feldmeyer, Lubke et al. 2006), L5A-L5A (Frick, Feldmeyer et al. 2008), L5B-L5B thick-tufted (Markram, Lubke et al. 1997), L5B-L5B corticocallosal (Le Be, Silberberg et al. 2007)) and interlaminar connections (L4-L2/3 (Feldmeyer, Lubke et al. 2002), L4-L5A (Feldmeyer, Roth et al. 2005), L2/3-L5 (Kampa, Letzkus et al. 2006; Sjostrom and Hausser 2006)).

L6A-L6A connections were recorded under the same experimental conditions. These intralaminar connections always show a fast rise time and a short latency like fSP connections but clearly different from SS and sSP connections (see Fig. 3.50, in which data of other corticocortical excitatory connections in the barrel cortex from previous publications are also given). The correlation between 20-80% rise time and latency for all L4-L6A connections is statistically significant with a relative high linear correlation coefficient ($r = 0.59$, $p = 6.80\times10^{-3}$). Furthermore, the correlation between the synapse-to-soma distance and the 20-80% rise time (Fig. 3.49D2) or latency (Fig. 3.49D3) is also significant ($r = 0.81$, $p = 6.28\times10^{-9}$ and $r = 0.79$, $p = 2.94\times10^{-8}$,

respectively). Here, for fSP connections, the synapse-to-soma distance is less than 200 µm (more proximal), while that for SS and sSP connections is normally larger than 200 µm (more distal).

3.4.2 Incomplete prediction of the synaptic location based solely on axo-dendritic overlap

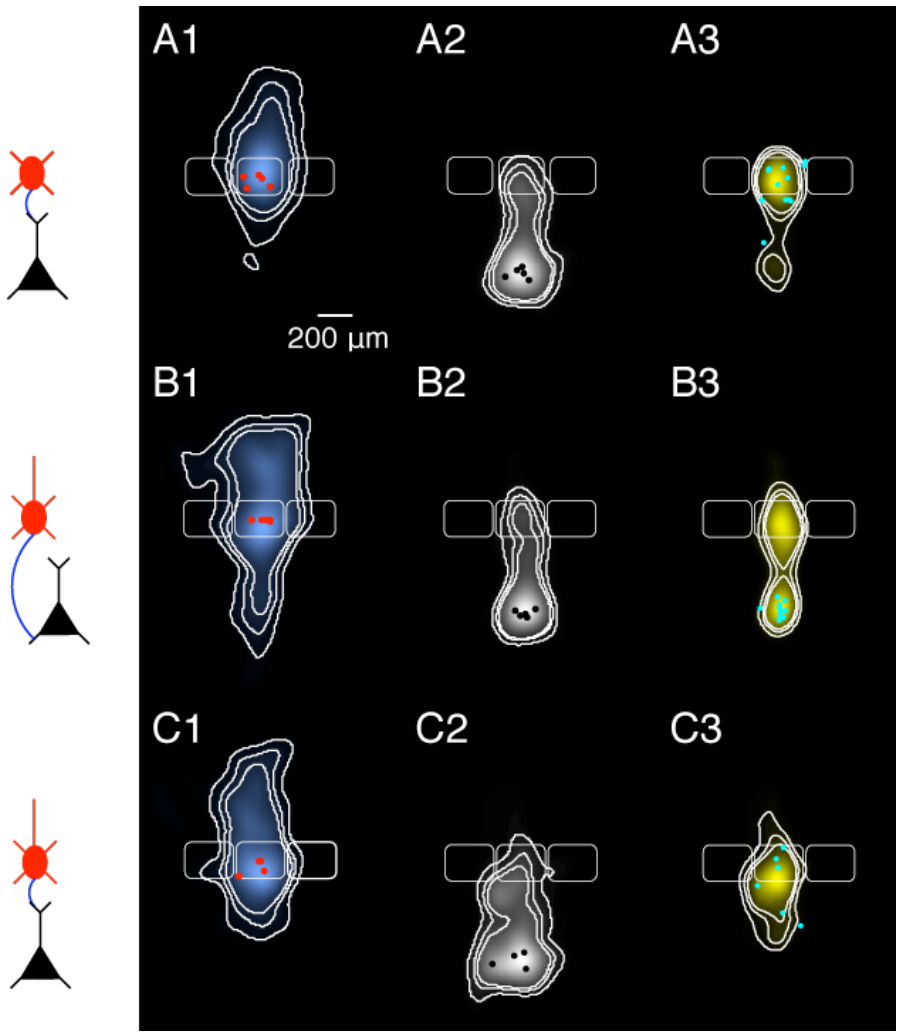


Fig. 3.51 Density maps of L4-to-L6A excitatory connections. A, 2D maps of axonal (A1) and dendritic (A2) length density of synaptically coupled L4 spiny stellate neurons and L6A pyramidal cells, respectively. L4 spiny stellate neurons and L6A pyramidal cells (n = 5) were aligned with respect to the barrel centre. The predicted innervation domain (A3) of L6A dendrites by L4 axons is given by the product of the L4 axonal density and the L6A dendritic density. Contours (thick white lines) enclosing 70, 80 and 90% of the integrated density are shown superimposed. Positions of L4 spiny stellate neuron soma (red dots), L6A pyramidal cell soma (black dots), putative synaptic contacts (light blue dots), and outlines of barrels (thinner white lines) are indicated symbolically. B, C, Same as in A but for five L4 star pyramid-L6A pyramidal cell pairs with fast EPSPs and four L4 star pyramid-L6A pyramidal cell pairs with slow EPSPs, respectively. Scale bar in A also applies to B and C.

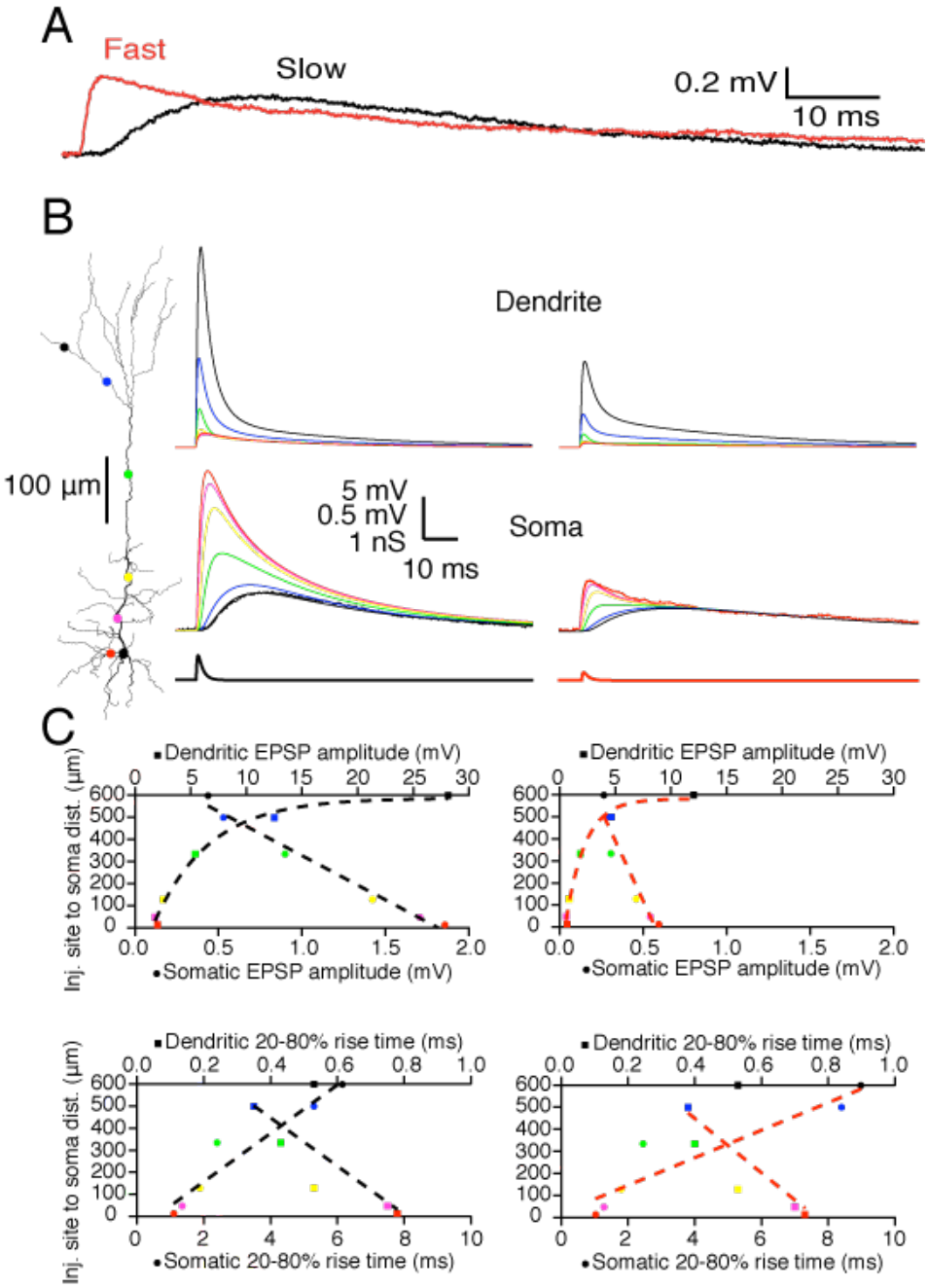


Fig. 3.52 Modeling the origin of 'slow' and 'fast' EPSPs. A, Two mean EPSP waveforms (slow *vs.* fast) of L4-L6A excitatory connections recorded experimentally. B, Left, Morphology of the L6A pyramidal cell used for neuronal modeling and the colour coded location of synaptic inputs. Right, Simulated somatic EPSPs (bottom left black and top right red smooth traces) were generated by inserting synaptic conductances composed of both AMPA and NMDA components (bottom traces) into the apical tuft (black dot) and the basal dendrite (red dot), respectively, which fitted well with two experimentally recorded EPSPs (slow EPSP, noisy black trace and fast EPSP, noisy red trace). Simulated somatic (middle traces) and dendritic (top traces) EPSP waveforms for different synaptic injection sites are also shown. C, Calculated somatic and dendritic EPSP amplitude (top) and rise time (bottom) based on the EPSP waveforms shown in B plotted against the injection site of synapse-to-soma distance. Best linear or exponential fits are shown in dashed lines.

Fig. 3.51 illustrates quantitatively the overlap of L4 spiny stellate axonal (Fig. 3.51A1) and L6A dendritic arbors (Fig. 3.51A2), suggesting that potential synaptic contacts might be predominantly located on the distal apical tuft dendrites of L6A pyramidal cells (Fig. 3.51A3). This prediction is largely consistent with the location of putative synaptic contacts we found under the light microscope (see light-blue dots in Fig. 3.51A3). The overlap of L4 star pyramid axonal (Fig. 3.51B1) and L6A dendritic arbors (Fig. 3.51B2), which is shown in Fig. 3.51B3, suggests that the potential synaptic contacts could be located on both the proximal basal and distal apical tuft dendrites of L6A pyramidal cells. However, the actual distribution of putative synaptic contacts does no fully correspond to the predicted innervation domain: Synaptic contacts are located only on the basal and proximal apical oblique dendrites near the somata of L6A pyramidal cells, but no synapse on distal apical tuft dendrites were found. The distribution of synaptic contacts is consistent with the EPSP properties, *i.e.,* pairs with a fast rise time and a short latency had proximal contacts while those with slow EPSP waveforms with long latencies had distal contacts. For sSP connections (Fig. 3.51C), a distribution of putative synaptic contacts similar to that of SS connections (Fig. 3.51A3) was found but contacts are generally more dispersed; this is in marked contrast to that of fSP connections (Fig. 3.51B3).

3.4.3 Modeling the origins of 'slow' and 'fast' synapses

In previous results on intralaminar (*e.g.*, L4-L4, L2/3-L2/3, L5-L5) and interlaminar (*e.g.*, L4-L2/3, L4-L5A, L2/3-L5) excitatory connections (see Fig. 3.50), as a group, none of above connections showed the EPSPs with so slow rise time and long latency as that of SS and sSP (but not fSP) connections given here. Where do these slow EPSPs come from? One possibility is that there exists specificity for the components of glutamatergic receptors. For example, pure NMDA receptor could induce very slow EPSP in the postsynaptic neuron (Radnikow, Feldmeyer et al. 2002). To check this, we have done several pharmacological experiments and found that there was no obvious

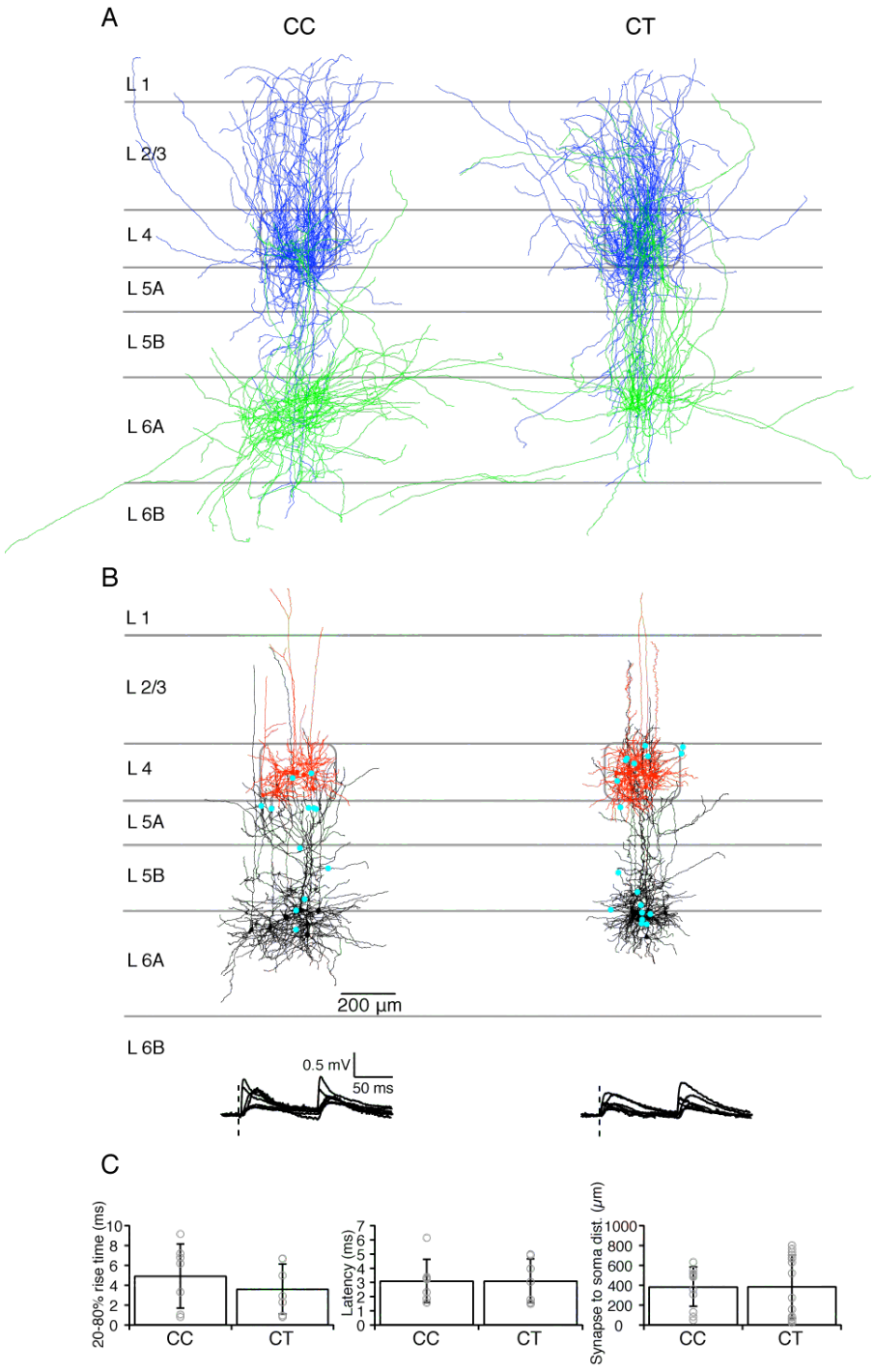


Fig. 3.53. Comparison of L4-to-L6A excitatory connections with L6A CC and CT short pyramids as postsynaptic neurons. A, Pre- and postsynaptic axonal domains of L4-L6A excitatory connections with L6A CC (left) and CT (right) short pyramids as postsynaptic neurons. The axonal arbors of the L4 spiny neurons and the L6A pyramidal cells are shown in blue and green, respectively. Note the columnar confinement of L6A CT axons. B, The somatodendritic arbors of the L4 spiny neurons and the L6A pyramidal cells are shown in red and black, respectively. Light-microscopically identified putative synaptic contacts are marked by filled light-blue circles. Bottom, Overlay of mean EPSPs of individual L4-L6A pairs within their corresponding groups. C, Comparison of 20-80% rise time, latency, and synapse-to-soma distance histograms. Grey open circles show data from individual pairs (n = 7 for CC and n = 7 for CT).

difference on the receptor components between slow and fast EPSPs. Adding the AMPA receptor antagonist CNQX (10 μM) could suppress the response for both slow and fast EPSPs (n = 3) nearly completely. In contrast, when the NMDA receptor blocker AP5 (50 μM) was applied, there was no obvious effect on the response for both slow and fast EPSPs (n = 2). Another factor that may account for the difference in the EPSP time course is electrotonic filtering during EPSP propagation along the dendrite from the synaptic location to the soma. To test this a neuronal model was constructed containing a detailed, realistic L6A pyramidal cell morphology and appropriate channel type, kinetics, and distribution. By calibrating the simulated EPSPs with the experimentally recorded slow and fast somatic EPSPs (Fig. 3.52A), respectively, we found that, as expected, synaptic inputs with identical conductances but on different sites could induce very different EPSP waveform at the postsynaptic soma (Fig. 3.52B). More distal synapses generated slower and smaller EPSPs at the soma than proximal ones but faster and bigger local dendritic EPSPs, whereas more proximal synapses generated faster and bigger EPSPs at the soma than distal ones but slower and smaller local dendritic EPSPs (Figs. 3.52B and 3.52C).

3.4.4 Pre but not postsynaptic cell-type specific selection of the postsynaptic target region

In layer 6A, short pyramidal cells can be divided into two types (CC *vs.* CT) according to the projection patterns of their axons. In L4-L6A connections, L4 neurons formed synapses with both CC and CT neurons in layer 6A. Furthermore, putative synaptic contacts were established on both the proximal basal and distal apical dendrites of L6A CC and CT pyramidal cells. There were no significant differences in the EPSP characteristics (*e.g.*, 20-80% rise time and latency) and the synapse-to-soma distance between CC and CT as postsynaptic neurons in L4-L6A connections (see Fig. 3.53). This result is consistent with a recent study showing that, for CC and CT neurons, the apical dendritic properties were homogeneously distributed (Ledergerber and Larkum 2010). In that study it has been suggested that the dendritic computation in L6 pyramidal neurons is independent

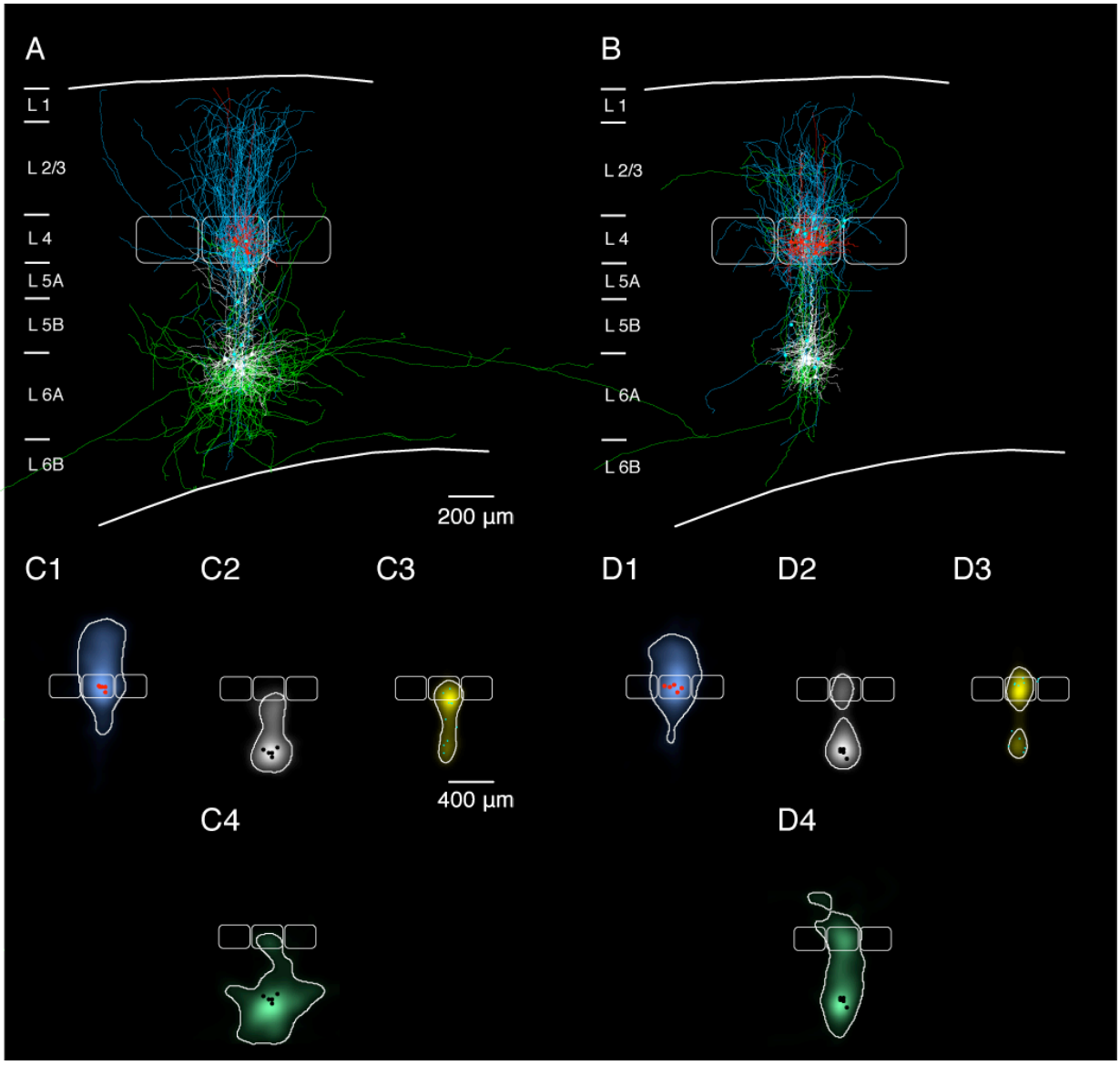


Fig. 3.54 Overlay and density maps of L4-to-L6A excitatory connections with L6A CC and CT short pyramids as postsynaptic neurons. A, Barrel-centred overlay of five synaptically coupled pairs of L4 spiny neurons and L6A CC short pyramidal cells. The average barrel in the centre is outlined in white; two neighbouring barrels are added symbolically. Light-microscopically identified putative synaptic contacts are marked by filled light-blue circles. B, Same as in A but for five L4 spiny-L6A CT short pyramidal cell pairs. C, 2D maps of axonal (C1) and dendritic (C2) length density of synaptically coupled L4 spiny neurons and L6A CC pyramidal cells, respectively. The predicted innervation domain (C3) of L6A dendrites by L4 axons is given by the product of the L4 axonal density and the L6A dendritic density. 2D map of axonal (C4) length density of L6A CC pyramidal cells is also shown. Contours (thick white lines) enclosing 80% of the integrated density are shown superimposed. Positions of L4 spiny stellate neuron soma (red dots), L6A pyramidal cell soma (black dots), putative synaptic contacts (light-blue dots), and outlines of barrels (thinner white lines) are indicated symbolically. D, Same as in C but for the same five L4 spiny-L6A CT pyramidal cell pairs as shown in B. Scale bars in A, C also apply to B, D, respectively.

of the axonal projection pattern of the L6A pyramidal neuron. Furthermore, in this study it was found that, for both CC and CT connections, the axo-dendritic overlap alone is sufficient to describe the synaptic pattern as shown in Fig. 3.54. However, as shown above this is not the case for L4-L6A fSP connections: the axo-dendritic overlap predicted that synapses should be on both proximal and distal dendrites of L6A pyramidal cells but synaptic contacts are only identified on proximal dendrites near the somata of L6A pyramidal cells and not on distal dendrites (see Fig. 3.51).

4 Discussion

4.1 The functional role of L4-L6A connections

The data shown here provides direct evidence for a monosynaptic connection between L4 spiny neurons and L6A pyramidal cells via relatively "reliable" synapses. Therefore, the sensory excitation arriving via the lemniscal (VPM-to-L4) afferents is then fed back from layer 4 to the thalamus through L6A corticothalamic axons. The L4-to-L6A connections might form a "short circuit" between afferent signals to neocortical layer 4 and efferent signals that leave the cortex from layer 6A and went back to the thalamus. In addition to the so-called "canonical" microcircuit innervated via the lemniscal thalamic afferents (Gilbert and Wiesel 1979; Douglas and Martin 2004) and the microcircuit innervated via paralemniscal afferents (Koralek, Jensen et al. 1988; Lu and Lin 1993), this suggests the existence of a thalamo-cortical-cortico-thalamic feedback circuit in the rat barrel cortex (Lubke and Feldmeyer 2007). Furthermore, it has been shown previously that, in the rodent barrel cortex, a major route for excitation of the infragranular layers is provided by L2/3-to-L5 excitatory synapses (Thomson and Bannister 1998; Reyes and Sakmann 1999). Here, we found another parallel descending excitation pathway from L4 spiny neurons to L6A pyramidal cells. Due to the different projecting patterns of pyramidal cells in layer 5 (Hattox and Nelson 2007; Larsen, Wickersham et al. 2007) (mainly to other cortical and subcortical areas) and layer 6A (Zhang and Deschenes 1997; Zhang and Deschenes 1998) (mainly back to the thalamus, but also to other cortical areas), these two parallel pathways may process different sensory modalities received from the periphery.

4.2 Different roles of L4 spiny neurons

The excitatory connections to layer 6A (shown here) and to other layers (*e.g.*, L4, L2/3, and L5A) provided by L4 spiny neurons imply that L4 spiny neurons are almost 'hub' neurons that connect to neurons located in almost all cortical layers with different connectivity ratios in a columnar manner.

Furthermore, the synapses formed by L4 spiny stellate neurons with other neurons are mainly confined to local regions near their somata whereas the synapses provided by L4 star pyramidal cells are in both local and distant regions (e.g., L4-L6A fSP connections given above) with respect to their somata. It has been shown that excitatory inputs to L4 spiny neurons also differentiate between spiny stellate and star pyramid in the barrel cortex (Schubert, Kotter et al. 2003): L4 spiny stellate inputs were mainly confined to the local region, while the inputs to star pyramids were from more distributed regions. Combining the results about the input and output patterns of L4 excitatory neurons, we hypothesize that spiny stellate neurons process the excitatory information locally, while star pyramidal neurons show a more distributed signal processing in the neuronal microcircuit of rat barrel cortex.

For L2/3-to-L5 connections it has been demonstrated that L2/3 pyramidal cells send excitatory synapses mainly to the proximal basal and apical oblique dendrites of L5 pyramidal cells with some synapses being located on the distal apical tuft dendrites (Thomson and Bannister 1998; Reyes and Sakmann 1999; Bannister 2005; Letzkus, Kampa et al. 2006; Sjostrom and Hausser 2006; Williams and Atkinson 2007; Hardingham, Read et al. 2010). This is reminiscent of the finding in L4-to-L6A connections here. Therefore, L4 star pyramidal neurons act more like the typical pyramidal cells in layer 2/3, while L4 spiny stellate neurons behave differently probably because of their unique morphological characteristics. Differential functional roles of spiny stellate and pyramidal neurons from primary visual cortex to dorsal visual cortical areas were also found in monkey visual cortex: spiny stellate neurons received strong M input through layer 4Cα and no significant P input through layer 4Cβ. In contrast, pyramidal neurons in layer 4B received strong input from both layers 4Cα and 4Cβ (Yabuta, Sawatari et al. 2001).

4.3 Development of L4-L6A connections

Most experiments for this study were done in juvenile rats (18-22 days old). For these L4-L6A connections we found that presynaptic L4 neurons include both spiny stellate and star pyramidal cells. We also did some experiments in more mature rats (27-28 days old) and found three L4-L6A connections. Compared with juvenile rats, the probability of finding a L4-L6A connection is a little higher in mature rats. However, the prominent difference is that in mature L4-L6A connections the presynaptic L4 neurons are exclusively star pyramids with fast EPSPs and synapses located near the postsynaptic somata. Concerned with this difference between juvenile and mature rats, one possibility is that the connection with spiny stellate as presynaptic neuron type becomes weaker or is less readily detectable in mature animals due to the decrease in input resistance of the postsynaptic L6A pyramidal cell. Therefore, it could be tested in dendritic recordings which are, however, out of the scope of the present study. As described before, a significant positive linear correlation was found between the EPSP amplitude and the input resistance of postsynaptic L6A pyramidal cell for L4-L6A connections. In addition, we found that the input resistance of postsynaptic L6A pyramidal cell became smaller during development (data not shown). Another possibility that may account for the difference in L4-L6A connections found for less and more mature animals is long-term plasticity such as spike-timing dependent plasticity (STDP). In L2/3-L5 excitatory connections in rat visual cortex (Sjostrom and Hausser 2006) and barrel cortex (Letzkus, Kampa et al. 2006), it has been shown that the form of STDP depends on the location of synapses (Froemke, Poo et al. 2005): distal synapses normally showed depression in STDP while proximal ones showed potentiation. With regard to the results presented here, we think that, for a similar reason as shown in L2/3-L5 connections, the synapses of L4-L6A connections with slow EPSPs (the synaptic location is far from the soma) weaken or even disappear during the development of rat barrel cortex due to the spike-timing dependent depression. Which is highly worthy being tested in the future.

4.4 Comparison with previous findings

In the framework of the present study, excitatory L4-L6A connections were identified. The connectivity is low, but not as low as expected based on previous studies. In the same region of rat barrel cortex, several L6A-L4 excitatory connections including one onto a L4 inhibitory interneuron were also found in our laboratory (Günter and Feldmeyer, unpublished observations). However, the connectivity of L6A-L4 connections is much lower than that of L4-L6A connections. Similar findings have been reported for the mouse barrel cortex (Lefort, Tomm et al. 2009) in which connectivity for L4-L6 connections was 3.2% (three out of 93 pairs) and no L6-L4 connections were observed. This situation is different from that in cat visual cortex (Stratford, Tarczy-Hornoch et al. 1996; Tarczy-Hornoch, Martin et al. 1999): seven connections from layer 6 to layer 4 and only one L4-to-L6 connection were found. For L6-L4 connections, some indirect evidence using extracellular stimulation and/or photostimulation techniques have been presented for the mouse barrel and auditory cortices (Lee and Sherman 2008; Lee and Sherman 2009). Maybe this inconsistency is due to different cortical regions (barrel *vs.* visual cortex) and species (rat *vs.* cat). Other possibilities such as a reduced connectivity because of slicing artifact should also be taken into account. Because all of our searchings and paired recordings were performed *in vitro* in brain slices, the connectivity between neurons located in different layers is likely to be underestimated compared to that *in vivo* especially for the long-range interlaminar connections due to the truncation of dendritic and especially axonal branches. It was shown in computer simulations of cat visual cortex that the ascending interlaminar connections were more likely to be truncated than the descending ones in brain slice preparations (Stepanyants, Martinez et al. 2009). This may explain why more connections from layer 4 to layer 6A than the opposite direction were found in our laboratory and others.

Cell-type specific connection properties were discovered previously for both inhibitory and excitatory connections. It has been demonstrated that the synaptic connections provided or received by fast spiking and low-threshold spike interneurons demonstrated different anatomical and dynamical properties in rat barrel cortex (Markram, Wang et al. 1998; Reyes, Lujan et al. 1998; Gupta, Wang et al. 2000; Koester and Johnston 2005), visual cortex (Xiang, Huguenard et al. 2002) and hippocampus (Mori, Abegg et al. 2004; Pouille and Scanziani 2004). Such a projection or target region specificity of synaptic connections has only recently been discussed for excitatory connections. Several lines of evidence suggested that connections between pyramidal cells form subnetworks within the neocortical network. Simultaneous multiple whole-cell recordings from several excitatory neurons showed that once a synaptic connection has been identified in a small group of L5 pyramidal cells, the likelihood of finding additional connections within this group was greater than expected from the average connectivity (Song, Sjostrom et al. 2005). Moreover, the probability of connection between a L2/3 pyramidal cell and a pair of L5 pyramidal cells was higher when the L5 neurons were synaptically connected (Kampa, Letzkus et al. 2006) or when the L5 neurons shared similar firing patterns (Otsuka and Kawaguchi 2008). Similarly, pairs of connected L2/3 pyramidal cells were more likely to share excitatory input from L2/3 and L4 neurons as compared with unconnected neurons (Yoshimura and Callaway 2005; Yoshimura, Dantzker et al. 2005). In addition, radial clones of pyramidal neurons that originate developmentally from the same mother cell are preferentially connected as compared to randomly selected neighboring pyramidal cells (Yu, Bultje et al. 2009). Besides the fine connection structures discussed above, the synaptic properties of excitatory connections in local cortical microcircuits are also diverse and cell-type dependent. In mouse auditory cortex, two types of synapses between pairs of L2/3 pyramidal neurons, which were called ‘weak’ and ‘strong’ synapses, were identified. The ‘weak’ synapses showed a small EPSP amplitude and high failure rate, while the ‘strong’ ones demonstrated a large EPSP amplitude and low failure rate (Atzori, Lei et al. 2001). Furthermore, in

the ferret prefrontal cortex, both ‘depressing’ and ‘facilitating’ synapse types have been reported. Synapses formed between so-called ‘complex’ pyramidal cells with dual main apical dendritic branches demonstrated facilitations while those formed between ‘simple’ pyramidal cells with single main apical dendritic branches showed depressions (Wang, Markram et al. 2006). Eexperiments in which fluorescent beads were used to retrogradely label the target brain regions of the long-range axon collaterals of pyramidal cells in mouse visual cortex, showed that the connectivity among neighboring pyramidal cells were dependent on the identity of both presynaptic and postsynaptic cell types. The connection probability of a L5 corticocortical pyramidal cell with a neighbouring L5 corticotectal pyramidal cell was almost fourfold higher than the connection probability with another L5 corticocortical pyramidal cell (Brown and Hestrin 2009). In addition, by selectively expressing light-gated cation channel, channelrhodopsin-2, throughout the axonal arbor of different cortical afferents and selectively stimulating these afferents by light, the strength of different inputs onto L3, L5A and L5B pyramidal cells in mouse barrel cortex was studied. Different synaptic input patterns at the subcellular level were given, which revealed high specificity in the subcellular organization of excitatory circuits (Petreanu, Mao et al. 2009). Both of the two studies mentioned above demonstrated that the axo-dendritic overlap alone was insufficient to describe both the strength and pattern of synaptic connections at either cellular or subcellular level, *i.e.*, they did not obey the Peter’s rule, like the thalamic input to the cerebral cortex did (Peters 1979). Our findings here: two types of synapses (‘slow’ *vs.* ‘fast’), presynaptic cell-type specific connection probability and subcellular innervation pattern supply another firm evidence for the fine structure of synaptic connections between excitatory neurons in the neocortex with a much higher resolution than that of (Brown and Hestrin 2009; Petreanu, Mao et al. 2009).

4.5 Advantage and shortcoming of present methods

A growing body of evidence shows that the neuronal networks in the mammalian brain are neither random nor uniform (Callaway 2002; Thomson and Morris 2002; White 2002; Ohki and Reid 2007). They are structured and hierarchically organised into fine subnetworks comprising heterogeneous neuronal populations. Between different types of neurons, the connectivity and connection dynamics are dependent on either the pre- or postsynaptic neuron type or possibly even both. Therefore, knowing the cell-identity is very important to for the studying the functional and structural properties of neuronal microcircuits (Brown and Hestrin 2009). Using paired recordings with dye injection, we could unambiguously identify the cell types of both pre- and postsynaptic neurons and obtained all information concerning both the electrophysiological and the morphological characteristics of the connection under study. Alternative techniques such as laser scanning photostimulation including the photo-release of caged glutamate and channelrhodopsin-2-assisted circuit mapping (Callaway and Katz 1993; Dantzker and Callaway 2000; Schubert, Staiger et al. 2001; Dodt, Schierloh et al. 2003; Kotter, Schubert et al. 2005; Shepherd, Stepanyants et al. 2005; Yoshimura and Callaway 2005; Yoshimura, Dantzker et al. 2005; Bureau, von Saint Paul et al. 2006; Petreanu, Huber et al. 2007) and calcium imaging (Peterlin, Kozloski et al. 2000; Kozloski, Hamzei-Sichani et al. 2001; Aaron and Yuste 2006) cannot identify either the projection or the target cell type, respectively. Furthermore, using the laser scanning photostimulation technique, the patched neuron was normally recorded in the voltage-clamp mode, but see (Schubert, Staiger et al. 2001; Kotter, Schubert et al. 2005). It is known that, the more distal the synaptic input is, the larger the voltage-clamp error and distortion of current measured at the soma becomes (Williams and Mitchell 2008). Especially for the case of L4-to-L6A connections shown here, different types of presynaptic neurons innervated different dendritic domains of postsynaptic neurons and elicited different forms of EPSPs in postsynaptic somata, a finding we would not have observed when using photostimulation approaches. Two other points are also relevant: first, caged glutamate release is a technique with a relatively low spatial resolution and it is therefore not certain

whether the observed connections are single, unitary connections. And second, the glutamate uncaging method is adequate for studying long-range connection, however there are severe problems with short-range connection because of direct excitation of the postsynaptic neuron (Schubert, Staiger et al. 2001; Kotter, Schubert et al. 2005; Shepherd, Stepanyants et al. 2005; Shepherd and Svoboda 2005; Bureau, von Saint Paul et al. 2006; Hooks, Hires et al. 2011).

Channelrhodopsin-assisted photostimulation needs a highly selective expression to ensure that only a defined subpopulation of neurons is activated. For this expression of the channelrhodopsin is coupled to that of a cell-specific promotor protein; however, most of the promotor genes used at present are not sufficiently selective so that more than channelrhodopsin (or any other gene) is expressed in more than one subpopulation of neurons.

The shortcoming of the paired recording approach are also obvious, *i.e.*, it is laborious, inefficient and time-consuming especially for the cell pairs with low connection probabilities. The paired recording method is not useful for a rapid overview of connection patterns - here the laser scanning photostimulation and calcium imaging methods are superior although at present there most serious disadvantage is the unknown cellular identity of the pre- or postsynaptic neuron. Paired recording experiments normally take more time to obtain sufficient and meaningful results; however, the wealth for structural and functional data is much greater.

4.6 Future directions

Understanding the functional organisation of the brain at the circuit level will have important implications for both basic and clinical neuroscience. Cell-type specific expression of light sensitive rhodopsins or halorhodopsins (Boyden, Zhang et al. 2005; Zhang, Wang et al. 2006; Zhang, Wang et al. 2007; Zhang, Prigge et al. 2008; Zhang, Gradinaru et al. 2010) combining electrophysiological

(*e.g.*, patch clamping) and optical (*e.g.*, laser stimulation) methods provide a powerful genetic tool to dissect neural circuits both *in vitro* (Wang, Peca et al. 2007) and especially *in vivo* (Airan, Thompson et al. 2009; Cardin, Carlen et al. 2009; Sohal, Zhang et al. 2009). This approach is refered to as 'optogenetics'. Furthermore, using a combination of optogenetics and fMRI, it was verified that the firing of local excitatory neurons is fully sufficient to trigger the complex signals detected by fMRI scanners (Lee, Durand et al. 2010). In addition, using optogenetics to study an animal model of Parkinson's disease fundamental insight into the nature of the diseased circuitry and the mechanisms of action of therapeutic interventions was obtained (Gradinaru, Mogri et al. 2009).

Another recently introduced technique, retrograde neuronal tracing with a deletion-mutant rabies virus (Wickersham, Finke et al. 2007), may allow significant steps forward in circuitry research (Callaway 2008). It has been demonstrated that, after injecting a modified rabies virus into a single neuron, many, if not all the neurons presynaptic to that single infected neuron became infected and labelled both *in vitro* (Wickersham, Lyon et al. 2007) and *in vivo* (Marshel, Mori et al. 2010). Furthermore, by intracellular recording both that injected neuron and the labelled neurons, it was verified that they were really connected functionally.

Advances in confocal and multi-photon technology and increasingly elegant ways of labeling molecules with fluorescent and electron-dense molecules, together with the advances in molecular biology and the many different types of genetically modified mice becoming available, offer other ways to combine functional with structural studies of the brain (Thomson and Armstrong 2011).

5 Abbreviations

AMPA α-amino-3-hydroxy-5-methyl-4-isoxazolepropionic acid

AP Action potential

AP5 (2R)-amino-5-phosphonovaleric acid

CC Cortiocortical

CNQX 6-cyano-7-nitroquinoxaline-2,3-dione

CT Corticothalamic

CV Coefficient of variation

EPSC Excitatory postsynaptic current

EPSP Excitatory postsynaptic potential

IR-DIC Infrared differential interference contrast

ISI Interstimulus interval

L4 Layer 4

NMDA N-Methyl-D-Aspartate

POm Posterior medial nucleus

PPR Paired-pulse ratio

S1 Primary somatosensory cortex

SD Standard deviation

SP Star pyramidal

SS Spiny stellate

VPM Ventroposterior medial nucleus

V_{rest} Resting membrane potential

6 Summary

In the primary somatosensory (barrel) cortex of rodents, layer 4 (L4) and 6A are the main recipient layers of thalamocortical projections. In addition, a subset of L6A pyramidal neurons provide a direct corticothalamic feedback to the thalamus. Thus, neurons in layer 4 and 6A are an integral part of a thalamo-cortical-cortico-thalamic feedback circuit. To better understand the role of the intracortical unit in this circuit, we studied the anatomical and functional properties of excitatory synaptic connections from layer 4 to layer 6A in the rat barrel cortex by making dual whole-cell recordings with dye injection from L4 spiny neurons and L6A pyramidal cells in acute brain slices.

Interlaminar monosynaptic L4-to-L6A excitatory connections (n = 17) were relatively rare. They were of low efficacy with an average excitatory postsynaptic potentials (EPSPs) of 0.32 ± 0.19 mV (n = 17) but of moderately high reliability with failure rate of 24.2 ± 17.7% (n = 16) and coefficient of variation (CV) of 0.56 ± 0.16 (n = 16). The EPSP amplitude was either depressing or weakly facilitating with paired-pulse ratio (PPR) of 0.45 - 1.38 (n = 17) at an interstimulus interval of 100 ms. Notably, we found a spatial separation of synaptic inputs on the dendritic domain of the postsynaptic L6A pyramidal cells depending on the presynaptic L4 neuron type: L4 spiny stellate neurons innervated predominantly the distal apical tuft dendrites of L6A pyramidal cells with synapse-to-soma distance of 591 ± 137 μm (n = 6) and elicited slow EPSPs (20-80% rise time = 6.7 ± 2.1 ms and latency = 3.8 ± 1.6 ms, n = 6) in L6A somata, while most of L4 star pyramidal neurons preferentially innervated the proximal basal and apical oblique dendrites with synapse-to-soma distance of 86 ± 54 μm (n = 7) and elicited fast EPSPs (20-80% rise time = 1.5 ± 0.9 ms and latency = 1.7 ± 0.2 ms, n = 7) in L6A somata with some star pyramids also forming synapses on the L6A apical tuft or oblique dendrites (synapse-to-soma distance = 524 ± 167 μm, n = 4) and eliciting relatively slow EPSPs (20-80% rise time = 5.4 ± 1.7 ms and latency = 3.7 ± 0.8 ms, n = 4). Other EPSP characteristics (*i.e.,* amplitude, PPR, failure rate and CV) were not significantly different for

the three types of L4-L6A connections. There was a tight correlation between the EPSP rise time, latency, and the synapse-to-soma distance. The synaptic location could not completely predicted solely on the basis of the axo-dendritic overlap suggesting that Peter's rule of synaptic connectivity was not completely correct here. Using pharmacological treatment and neuronal modeling, we found that the occurrence of 'slow' and 'fast' EPSPs was not due to different receptor components in the postsynaptic densities but mainly due to the dendritic filtering effect during the EPSP propagation from synaptic location to soma. In addition, the cell-type specific selection of postsynaptic target region was a pre- but not postsynaptic phenomenon.

As a comparison, we also performed some paired recordings in layer 4 and 6A and studied the characteristics of excitatory connections in layer 4 and 6A, respectively. For intralaminar monosynaptic L4-L4 and L6A-L6A excitatory connections, we found homogeneous dynamical properties of EPSPs, *i.e.,* fast rise time (20-80% rise time = 1.59 ± 0.49 ms (n = 10) for L4-L4 and 1.39 ± 0.59 ms (n = 5) for L6A-L6A connections) and short latency (latency = 1.17 ± 0.41 ms (n = 10) for L4-L4 and 1.69 ± 0.65 ms (n = 5) for L6A-L6A connections), implying that, for both connections, synaptic inputs to postsynaptic neurons were electrotonically close to somata. The synaptic efficacy of L4-L4 connections were widely distributed from very weak connections (0.30 mV) to very strong ones (4.71 mV) with an average EPSP amplitude of 1.02 ± 1.33 mV (n = 10) compared with L6A-L6A connections that had a substantially lower average EPSP amplitude (0.58 ± 0.50 mV, n = 5), a relatively higher failure rate (17.5 ± 15.0%, n = 5) and a little higher CV (0.53 ± 0.23, n = 5).

7 Acknowledgements

Firstly, I would like to thank my supervisor, Prof. Dirk Feldmeyer, whose guidance and insight provided the basis for this thesis. Without his continuous help and advice, this work would not have been possible. Furthermore, I want to thank Prof. Karl Zilles for giving me the opportunity to perform my PhD work in Institute of Neuroscience and Medicine (INM-2), Research Centre Jülich, Germany.

I would like to thank Prof. Joachim Lübke (Research Centre Jülich) for helpful discussions, Dr. Arnd Roth (University College London) for sending me the program for density maps and Prof. Edwin Abel (University of Pennsylvania) for reviewing this thesis.

I would like to thank Dr. Gina Haack for introducing me to patch clamp and other related experimental techniques; Dr. Karlijn van Aerde for teaching me Igor programming; Dr. Robert Günter for helping me with computer things; Manuel Marx for showing me Neurolucida reconstructions.

A special thank to Werner Hucko for staining the neurons. He was always available to help with any technical problem in the laboratory that occurred during the experimental phase of this work.

A big thank you to all the members of Feldmeyer's group - 'Function of neuronal microcircuits' (Dr. Gabriele Radnikow, Dr. Gina Haack, Dr. Karlijn van Aerde, Dr. Robert Günter, Manuel Marx, Claudia Schreiner and Werner Hucko) in Institute of Neuroscience and Medicine (INM-2), Research Centre Jülich, Germany, for their help through the thesis.

I would like to thank the members of my thesis committee (Prof. Henner Hollert, Prof. Dirk Feldmeyer, Prof. Marc Spehr and Prof. Werner Baumgartner), for their valuable time and insight.

Finally, I would like to thank my parents, my little sister, my girl friend Stacey R. Dong and all my friends, who have been supportive and patient with me during the whole process of finishing this thesis.

During the period of pursuing this thesis, I was financially supported by CSC-Helmholtz scholarship for PhD students. This work was also supported in part by the DFG research group on Barrel Cortex Function (BaCoFun).

8 References

Aaron, G. and R. Yuste (2006). "Reverse optical probing (ROPING) of neocortical circuits." Synapse **60**(6): 437-440.

Adesnik, H. and M. Scanziani (2010). "Lateral competition for cortical space by layer-specific horizontal circuits." Nature **464**(7292): 1155-1160.

Ahissar, E., R. Sosnik, et al. (2000). "Transformation from temporal to rate coding in a somatosensory thalamocortical pathway." Nature **406**(6793): 302-306.

Airan, R. D., K. R. Thompson, et al. (2009). "Temporally precise in vivo control of intracellular signalling." Nature **458**(7241): 1025-1029.

Ajima, A. and S. Tanaka (2006). "Spatial patterns of excitation and inhibition evoked by lateral connectivity in layer 2/3 of rat barrel cortex." Cereb Cortex **16**(8): 1202-1211.

Ascoli, G. A., L. Alonso-Nanclares, et al. (2008). "Petilla terminology: nomenclature of features of GABAergic interneurons of the cerebral cortex." Nat Rev Neurosci **9**(7): 557-568.

Atzori, M., S. Lei, et al. (2001). "Differential synaptic processing separates stationary from transient inputs to the auditory cortex." Nat Neurosci **4**(12): 1230-1237.

Bannister, A. P. (2005). "Inter- and intra-laminar connections of pyramidal cells in the neocortex." Neurosci Res **53**(2): 95-103.

Bannister, A. P. and A. M. Thomson (2007). "Dynamic properties of excitatory synaptic connections involving layer 4 pyramidal cells in adult rat and cat neocortex." Cereb Cortex **17**(9): 2190-2203.

Beierlein, M. and B. W. Connors (2002). "Short-term dynamics of thalamocortical and intracortical synapses onto layer 6 neurons in neocortex." J Neurophysiol **88**(4): 1924-1932.

Boyden, E. S., F. Zhang, et al. (2005). "Millisecond-timescale, genetically targeted optical control of neural activity." Nature neuroscience **8**(9): 1263-1268.

Briggs, F. and E. M. Callaway (2001). "Layer-specific input to distinct cell types in layer 6 of monkey primary visual cortex." J Neurosci **21**(10): 3600-3608.

Brown, S. P. and S. Hestrin (2009). "Cell-type identity: a key to unlocking the function of neocortical circuits." Curr Opin Neurobiol **19**(4): 415-421.

Brown, S. P. and S. Hestrin (2009). "Intracortical circuits of pyramidal neurons reflect their long-range axonal targets." Nature **457**(7233): 1133-1136.

Bureau, I., F. von Saint Paul, et al. (2006). "Interdigitated paralemniscal and lemniscal pathways in the mouse barrel cortex." PLoS Biol **4**(12): e382.

Callaway, E. M. (2002). "Cell type specificity of local cortical connections." J Neurocytol **31**(3-5): 231-237.

Callaway, E. M. (2008). "Transneuronal circuit tracing with neurotropic viruses." Curr Opin Neurobiol **18**(6): 617-623.

Callaway, E. M. and L. C. Katz (1993). "Photostimulation using caged glutamate reveals functional circuitry in living brain slices." Proceedings of the National Academy of Sciences of the United States of America **90**(16): 7661-7665.

Cardin, J. A., M. Carlen, et al. (2009). "Driving fast-spiking cells induces gamma rhythm and controls sensory responses." Nature **459**(7247): 663-667.

Chmielowska, J., G. E. Carvell, et al. (1989). "Spatial organization of thalamocortical and corticothalamic projection systems in the rat SmI barrel cortex." J Comp Neurol **285**(3): 325-338.

Connors, B. W. and M. J. Gutnick (1990). "Intrinsic firing patterns of diverse neocortical neurons." Trends Neurosci **13**(3): 99-104.

Cowan, A. I. and C. Stricker (2004). "Functional connectivity in layer IV local excitatory circuits of rat somatosensory cortex." J Neurophysiol **92**(4): 2137-2150.

Dantzker, J. L. and E. M. Callaway (2000). "Laminar sources of synaptic input to cortical inhibitory interneurons and pyramidal neurons." Nat Neurosci **3**(7): 701-707.

Diamond, M. E., M. von Heimendahl, et al. (2008). "'Where' and 'what' in the whisker sensorimotor system." Nat Rev Neurosci **9**(8): 601-612.

Dodt, H. U., A. Schierloh, et al. (2003). "Circuitry of rat barrel cortex investigated by infrared-guided laser stimulation." Neuroreport **14**(4): 623-627.

Dodt, H. U. and W. Zieglgansberger (1990). "Visualizing unstained neurons in living brain slices by infrared DIC-videomicroscopy." Brain Res **537**(1-2): 333-336.

Douglas, R. J. and K. A. Martin (2004). "Neuronal circuits of the neocortex." Annu Rev Neurosci **27**: 419-451.

Egger, V., D. Feldmeyer, et al. (1999). "Coincidence detection and changes of synaptic efficacy in spiny stellate neurons in rat barrel cortex." Nat Neurosci **2**(12): 1098-1105.

Egger, V., T. Nevian, et al. (2008). "Subcolumnar dendritic and axonal organization of spiny stellate and star pyramid neurons within a barrel in rat somatosensory cortex." Cereb Cortex **18**(4): 876-889.

Feldmeyer, D. (2010). "Neuroscience: Signals far and away." Nature **464**(7292): 1134-1136.

Feldmeyer, D., V. Egger, et al. (1999). "Reliable synaptic connections between pairs of excitatory layer 4 neurones within a single 'barrel' of developing rat somatosensory cortex." J Physiol **521 Pt 1**: 169-190.

Feldmeyer, D., J. Lubke, et al. (2006). "Efficacy and connectivity of intracolumnar pairs of layer 2/3 pyramidal cells in the barrel cortex of juvenile rats." J Physiol **575**(Pt 2): 583-602.

Feldmeyer, D., J. Lubke, et al. (2002). "Synaptic connections between layer 4 spiny neurone-layer 2/3 pyramidal cell pairs in juvenile rat barrel cortex: physiology and anatomy of interlaminar signalling within a cortical column." J Physiol **538**(Pt 3): 803-822.

Feldmeyer, D., A. Roth, et al. (2005). "Monosynaptic connections between pairs of spiny stellate cells in layer 4 and pyramidal cells in layer 5A indicate that lemniscal and paralemniscal afferent pathways converge in the infragranular somatosensory cortex." J Neurosci **25**(13): 3423-3431.

Finnerty, G. T., L. S. Roberts, et al. (1999). "Sensory experience modifies the short-term dynamics of neocortical synapses." Nature **400**(6742): 367-371.

Frick, A., D. Feldmeyer, et al. (2008). "Monosynaptic connections between pairs of L5A pyramidal neurons in columns of juvenile rat somatosensory cortex." Cereb Cortex **18**(2): 397-406.

Froemke, R. C., M. M. Poo, et al. (2005). "Spike-timing-dependent synaptic plasticity depends on dendritic location." Nature **434**(7030): 221-225.

Gilbert, C. D. and T. N. Wiesel (1979). "Morphology and intracortical projections of functionally characterised neurones in the cat visual cortex." Nature **280**(5718): 120-125.

Gradinaru, V., M. Mogri, et al. (2009). "Optical deconstruction of parkinsonian neural circuitry." Science **324**(5925): 354-359.

Gupta, A., Y. Wang, et al. (2000). "Organizing principles for a diversity of GABAergic interneurons and synapses in the neocortex." Science **287**(5451): 273-278.

Hardingham, N. R., J. C. Read, et al. (2010). "Quantal analysis reveals a functional correlation between presynaptic and postsynaptic efficacy in excitatory connections from rat neocortex." J Neurosci **30**(4): 1441-1451.

Hattox, A. M. and S. B. Nelson (2007). "Layer V neurons in mouse cortex projecting to different targets have distinct physiological properties." Journal of neurophysiology **98**(6): 3330-3340.

Helmstaedter, M., C. P. de Kock, et al. (2007). "Reconstruction of an average cortical column in silico." Brain Res Rev **55**(2): 193-203.

Helmstaedter, M. and D. Feldmeyer (2010). Axons predict neuronal connectivity within and between cortical columns and serve as primary classifiers of interneurons in a cortical column. New Aspects of Axonal Structure and Function. D. Feldmeyer and J. Lubke, Springer**:** 141-155.

Hines, M. L. and N. T. Carnevale (1997). "The NEURON simulation environment." Neural Comput **9**(6): 1179-1209.

Hooks, B. M., S. A. Hires, et al. (2011). "Laminar analysis of excitatory local circuits in vibrissal motor and sensory cortical areas." PLoS Biol **9**(1): e1000572.

Hubel, D. H. and T. N. Wiesel (1959). "Receptive fields of single neurones in the cat's striate cortex." The Journal of physiology **148**: 574-591.

Hubel, D. H. and T. N. Wiesel (1962). "Receptive fields, binocular interaction and functional architecture in the cat's visual cortex." The Journal of physiology **160**: 106-154.

Kampa, B. M., J. J. Letzkus, et al. (2006). "Cortical feed-forward networks for binding different streams of sensory information." Nat Neurosci **9**(12): 1472-1473.

Katz, L. C. (1987). "Local circuitry of identified projection neurons in cat visual cortex brain slices." J Neurosci **7**(4): 1223-1249.

Koester, H. J. and D. Johnston (2005). "Target cell-dependent normalization of transmitter release at neocortical synapses." Science **308**(5723): 863-866.

Koralek, K. A., K. F. Jensen, et al. (1988). "Evidence for two complementary patterns of thalamic input to the rat somatosensory cortex." Brain Res **463**(2): 346-351.

Kotter, R., D. Schubert, et al. (2005). "Optical release of caged glutamate for stimulation of neurons in the in vitro slice preparation." Journal of biomedical optics **10**(1): 11003.

Kozloski, J., F. Hamzei-Sichani, et al. (2001). "Stereotyped position of local synaptic targets in neocortex." Science **293**(5531): 868-872.

Kumar, P. and O. Ohana (2008). "Inter- and intralaminar subcircuits of excitatory and inhibitory neurons in layer 6a of the rat barrel cortex." J Neurophysiol **100**(4): 1909-1922.

Larsen, D. D., I. R. Wickersham, et al. (2007). "Retrograde tracing with recombinant rabies virus reveals correlations between projection targets and dendritic architecture in layer 5 of mouse barrel cortex." Frontiers in neural circuits **1**: 5.

Le Be, J. V., G. Silberberg, et al. (2007). "Morphological, electrophysiological, and synaptic properties of corticocallosal pyramidal cells in the neonatal rat neocortex." Cereb Cortex **17**(9): 2204-2213.

Ledergerber, D. and M. E. Larkum (2010). "Properties of layer 6 pyramidal neuron apical dendrites." J Neurosci **30**(39): 13031-13044.

Lee, C. C. and S. M. Sherman (2008). "Synaptic properties of thalamic and intracortical inputs to layer 4 of the first- and higher-order cortical areas in the auditory and somatosensory systems." J Neurophysiol **100**(1): 317-326.

Lee, C. C. and S. M. Sherman (2009). "Modulator property of the intrinsic cortical projection from layer 6 to layer 4." Front Syst Neurosci **3**: 3.

Lee, J. H., R. Durand, et al. (2010). "Global and local fMRI signals driven by neurons defined optogenetically by type and wiring." Nature **465**(7299): 788-792.

Lefort, S., C. Tomm, et al. (2009). "The excitatory neuronal network of the C2 barrel column in mouse primary somatosensory cortex." Neuron **61**(2): 301-316.

Letzkus, J. J., B. M. Kampa, et al. (2006). "Learning rules for spike timing-dependent plasticity depend on dendritic synapse location." J Neurosci **26**(41): 10420-10429.

Lu, S. M. and R. C. Lin (1993). "Thalamic afferents of the rat barrel cortex: a light- and electron-microscopic study using Phaseolus vulgaris leucoagglutinin as an anterograde tracer." Somatosens Mot Res **10**(1): 1-16.

Lubke, J., V. Egger, et al. (2000). "Columnar organization of dendrites and axons of single and synaptically coupled excitatory spiny neurons in layer 4 of the rat barrel cortex." J Neurosci **20**(14): 5300-5311.

Lubke, J. and D. Feldmeyer (2007). "Excitatory signal flow and connectivity in a cortical column: focus on barrel cortex." Brain Struct Funct **212**(1): 3-17.

Lubke, J., A. Roth, et al. (2003). "Morphometric analysis of the columnar innervation domain of neurons connecting layer 4 and layer 2/3 of juvenile rat barrel cortex." Cereb Cortex **13**(10): 1051-1063.

Mainen, Z. F., J. Joerges, et al. (1995). "A model of spike initiation in neocortical pyramidal neurons." Neuron **15**(6): 1427-1439.

Mainen, Z. F. and T. J. Sejnowski (1996). "Influence of dendritic structure on firing pattern in model neocortical neurons." Nature **382**(6589): 363-366.

Markram, H., J. Lubke, et al. (1997). "Physiology and anatomy of synaptic connections between thick tufted pyramidal neurones in the developing rat neocortex." J Physiol **500 (Pt 2)**: 409-440.

Markram, H., Y. Wang, et al. (1998). "Differential signaling via the same axon of neocortical pyramidal neurons." Proc Natl Acad Sci U S A **95**(9): 5323-5328.

Marshel, J. H., T. Mori, et al. (2010). "Targeting single neuronal networks for gene expression and cell labeling in vivo." Neuron **67**(4): 562-574.

Mendizabal-Zubiaga, J. L., C. Reblet, et al. (2007). "The underside of the cerebral cortex: layer V/ VI spiny inverted neurons." J Anat **211**(2): 223-236.

Mercer, A., D. C. West, et al. (2005). "Excitatory connections made by presynaptic cortico-cortical pyramidal cells in layer 6 of the neocortex." Cereb Cortex **15**(10): 1485-1496.

Mori, M., M. H. Abegg, et al. (2004). "A frequency-dependent switch from inhibition to excitation in a hippocampal unitary circuit." Nature **431**(7007): 453-456.

Mountcastle, V. B. (1957). "Modality and topographic properties of single neurons of cat's somatic sensory cortex." J Neurophysiol **20**(4): 408-434.

Mountcastle, V. B. (1997). "The columnar organization of the neocortex." Brain **120 (Pt 4)**: 701-722.

Ohki, K. and R. C. Reid (2007). "Specificity and randomness in the visual cortex." Curr Opin Neurobiol **17**(4): 401-407.

Otsuka, T. and Y. Kawaguchi (2008). "Firing-pattern-dependent specificity of cortical excitatory feed-forward subnetworks." J Neurosci **28**(44): 11186-11195.

Peterlin, Z. A., J. Kozloski, et al. (2000). "Optical probing of neuronal circuits with calcium indicators." Proceedings of the National Academy of Sciences of the United States of America **97**(7): 3619-3624.

Peters, A. (1979). "Thalamic input to the cerebral cortex." Trends Neurosci **2**: 183-185.

Petersen, C. C. (2002). "Short-term dynamics of synaptic transmission within the excitatory neuronal network of rat layer 4 barrel cortex." J Neurophysiol **87**(6): 2904-2914.

Petersen, C. C. and B. Sakmann (2000). "The excitatory neuronal network of rat layer 4 barrel cortex." J Neurosci **20**(20): 7579-7586.

Petreanu, L., D. Huber, et al. (2007). "Channelrhodopsin-2-assisted circuit mapping of long-range callosal projections." Nat Neurosci **10**(5): 663-668.

Petreanu, L., T. Mao, et al. (2009). "The subcellular organization of neocortical excitatory connections." Nature **457**(7233): 1142-1145.

Pierret, T., P. Lavallee, et al. (2000). "Parallel streams for the relay of vibrissal information through thalamic barreloids." J Neurosci **20**(19): 7455-7462.

Pouille, F. and M. Scanziani (2004). "Routing of spike series by dynamic circuits in the hippocampus." Nature **429**(6993): 717-723.

Radnikow, G., D. Feldmeyer, et al. (2002). "Axonal projection, input and output synapses, and synaptic physiology of Cajal-Retzius cells in the developing rat neocortex." J Neurosci **22**(16): 6908-6919.

Reyes, A., R. Lujan, et al. (1998). "Target-cell-specific facilitation and depression in neocortical circuits." Nat Neurosci **1**(4): 279-285.

Reyes, A. and B. Sakmann (1999). "Developmental switch in the short-term modification of unitary EPSPs evoked in layer 2/3 and layer 5 pyramidal neurons of rat neocortex." J Neurosci **19**(10): 3827-3835.

Sarid, L., R. Bruno, et al. (2007). "Modeling a layer 4-to-layer 2/3 module of a single column in rat neocortex: interweaving in vitro and in vivo experimental observations." Proc Natl Acad Sci U S A **104**(41): 16353-16358.

Schaefer, A. T., M. Helmstaedter, et al. (2003). "Correction of conductance measurements in non-space-clamped structures: 1. Voltage-gated K+ channels." Biophysical journal **84**(6): 3508-3528.

Schubert, D., R. Kotter, et al. (2003). "Cell type-specific circuits of cortical layer IV spiny neurons." J Neurosci **23**(7): 2961-2970.

Schubert, D., J. F. Staiger, et al. (2001). "Layer-specific intracolumnar and transcolumnar functional connectivity of layer V pyramidal cells in rat barrel cortex." The Journal of neuroscience : the official journal of the Society for Neuroscience **21**(10): 3580-3592.

Shepherd, G. M., A. Stepanyants, et al. (2005). "Geometric and functional organization of cortical circuits." Nat Neurosci **8**(6): 782-790.

Shepherd, G. M. and K. Svoboda (2005). "Laminar and columnar organization of ascending excitatory projections to layer 2/3 pyramidal neurons in rat barrel cortex." J Neurosci **25**(24): 5670-5679.

Sjostrom, P. J. and M. Hausser (2006). "A cooperative switch determines the sign of synaptic plasticity in distal dendrites of neocortical pyramidal neurons." Neuron **51**(2): 227-238.

Sohal, V. S., F. Zhang, et al. (2009). "Parvalbumin neurons and gamma rhythms enhance cortical circuit performance." Nature **459**(7247): 698-702.

Song, S., P. J. Sjostrom, et al. (2005). "Highly nonrandom features of synaptic connectivity in local cortical circuits." PLoS Biol **3**(3): e68.

Staiger, J. F., I. Flagmeyer, et al. (2004). "Functional diversity of layer IV spiny neurons in rat somatosensory cortex: quantitative morphology of electrophysiologically characterized and biocytin labeled cells." Cereb Cortex **14**(6): 690-701.

Stepanyants, A., L. M. Martinez, et al. (2009). "The fractions of short- and long-range connections in the visual cortex." Proc Natl Acad Sci U S A **106**(9): 3555-3560.

Stratford, K. J., K. Tarczy-Hornoch, et al. (1996). "Excitatory synaptic inputs to spiny stellate cells in cat visual cortex." Nature **382**(6588): 258-261.

Stuart, G. J., H. U. Dodt, et al. (1993). "Patch-clamp recordings from the soma and dendrites of neurons in brain slices using infrared video microscopy." Pflugers Arch **423**(5-6): 511-518.

Tarczy-Hornoch, K., K. A. Martin, et al. (1999). "Intracortical excitation of spiny neurons in layer 4 of cat striate cortex in vitro." Cereb Cortex **9**(8): 833-843.

Thomson, A. M. and W. E. Armstrong (2011). "Biocytin-labelling and its impact on late 20th century studies of cortical circuitry." Brain research reviews **66**(1-2): 43-53.

Thomson, A. M. and A. P. Bannister (1998). "Postsynaptic pyramidal target selection by descending layer III pyramidal axons: dual intracellular recordings and biocytin filling in slices of rat neocortex." Neuroscience **84**(3): 669-683.

Thomson, A. M. and O. T. Morris (2002). "Selectivity in the inter-laminar connections made by neocortical neurones." J Neurocytol **31**(3-5): 239-246.

Urbain, N. and M. Deschenes (2007). "A new thalamic pathway of vibrissal information modulated by the motor cortex." J Neurosci **27**(45): 12407-12412.

Wang, H., J. Peca, et al. (2007). "High-speed mapping of synaptic connectivity using photostimulation in Channelrhodopsin-2 transgenic mice." Proceedings of the National Academy of Sciences of the United States of America **104**(19): 8143-8148.

Wang, Y., H. Markram, et al. (2006). "Heterogeneity in the pyramidal network of the medial prefrontal cortex." Nat Neurosci **9**(4): 534-542.

Welker, C. and T. A. Woolsey (1974). "Structure of layer IV in the somatosensory neocortex of the rat: description and comparison with the mouse." J Comp Neurol **158**(4): 437-453.

West, D. C., A. Mercer, et al. (2006). "Layer 6 cortico-thalamic pyramidal cells preferentially innervate interneurons and generate facilitating EPSPs." Cereb Cortex **16**(2): 200-211.

White, E. L. (2002). "Specificity of cortical synaptic connectivity: emphasis on perspectives gained from quantitative electron microscopy." J Neurocytol **31**(3-5): 195-202.

Wickersham, I. R., S. Finke, et al. (2007). "Retrograde neuronal tracing with a deletion-mutant rabies virus." Nature methods **4**(1): 47-49.

Wickersham, I. R., D. C. Lyon, et al. (2007). "Monosynaptic restriction of transsynaptic tracing from single, genetically targeted neurons." Neuron **53**(5): 639-647.

Williams, S. R. and S. E. Atkinson (2007). "Pathway-specific use-dependent dynamics of excitatory synaptic transmission in rat intracortical circuits." The Journal of physiology **585**(Pt 3): 759-777.

Williams, S. R. and S. J. Mitchell (2008). "Direct measurement of somatic voltage clamp errors in central neurons." Nat Neurosci **11**(7): 790-798.

Williams, S. R. and G. J. Stuart (2002). "Dependence of EPSP efficacy on synapse location in neocortical pyramidal neurons." Science **295**(5561): 1907-1910.

Wirth, C. and H. R. Luscher (2004). "Spatiotemporal evolution of excitation and inhibition in the rat barrel cortex investigated with multielectrode arrays." J Neurophysiol **91**(4): 1635-1647.

Woolsey, T. A. and H. Van der Loos (1970). "The structural organization of layer IV in the somatosensory region (SI) of mouse cerebral cortex. The description of a cortical field composed of discrete cytoarchitectonic units." Brain Res **17**(2): 205-242.

Xiang, Z., J. R. Huguenard, et al. (2002). "Synaptic inhibition of pyramidal cells evoked by different interneuronal subtypes in layer v of rat visual cortex." J Neurophysiol **88**(2): 740-750.

Yabuta, N. H., A. Sawatari, et al. (2001). "Two functional channels from primary visual cortex to dorsal visual cortical areas." Science **292**(5515): 297-300.

Yoshimura, Y. and E. M. Callaway (2005). "Fine-scale specificity of cortical networks depends on inhibitory cell type and connectivity." Nat Neurosci **8**(11): 1552-1559.

Yoshimura, Y., J. L. Dantzker, et al. (2005). "Excitatory cortical neurons form fine-scale functional networks." Nature **433**(7028): 868-873.

Yu, C., D. Derdikman, et al. (2006). "Parallel thalamic pathways for whisking and touch signals in the rat." PLoS Biol **4**(5): e124.

Yu, Y. C., R. S. Bultje, et al. (2009). "Specific synapses develop preferentially among sister excitatory neurons in the neocortex." Nature **458**(7237): 501-504.

Zarrinpar, A. and E. M. Callaway (2006). "Local connections to specific types of layer 6 neurons in the rat visual cortex." J Neurophysiol **95**(3): 1751-1761.

Zhang, F., V. Gradinaru, et al. (2010). "Optogenetic interrogation of neural circuits: technology for probing mammalian brain structures." Nature protocols **5**(3): 439-456.

Zhang, F., M. Prigge, et al. (2008). "Red-shifted optogenetic excitation: a tool for fast neural control derived from Volvox carteri." Nature neuroscience **11**(6): 631-633.

Zhang, F., L. P. Wang, et al. (2006). "Channelrhodopsin-2 and optical control of excitable cells." Nature methods **3**(10): 785-792.

Zhang, F., L. P. Wang, et al. (2007). "Multimodal fast optical interrogation of neural circuitry." Nature **446**(7136): 633-639.

Zhang, Z. W. and M. Deschenes (1997). "Intracortical axonal projections of lamina VI cells of the primary somatosensory cortex in the rat: a single-cell labeling study." J Neurosci **17**(16): 6365-6379.

Zhang, Z. W. and M. Deschenes (1998). "Projections to layer VI of the posteromedial barrel field in the rat: a reappraisal of the role of corticothalamic pathways." Cereb Cortex **8**(5): 428-436.

Zhou, Y., B. H. Liu, et al. (2010). "Preceding inhibition silences layer 6 neurons in auditory cortex." Neuron **65**(5): 706-717.

Zilles, K. and K. Amunts (2010). "Centenary of Brodmann's map--conception and fate." Nat Rev Neurosci **11**(2): 139-145.

9 Curriculum Vitae

Personal information:

Surname: Qi

First name: Guanxiao

Date of birth: August 20, 1980

Place of birth: Shandong, P.R. China

Nationality: Chinese

Qualification:

1994-1998: High school graduation

1998-2002: B.Sc. (Applied Physics), Southeast University, Nanjing, P.R. China

2002-2005: M.Sc. (Optics), Southeast University, Nanjing, P.R. China

Since 2007: PhD study in Institute of Neuroscience and Medicine (INM-2), Research Centre Jülich, Germany